2012

Wireless Channel Equalization in Digital Communication Systems

Sammuel Jalali
Claremont Graduate University

Recommended Citation

Jalali, Sammuel, "Wireless Channel Equalization in Digital Communication Systems" (2012). *CGU Theses & Dissertations.* Paper 42.
http://scholarship.claremont.edu/cgu_etd/42

DOI: 10.5642/cguetd/42

Wireless Channel Equalization in Digital Communication Systems

By

Sammuel Jalali

A dissertation submitted to the faculty of Claremont Graduate University and California State University, Long Beach in partial fulfillment of the requirements for the degree of Doctor of Philosophy in the Graduate Faculty of Engineering and Industrial Applied Mathematics

Claremont, California and Long Beach, California

2012

Wireless Channel Equalization in Digital Communication Systems

By

Sammuel Jalali

Claremont Graduate University

2012

Abstract

Our modern society has transformed to an information-demanding system, seeking voice, video, and data in quantities that could not be imagined even a decade ago. The mobility of communicators has added more challenges. One of the new challenges is to conceive highly reliable and fast communication system unaffected by the problems caused in the multipath fading wireless channels. Our quest is to remove one of the obstacles in the way of achieving ultimately fast and reliable wireless digital communication, namely Inter-Symbol Interference (ISI), the intensity of which makes the channel noise inconsequential.

The theoretical background for wireless channels modeling and adaptive signal processing are covered in first two chapters of dissertation.

The approach of this thesis is not based on one methodology but several algorithms and configurations that are proposed and examined to fight the ISI problem. There are two main categories of channel equalization techniques, supervised (training) and blind unsupervised (blind) modes. We have studied the application of a new and specially modified neural network requiring very short training period for the proper channel equalization in supervised mode. The promising performance in the graphs for this network is presented in chapter 4.

For blind modes two distinctive methodologies are presented and studied. Chapter 3 covers the concept of multiple "cooperative" algorithms for the cases of two and three cooperative algorithms. The "select absolutely larger equalized signal" and "majority vote" methods have been used in 2-

and 3-algoirithm systems respectively. Many of the demonstrated results are encouraging for further research.

Chapter 5 involves the application of general concept of simulated annealing in blind mode equalization. A limited strategy of constant annealing noise is experimented for testing the simple algorithms used in multiple systems. Convergence to local stationary points of the cost function in parameter space is clearly demonstrated and that justifies the use of additional noise. The capability of the adding the random noise to release the algorithm from the local traps is established in several cases.

Acknowledgement

My deep and sincere thanks to my advisor, Professor Rajendra Kumar from California State University, Long Beach (CSULB) for his knowledgeable and kind guidance and help that I have received in three interesting courses I took with him, and continuously since 2008 to 2012. I am also indebted to Professor Ellis Cumberbatch from Claremont Graduate University (CGU) for his fantastic applied mathematics courses and priceless help in the course of my education.

My especial thanks to Professor Burkhard Englert from CSULB, and Professor Allon Percus from CGU for being encouraging dissertation committee memeber. I would like to extend my appreciation to Professor Chit-Sang Tsang and Professor Henry Schellhorn and to the memory of Professor Hedley Morris.

Table of Contents

Chapter 5: Adaptive Simulated Annealing

List of Figures

Thesis Outlook

Our modern society has transformed to an information-demanding system, seeking voice, video, and data in quantities that could not be imagined even a decade ago. Mobility of communicators has added new challenges in the path to accomplish the goal of providing all the information asked for in any possible location. One of the new challenges is to conceive highly reliable and fast communication system unaffected by the problems caused in the multipath fading wireless channel.

Our quest in this thesis is to help remove one of the obstacles in the way of achieving ultimately fast and reliable wireless digital communication, namely Inter-Symbol Interference (ISI), the severity of which makes the channel noise inconsequential.

An introduction to wireless channel characteristics and modeling is given in chapter one. This includes the large scale and small scale fading phenomena in section 1.2 and 1.3 respectively, and the mathematical models for wireless channels in section 1.5. An emerging ISI cancellation technique by space diversity is also discussed in the last section of chapter one.

Since most of the techniques used to achieve the aforementioned goal are adaptive in nature, chapter two is dedicated to a review of the main adaptive algorithms as well as some other methods to invert a-priori known channels. The deconvolution technique for inverting known channels (by their approximate impulse response) is discussed in section 2.3; when other techniques for the known channel are given in section 2.4. Blind equalization techniques with relatively low computational cost are discussed in section 2.5. A major family of these techniques that are collectively called Bussgang algorithms are reviewed in the concluding section of chapter 2.

Our contributions are mainly in chapter 3 and 4. A new methodology to approach the blind equalization which was mentioned in the research proposal by using diverse algorithms is treated in chapter 3. First a few more algorithms with relatively simple computations that are being incorporated in diversified systems in chapter 3 are given in section 3.2. These include RLS, EWRLS, and Quantized State recursive methods. In section 3.3 the general idea of cooperation of two or more algorithms is discussed and with some very optimistic expectations the effectiveness of them are shown. Section 3.4 introduces the configuration that uses two algorithms with corresponding simulation results, while the main idea of majority vote among the algorithms contributing to the systems with 3 simultaneous ones is given in section 3.5. The latter section includes the important simulation results for the system of three that is the pinnacle of this chapter. Chapter 3 concludes with a brief summary of the results.

An alternative to blind methods that can use a very short training period seems attractive in practice. Especially if the proposed method is simple in architecture, it can be employed to replace the less reliable blind equalization techniques. After an introduction, and the review of the fundamental theory of neural networks in sections 4.1 and 4.2 the well-known back propagation algorithm for neural networks is presented in section 4.3. The application of the proposed architecture to the problem of wireless channel equalization is formulated in section 4.4. The learning algorithm details for the proposed network are summarized in section 4.5. The performance and the simulation results are included in section 4.6 of this chapter. A weak convergence analysis of the output layer is discussed in section 4.7 (this is different from the well-known Rosenblatt perceptron convergence that does not include any activation function, such as the hyperbolic tangent blocks in our proposed network). While the input layer convergence analysis seems out of reach at present, it is left to the future research.

Another concept that was originally intended to be developed also for blind mode systems as a promising methodology is approached in chapter 5 under the Adaptive Simulated Annealing terminology. After an introduction to the elements of simulated annealing and a short history of its application are given in section 5.2, in section 5.3 we argue that this technique should facilitate the convergence, at least in theory. Some preliminary results are shown in the following section.

Finally chapter 6 presents an overall collective summary of the results obtained in this thesis and delineates the path for future continuation of related research by the author and the research community, in particular in the field of adaptive signal processing.

Chapter 1: Wireless Channel Models and Diversity techniques

1.1 Introduction

Wireless communication has gone through major changes in the last few decades. While it mostly had been used for satellite, terrestrial links and broadcasting until the 1970s, cellular and wireless networking and other Personal Communication Systems (PCS) presently dominate the technology of modern wireless communications.

The generally used Additive White Gaussian Noise (AWGN) model does not adequately represent the channel for these modern applications. Moreover, the Line-Of-Sight (LOS) path between the transmitter and the receiver may or may not exist in such a channel.

An important characteristic of the wireless channel is the presence of many different paths between the transmitter and the receiver (See Figure 1-1).

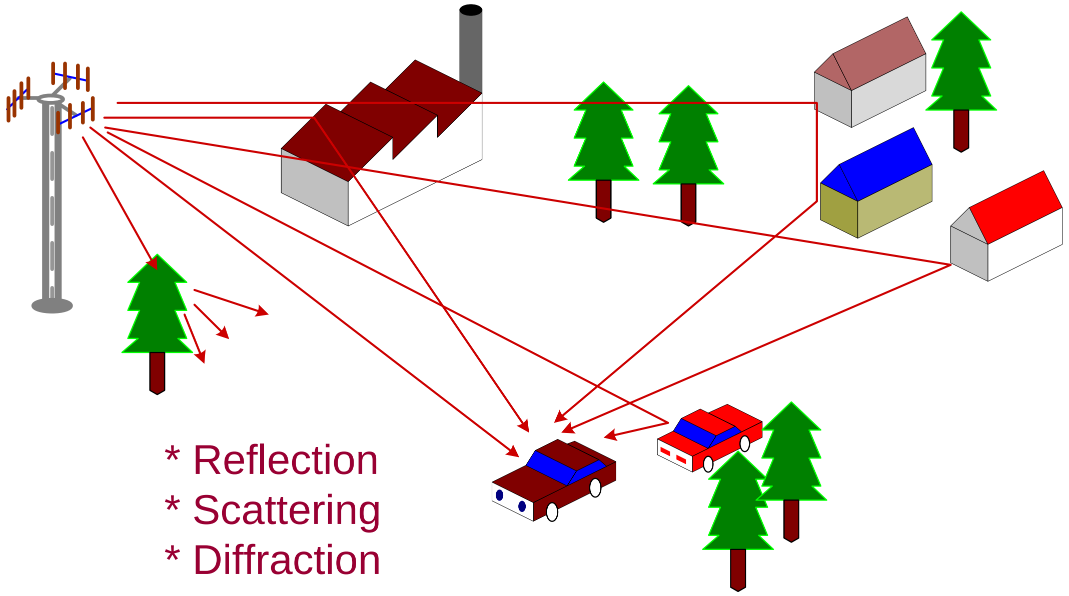

Figure 1-1 Multipath channel in wireless communications.

Basic Electromagnetic (EM) wave propagation phenomena such as scattering that occurs along these paths further increases the number of the paths between the communicators.

Common propagation phenomena encountered are:

1. Reflection: EM waves are reflected when impinging on objects in their paths if the physical size of the objects are much greater than the wavelength λ of the EM waes.
2. Diffraction: Characterized as the sharp changes in the propagation path of EM waves that occur when they hit an obstacle with surface irregularities such as sharp edges.
3. Scattering: Occurs when EM waves visit a cluster of objects smaller in size than the wavelength, such as water vapor and foliage. Scattering causes many copies of the EM wave to propagate in different directions.

There are other infrequent phenomena such as absorption and refraction that might take place in common wireless channels.

The signal power is the critical parameter in a communication channel. The power reducing effects have been studied in two major cases:

1. Large-scale effect characterizes the signal power usually with respect to long propagation distances and results in the mean path loss of the signal.
2. Small-scale effect or fading concerns the relatively fast changes in the signal amplitude and its power. It characterizes the signal power fluctuations over short distance and time intervals around the mean signal power.

1.2 Large Scale Fading or Attenuation

In general, the average power of the received signal decreases logarithmically with the distance between the transmitter and the receiver. The attenuation caused by the distance is called *large scale effect* or *path loss*. The propagation medium and the environment would also have some effect on the total loss of the signal strength.

The averaged received power at a certain distance from the transmitted is measured by keeping the distance to the transmitter constant (as the radius of a circle) and moving the mobile antenna on the circle. The difference between the transmitted power $\mathcal{P}_t$ and the averaged received signal power $\mathcal{P}(d)$ (expressed in dBm) at certain distance d is the path loss in dB, which is denoted by $L(d)$.

$$\mathcal{P}(d) = \mathcal{P}_t - L(d)\,, d > d_o \qquad (1\text{-}1)$$

The average of the path loss in dB units, with respect to a referenced distance d_o at which the path loss is measured and is known, is given by:

$$\bar{L}(d) = \bar{L}(d_o) + 10n\ \log_{10}\left(\frac{d}{d_o}\right) \qquad (1\text{-}2)$$

The order n has the constant value of 2 for LOS links but is usually higher than 2 for multipath channels in cities and urban areas. The model in (1-20 is known as the *log-distance* path loss model. The measured path loss $L(d)$ at distance d can be significantly different from the average value due to, for example, shadowing effects, and in fact, is a Gaussian random variable given by:

$$L(d) = \bar{L}(d_o) + 10n\ \log_{10}\left(\frac{d}{d_o}\right) + X_\sigma \qquad (1\text{-}3)$$

X_σ is a zero-mean Gaussian random variable (in dB) with standard deviation σ also in dB. The path loss so described is known as log-normal shadowing.

The various measurements of path loss at different distances are collected in a graph of the loss in dB versus the distance in dB $(\text{that is } 10\log_{10} d)$. The constant n can be approximated by the best fitted line (Least-Squares, for example) of the data.[1]

With the distance d equal to the radius of the wireless cellular network, the probability $[\mathcal{P}_r(d) > \gamma]$ is equal to the *likelihood of the coverage* within the cell.

[1] See Jake, 1974, pp. 126-127
Rappaport, 2002, pp. 141-143

The percentage of coverage area (that is, the fraction of the area within the cell that will have an acceptable power level) is:

$$U(\gamma) = \frac{1}{\pi d^2} \int_0^{2\pi} \int_0^{d} P[\mathcal{P}r(d) > \gamma] \, r dr d\theta \qquad (1\text{-}4)$$

This percentage may be computed in terms of the error function erf as follows(see [6] and [7]):

$$U(\gamma) = \frac{1}{2}\left(1 - \operatorname{erf}(a) + \exp\left(1 - \frac{2ab}{b^2}\right)\left[1 - \operatorname{erf}\left(1 - \frac{ab}{b}\right)\right]\right) \qquad (1\text{-}5)$$

where $a = \gamma - \frac{\overline{\mathcal{P}r}(d)}{\sigma\sqrt{2}}, b = \frac{10n \log_{10} e}{\sigma\sqrt{2}}$, and $\operatorname{erf}(x) = \frac{2}{\sqrt{\pi}} \int_0^x e^{-t^2} dt.$

When the signal level is $\overline{\mathcal{P}r}(d) = \gamma$ (that is $a = 0$), then:

$$U(\gamma) = \frac{1}{2}\left[1 + \exp\left(\frac{1}{b^2}\right)\left(1 - \operatorname{erf}\left(\frac{1}{b}\right)\right)\right] \qquad (1\text{-}6)$$

1.3 Small Scale Fading

Due to multipath propagation, more than one version of the transmitted signal arrive at the mobile receiver at slightly different times. The interference induced by these multiple copies, also known as multipath waves, has become the most significant cause of distortion known as fading and *Inter-Symbol Interference* (ISI). The radio signal experiences rapid changes of its amplitude over a relatively short period of time (See Figure 1-2).

The waves travelling different paths, therefore travelling different distances, sum up at the receiver antenna (or antenna array in some cases) to generate ISI of such a magnitude that the effects of large-scale path loss can be completely ignored by comparison.

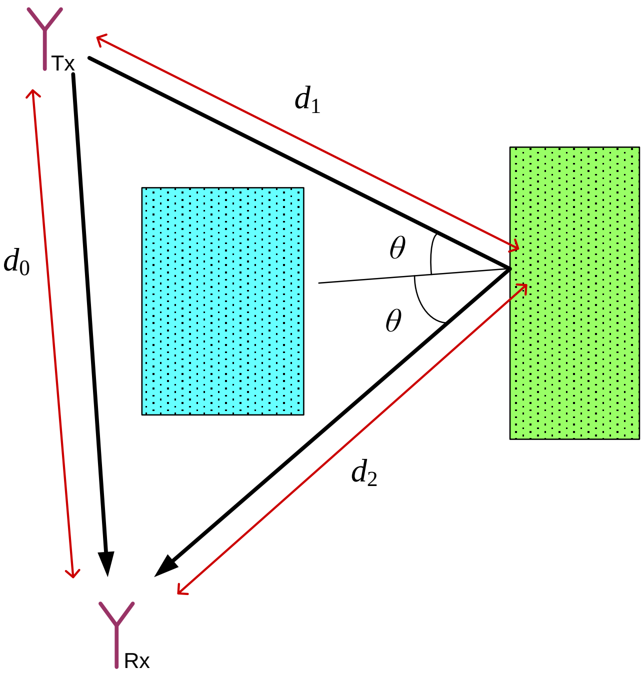

Figure 1-2 Example of two-ray geometry

There are a variety of ways to statistically model the wireless channels in order to represent the random behavior of multipath fading. One simple and popular model represents the fading channel with a linear and time-varying Channel Impulse Response (CIR) denoted by the function $h(t, \tau)$.

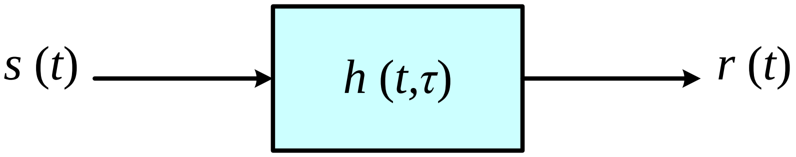

Figure 1-3 Channel modeling by Channel Impulse Response (CIR)

Time Dispersion Parameters

A perfect channel from a communications point of view is one that has a constant gain and a linear phase response, or at least possesses these features over a desired frequency range or bandwidth.

Such a frequency range should be larger than the frequency spectrum of the transmitted signal to preserve the signal spectral characteristics. Consequently, such an ideal channel can be symbolically shown as $h(t,\tau) = g_o\,\delta(\tau)$ (See Figure 1-4), with g_o as a constant.

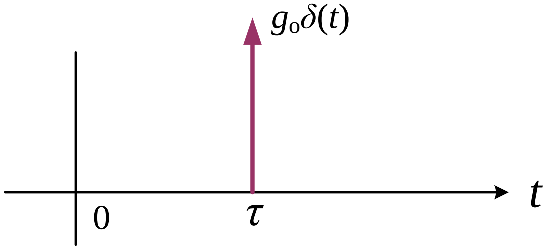

Figure 1-4 An ideal Channel Impulse Response (CIR)

Such channel impulse response implies only one received signal (delayed by τ), causing no ISI even when the gain varies with time as the varying CIR of $h(t,\tau) = g(t)\delta(\tau)$ where $g(t)$ is relatively slowly varying function of time and in general may be complex valued. If we assume that the multipath channel includes N different paths, and let the power and delay of k^{th} path be given by P_k and τ_k respectively, then the weighted average delay (also known as *mean excess delay*) is defined as:

$$\bar{\tau} = \frac{\sum_{k=1}^{N} g_k^2 \tau_k}{\sum_{k=1}^{N} g_k^2} \qquad (1\text{-}7)$$

The second statistical moment of the delay may also be computed by:

$$\overline{\tau^2} = \frac{\sum_{k=1}^{N} g_k^2 \tau_k^2}{\sum_{k=1}^{N} g_k^2} \qquad (1\text{-}8)$$

The channel *delay spread*, that is the rms value of the delay, is given by:

$$\sigma_\tau = \sqrt{\overline{\tau^2} - (\bar{\tau})^2} \qquad (1\text{-}9)$$

The channels with time-dependent response (CIR) given by $h(\tau, t)$ will have time-dependent frequency response $H(\omega, t)$ (In fact, as will be stressed later, the CIRs change very slowly with respect to time in most practical cases) with

$$H(\omega, t) = \int_{-\infty}^{+\infty} h(\tau, t) e^{-j\omega\tau} d\tau . \qquad (1\text{-}10)$$

To determine the wireless channel characteristics in the frequency domain, first we need to determine the *correlation coefficient or factor* of the channel frequency response, based on a change in frequency of the size $\Delta\omega$ or $2\pi\Delta f$.

$$P(\Delta\omega) = \frac{\mathbb{E}\{H^*(\omega, t)H(\omega + \Delta\omega, t)\}}{\mathbb{E}\{H^*(\omega, t)H(\omega, t)\}} = \frac{\mathbb{E}\{H^*(\omega, t)H(\omega + \Delta\omega, t)\}}{\mathbb{E}\{|H(\omega, t)|^2\}}$$

$$= \frac{\int_{-\infty}^{+\infty} |h(\tau, t)|^2 e^{-j\Delta\omega\tau} d\tau}{\int_{-\infty}^{+\infty} |h(\tau, t)|^2 d\tau} \quad (1-11)$$

The *coherence bandwidth* is the counterpart of the delay spread in the frequency domain, and it is the range of frequencies over which the channel gain remains about the same, or as is commonly known, over the range of frequencies the gain is *flat*, with a linear phase. Fortunately, the coherence bandwidth of the channel denoted by B_c can be approximated based on the specified correlation coefficient value.

The case when the correlation coefficient is about zero, $P(\Delta\omega) \approx 0, \Delta\omega = 2\pi B_c$. The coherence bandwidth for this case is approximated by $B_c \approx 1/\sigma_\tau$, which implies that changing the frequency by B_c results in a completely different (and statistically independent) gain.

For the more common value of $P(\Delta\omega) \approx 0.5$ (or 50%),the coherence bandwidth is estimated by $B_c \approx 1 / 5\sigma_\tau$, which implies that the channel gain at ω and $\omega + B_c$ are similar.

Finally, when considering $P(\Delta\omega) \approx 0.9$ (or 90%), the coherence bandwidth can be approximated as $B_c \approx 1\ /\ 50\sigma_\tau$. In this case, the channel gain at ω is almost exactly the same as the gain at $\omega + B_c$.

Based on the value of coherence bandwidth B_c, and given signal bandwidth B_s, one can evaluate the channel category. When $B_c > B_s$, the channel is considered flat or *flat fading*.

Denoting the symbol time duration by T_s then the minimum signal bandwidth can be estimated as $B_s = \frac{1}{T_s}$. This signal bandwidth therefore has to be quite a bit less than the channel coherence bandwidth so that the channel can be assumed to be flat fading. A rule of thumb is given by

$$B_s = \frac{1}{T_s} \leq \frac{1}{10\sigma_\tau} \text{ or equivalently by } \frac{\sigma_\tau}{T_s} \leq 0.1.$$

In the case of a flat fading channel, no compensation for the channel distortion is required. Consequently, the symbol rate in the channel has an upper bound $R_s \leq \frac{0.1}{\sigma_\tau}$.

When the above condition is not met, that is, $B_s > B_c$, the ISI exists and the received signal is distorted.

In most common multipath channels the ISI distortion effects are significant and dominate the channel noise. Such channels are said to be highly *dispersive*, and engineering efforts are focused on eliminating ISI by a process known as equalization in communication discipline, or de-convolution in some other applications such as geophysics.

In conclusion, we divide the channel behavior with respect to the signal bandwidth and according to the channel delay spread as follows:

- When $B_s \ll B_c$ and $T_s \gg \sigma_\tau$ the channel is known as flat fading or frequency-not-selective.
- When $B_s > B_c$ and $T_s < \sigma_\tau$ the channel is known as non-flat or frequency-selective.

1.4 Frequency Dispersion Parameters

The mobility of the communicator originates another parameter known as *Doppler shift* in frequency, or simply some change in frequency due to the mobile velocity.

When denoted by f_d, the Doppler shift is computed as $f_d = \frac{v}{\lambda}\cos\theta$, in which v is the relative mobile speed, λ is the radio wavelength, and θ is the angle between the wave direction and the mobile direction. The change in frequency is positive when the mobile approaches the transmitter and negative when the mobile is departing.

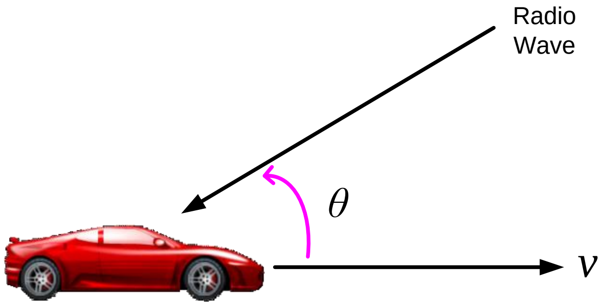

Figure 1-5 Doppler shift geometry

It is obvious that different paths have different Doppler shifts that possess random natures, as the angle θ can be considered random and in most cases uniformly distributed.

There are a number of copies of the transmitted waves at the mobile antenna, each travelling along different paths, which are characterized by various relative speeds and angles. Moreover, in specific scenarios, the surrounding objects might be moving and generating time varying Doppler shifts on multiple components.

The corresponding random change in frequency causes spectral broadening known as *Doppler spread*. Doppler spread is therefore defined as the range of frequencies over which the Doppler shift is not zero. We denote by B_d the maximum Doppler shift or Doppler spread of a specific wireless channel.

It is possible to categorize the wireless channel with respect to Doppler spread B_d as follows:

- If the signal bandwidth is much greater than Doppler spread, that is $B_s \gg B_d$, the fading is known as *slow fading* and, hence, the effects of Doppler spread are negligible. In this case, the channel (in particular, CIR) changes at a much slower rate and can be assumed to be static over several symbol time durations.
- If, on the contrary, the effects of the Doppler spread are significant and cannot be ignored in the case that $B_s < B_d$, the CIR changes rapidly with respect to the symbol time duration. Such channel is called *fast fading*.

The time domain properties of the wireless channel can be further specified by defining another parameter, *coherence time*, which is the duration of time in which the CIR is invariant. Two samples of the channel are highly correlated if their time separation is less than the coherence time. The given definition itself depends on the time correlation coefficient.

The correlation coefficient in the time domain as a function of time difference Δt is given by:

$$P(\Delta t) = \frac{\mathbb{E}\{h(t)h^*(t+\Delta t)\}}{\mathbb{E}\{|h(t)|^2\}} \qquad (1\text{-}12)$$

Generally, the coherence time is inversely proportional to the Doppler spread.

$$T_c \approx \frac{1}{B_d} \qquad (1\text{-}13)$$

If the coherence time for which the time correlation coefficient of Equation (1-12) remains above 0.5 or 50% it is approximated by:

$$T_c \approx \frac{9}{16\pi B_d} \qquad (1\text{-}14)$$

As a rule of thumb, the geometric average of 1-13 and 1-14 is used for digital communication.

$$T_c = \sqrt{\frac{1}{B_d} . \frac{9}{16\pi B_d}} \approx \frac{0.423}{B_d} \qquad (1\text{-}15)$$

The channel characteristics can be categorized using the coherence time T_c, and the symbol time duration T_s as follows:

- When $T_s < T_c$, the complete signal or symbol is affected similarly by the channel, and the channel is known as *slow fading*.
- When $T_s > T_c$, different parts of a signal are affected differently because the channel changes faster compared to a symbol duration. Consequently, the channel is called *fast fading*.

In summary, wireless channels can be divided into four types. Based on the delay spread, the channel is either flat (not frequency selective) or frequency selective, and based on Doppler spread (or, equivalently, coherence time) the channel is known as slow or fast fading.

As we will see, commonly encountered wireless channels in modern mobile communication systems are determined to be selective and slow fading. That is, the channels are usually highly dispersive. However, the variation of channels is slow with respect to time.

To investigate the time variation of typical wireless channels, consider the scenario of Figure 1-6 in which the mobile is travelling at 50 mph (approximately 23 m/s) at an angle of 40° to the cardinal East-West direction.

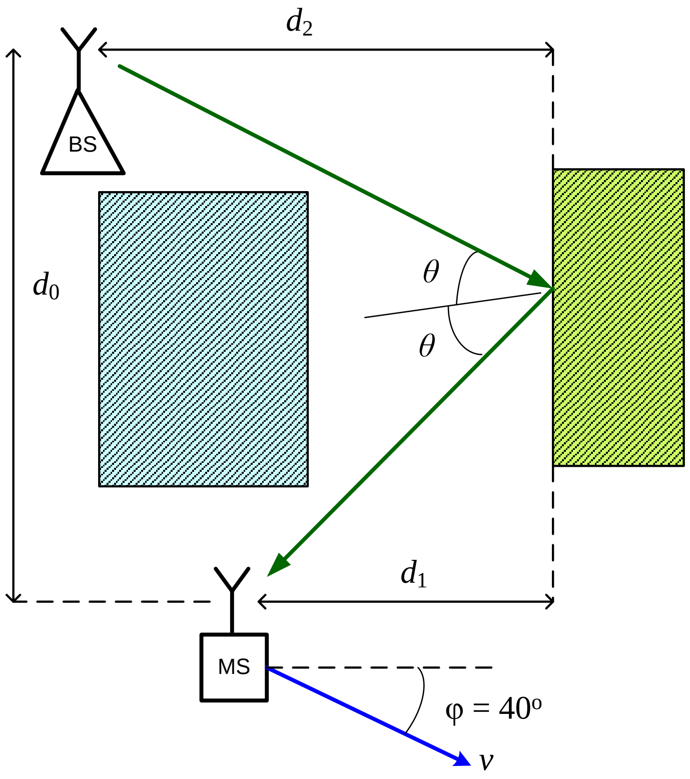

Figure 1-6 Example of the channel time-variation computing

The path length for the ray shown in the figure is computed by $d_T = \sqrt{d_o^2 + (d_1 + d_2)^2}$ in meters and the corresponding delay in seconds by $\tau_1 = \frac{d_T}{c}$. Given the geometric distances: $d_o = 600\text{m}, d_1 = 100$ m, and $d_2 = 350$ m, the delay $\tau = 2.5$ μs. If we assume a symbol rate of $R_s = 19.2$ ksps that is equivalent of symbol time $T_s \approx 52$ μs, the time delays after 10,000 symbols (0.52 s) is computed as $\tau_2 = 2.50224$ μs. That is a change of less than 0.1% in the time delay of the travelling ray. This example justifies the assumption that time variation of the wireless channels are significantly slow in comparison to common symbol rates (we have used a worst case scenario here.)

1.5 Wireless Channel Models

Analytical modeling of wireless channel variations and the evaluation of their effects on transmitted signals is essential for capacity and coverage optimization including radio resource management. One simple model based on the previous discussions is given in Figure 1-7. In this model large-scale path loss is compensated for by adjusting the signal amplitude with $\sqrt{\bar{L}(d)}$ factor.

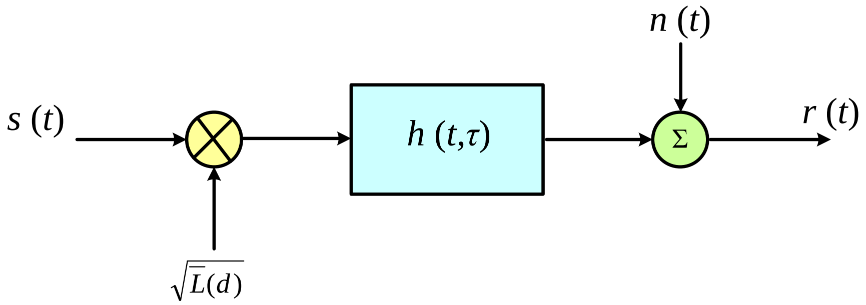

Figure 1-7 Simple wireless channel model

The small-scale variations are collected in CIR part of the model, namely $h(\tau, t)$. The received signal characteristics, including the amplitude and the phase, depend on the distance from the transmitter d, and the azimuth (horizontal plane) angle φ of the receiver with respect to a reference. The latter is justified even in cases when the transmitter antenna (or antenna array) is omni-directional due to the fact that the physical channel might not be azimuthally symmetric. When the dependence on the distance was explicitly shown in equation (1-3), the azimuth angle was ignored since an angular average of the pass loss at each specific distance was taken into account.

In the following, the dependence on d and φ is assumed to be implied and explicit notation is omitted in order to keep the mathematical expressions sharp and simple.

The dependence on time must also be acknowledged. So for the Channel Impulse Response (CIR), which in an accurate notation should be given as $h(d, \varphi, t)$ or $h_{d,\varphi}(t)$, it is simply shown by $h(t)$ in the discussion that follows.

The channel model of a linear time-varying impulse response is approximated by one or multiple delta functions for the flat-fading or frequency-selective cases respectively. The delta functions have variable and generally complex-valued amplitudes that need to be statistically modeled.

- In the first case we assume that no Line-Of-Sight (LOS) path between the transmitter and the receiver exist. Considering M available paths in the channel, the received signal comprises a collection of weighted and delayed signals (in terms of an unmodulated sinusoidal carrier signal) and an independent random noise process:

$$r(t) = \sum_{j=1}^{M} \alpha_j \cos\left(2\pi f_c t + \varphi_j\right) + n(t) \qquad (1\text{-}16)$$

$$r(t) = \cos(2\pi f_c t) \sum_{j-1}^{M} \alpha_j \cos\left(\varphi_j\right) - \sin(2\pi f_c t) \sum_{j=1}^{M} \alpha_j \ \sin\left(\varphi_j\right) + n(t)$$

$$= \cos(2\pi f_c t) * I(t) - \sin(2\pi f_c t) * Q(t) + n(t) \qquad (1\text{-}17)$$

By using the central-limit-theorem and fair assumptions about the physical environment, $I(t)$ and $Q(t)$ parameters are estimated as iid (identical and independently distributed) zero-mean Gaussian random variables with their variance noted by σ^2.

The envelope $R(t) = \sqrt{I^2(t) + Q^2(t)}$ is distributed according to Rayleigh pdf (probability distribution function) and is usually independent of time.

$$f_R(r) = \frac{r}{\sigma^2} \exp\left(-\frac{r^2}{2\sigma^2}\right), r \geq 0 \qquad (1\text{-}18)$$

The phase component is:

$$\Theta(\mathrm{t}) = \tan^{-1}\left(\frac{Q(t)}{I(t)}\right). \qquad (1\text{-}19)$$

The phase variable is commonly accepted to be uniformly distributed in $[-\pi, \pi]$ follows from iid assumption. The average power of the received signal can be evaluated as $\mathbb{E}[R^2] = \mathbb{E}[I^2] + \mathbb{E}[Q^2] = 2\sigma^2$.

The small-scale variations of the channel as collected in the CIR, $h(\tau, t)$, is modeled with one or multiple delta functions adjusted by a complex-valued path gain. The CIR is simplified and given by:

$$h(\tau, t) \approx \sum_{j=1}^{M} r_j e^{i\,\theta_j(t)}\,\delta(\tau - \tau_j) \qquad \text{(1-20)}$$

The CIR equation reduces a single delta function in flat-fading channels as $M = 1$. Moreover, the path gains r_j are assumed to be time-independent (in fact, slowly varying with time), when the phase components $\theta_j(t)$ may change rapidly in time. Their distributions have already been given in (1-19) and (1-20) for R and Θ respectively. The received baseband signal is usually normalized so that $\sum_{j=1}^{M} r_j^2 = 1$. When the channel is frequency-selective, all but one of the components in (1-20) are undesired and interfere with the main desired component. The desired component is specified by (r_d, θ_d). The important measure of the quality of ISI-elimination is known as residual ISI computed in dB:

$$ISI_R = 10\log_{10}\left(\frac{\sum_{j=1}^{M} r_j^2 - r_d^2}{r_d^2}\right) = 10\log_{10}\left(\frac{1 - r_d^2}{r_d^2}\right) \qquad \text{(1-21)}$$

The last term in Equation (1-21) is valid when the signal power is normalized.

The *power-delay profile* of multipath channels is defined by the square of the magnitude of path gains as a collection of delta or impulse functions $\sum_{j=1}^{M} r_j^2 \delta(\tau - \tau_j)$.

- The second case of modeling path gains includes a dominant approximately stationary LOS component in addition to random multipath components. In this case the path gain $I(t)$and $Q(t)$ are no longer zero-mean, nonetheless they are Gaussian with equal variance. Let $m_1 = \mathbb{E}[I]$ and $m_2 = \mathbb{E}[Q]$ with equal variance noted by σ^2. We define $s = \sqrt{m_1^2 + m_2^2}$ as a non-centrality parameter, and $k = \frac{m_1^2+m_2^2}{2\sigma^2} = \frac{s^2}{2\sigma^2}$ as the Rice factor. The pdf of the envelope $R = \sqrt{I^2 + Q^2}$ will be *Ricean* as follows:

$$f_R(r) = \frac{r}{\sigma^2} \exp\left(\frac{-r^2 + s^2}{2\sigma^2}\right) I_o\left(\frac{rs}{\sigma^2}\right) , r \geq 0 \qquad \text{(1-22)}$$

The $I_o(.)$ part is the modified Bessel function of the 0th order. This function, in closed form, can be written:

$$I_o(x) = \frac{1}{\pi} \int_0^{\pi} \cosh(x \sin \xi) d\xi = \frac{1}{2\pi} \int_0^{2\pi} \exp(x \sin \xi) d\xi \qquad \text{(1-23)}$$

It is computed using series expansions with $I_o(0) = 1$ (see for example, Jeffery 2005 or Abramowitz and Stegun 1964).

Obviously, when the LOS disappears, the non-centrality $s = 0$ and the pdf converges to Rayleigh.

- Finally, for urban zones and cities with closely spaced buildings where no dominant LOS or specular component exists, the small-scale multipath channel is more accurately modeled by the *Nakagami* distribution, which models the magnitude of the path gains relatively better as compared to the Rayleigh distribution.

Considering $\mathbb{E}[R^2] = \Omega(\Omega = 2\sigma^2)$ and defining $= \frac{\Omega^2}{\mathbb{E}[(R^2-\Omega)^2]}$, the Nakagami pdf is given as:

$$f_{R(r)} = \frac{2}{\Gamma(m)} \left(\frac{m}{\Omega}\right)^m r^{2m-1} \exp\left(-\frac{mr^2}{\Omega}\right), r \geq 0, m \leq 0.5 \qquad (1\text{-}24)$$

When $\Gamma(m) = \int_0^\infty \exp(-x)\, x^{m-1} dx$ is Gamma function with $\Gamma(1) = 1$.

The Nakagami distribution is equivalent to the well-known Gamma distribution with parameters $\alpha = m$ and $\beta = \frac{\Omega}{\mathrm{m}}$ and if we substitute random variable R^2 with x as in the following pdf:

$$f_x(x) = \frac{1}{\Gamma(\alpha)\beta^\alpha}\, x^{\alpha-1} \exp\left(-\frac{x}{\beta}\right), x \geq 0 \qquad (1\text{-}25)$$

Furthermore, the Nakagami reduces to the Rayleigh distribution when $m = 1$.

In concluding this section, we need to stress some important issues in the discussion presented above.

a. As was mentioned, the two components of the channel path gains $I(t)$and $Q(t)$ are independent and can be dealt with separately. In some cases, the envelope $R = \sqrt{I^2 + Q^2}$ is assumed to be relatively constant in time (slowly varying) and the phase $\theta = \tan^{-1}\left(\frac{Q}{I}\right)$ may be constant and ignored as it is tracked by the receiver. Such assumptions approximate the channel with a real impulse response.

b. In digital communication, the baseband signals (received signal), after processing with matched filter and the sample and hold circuit are represented by a discrete-time impulse response or equivalently by a transversal filter of finite length. Such CIR is written by the sequence $\{h[j]\}_{j=0}^{L-1}$, and in terms of unit impulses by $\sum_{j=0}^{L-1} h[j]\delta[k-j]$ when the CIR is approximated by a finite-length sequence of size L. In general, the components $\{h[k]\}$ can be complex or real-valued.

c. When the channel model is closer to a recursive filter representation, it can still be adequately modeled with an infinite, or more practically with a very large transversal filter.

1.6 Inter-Symbol-Interface Cancellation and Diversity

Highly dispersive channels require some advanced processes to reduce, and possibly eliminate the ISI effects. In practice, these channels are approximately invariant during the time that the necessary process is executed. Moreover, some means of adaptation to compensate and adjust for the slow variations of the channel must be applied.

a. The first of the algorithms introduced here can be one among various approaches employed to eliminate ISI in general. These techniques are all designed to nullify or at least mitigate the effect of the channel response. This group is known to perform channel equalization. When employing a training period the channel equalization has the form of a straightforward and relatively simple adaptive system. It is the blind equalization (no training period) that has generated a great amount of literature with regard to relevant research. Unsupervised (blind) channel equalization problems have been solved by many different approaches each employing different and possible-to-estimate channel characteristics.

b. The Orthogonal Frequency Division Multiplexing (OFDM) Technique can be considered an independent solution to ISI problems. Although the channel equalization should also be performed in OFDM systems, it should be noted that the channels seem to be different by having narrow frequency band in OFDM systems. In particular, they reduce to flat-fading or frequency nonselective as the signal is segmented into many component ……..

c. The performance measures, such as the probability of error in fading channels, can be improved by transmitting the same information through more than one (possibly many) independent channels. The techniques exploiting this idea are known as diversity techniques, and the information copies can be obtained in time, space, or frequency.

Modern digital communication systems incorporating diversity techniques are collectively MIMO (Multiple Input Multiple Output) systems. These systems can also have multiple inputs but single output (MISO), or only multiple outputs with single input (SIMO).

One diversity gain has been defined by [1]:

$$G_d = -\lim_{\gamma \to \infty} \frac{\log(P_e)}{\log(\gamma)} \qquad (1\text{-}26)$$

Where P_e is the probability of bit error or Bit Error Rate (BER) and γ is the Signal-to-Noise Ratio (SNR) entered in log-scale into the equation.

MIMO systems should offer answers to two essential questions: how to create diversity (in time, space and frequency) and how to use the diversity to achieve the highest performance via reduction in the probability of error.

The diversity can be gained by creating independently fading channels separated in time, frequency, or space as follows:

a. Using different carrier frequencies when frequency separation must be much greater than coherence bandwidth $\left(B_c \approx \frac{1}{\sigma_\tau}\right)$.
b. Using different time slots (temporal diversity) when the separation must be greater than coherence time $\left(T_c \approx \frac{1}{B_d}\right)$.

c. Using different antennas (spatial diversity) when the spatial separation of the transmitter or the receiver antennas must be at least equal to or more than the half-wavelength of the carrier frequency $\left(\frac{\lambda_C}{2}\right)$.

It must be mentioned that exploiting temporal diversity is possible only when the mobile is in motion, otherwise when the mobile is stationary (the moving objects surrounding the receiver can also create Doppler shift), the Doppler shift is zero, and creating independent channels in time is consequently not feasible.

Furthermore, polarization diversity, including vertical or horizontal polarization is not seriously accepted or considered, perhaps because it can only provide a diversity of order two.

The second question seeks some invention of a method to take advantage of the existing diversity in an efficient way. To see how this has been achieved in what appears to be the classic literature (See Jake 1974), we first consider the cases with multiple antennas at the receiver only, collectively called SIMO (Single-Input-Multiple-Output). We will include a short introduction to the cases containing multiple transmitter antennas also to visit MIMO systems.

The techniques employed to acquire high diversity gain in SIMO systems are based on the way the received signals are combined through different and independent channels. Combination methods include:

- Maximum Ratio Combination (MRC)
- Selective Combination (SC)
- Hybrid Combination (using both of the above)

Figure 1-8 illustrates MRC and SC systems in block diagrams picturing the basic concepts.

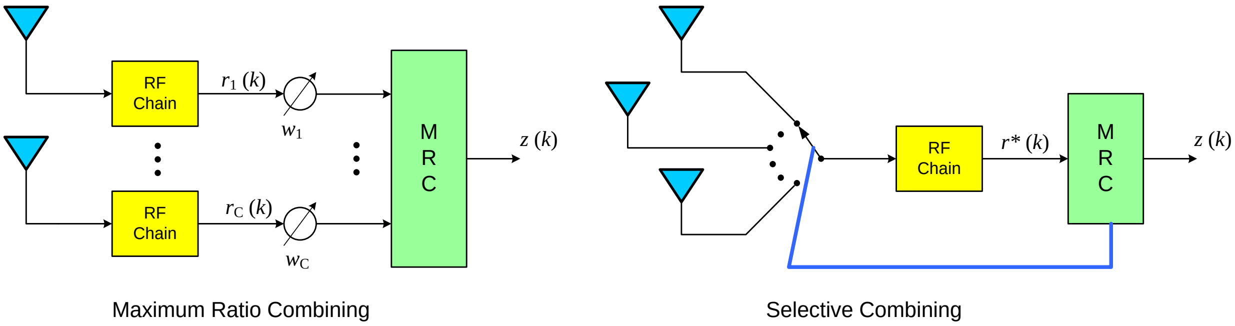

Figure 1-8 Basic diversity combination methods

Maximum Ratio Combination

When there are R independent paths, each having the same copy of the signal, the decision statistic is computed as the weighted sum of path signals:

$$z[k] = \sum_{j=1}^{R} w_j^* r_j[k] + n[k] \qquad (1\text{-}27)$$

where we denote by w_j^* the optimum combining weights, $r_j(k)$ are the received signals through each path at the k^{th} sample time, and $n(k)$ is the overall noise. Equation (1-27) incorporates an ML (Maximum Likelihood) decoder with coherent detection assumptions. If we assume that each path has equal SNR defined as the ratio of symbol energy and PSD of noise $\gamma_j = E_s/N_o$, the output SNR of the MRC system is given by:

$$\gamma_{MRC} = \sum_{j=1}^{R} \gamma_j \qquad (1\text{-}28)$$

Equation (1-28) indicates a possible R-times increase in SNR. In fact, the path SNRs are not equal, and one has to use the mean value $\mathbb{E}[\gamma_j]$ instead to get:

$$\gamma_{MRC} = R\,\mathbb{E}[\gamma_j] \qquad (1\text{-}29)$$

Selective Combination

MRC systems demand significant hardware for many Radio RF chains; SC is the design based on one single radio that picks the best received signal with respect to SNR of the channels. The selection can be realized, for example, by choosing one of the receiver antennas as the most efficient one. The diversity gain measured by SNR of the output signal has been determined, assuming Rayleigh fading and keeping other regular assumptions applied in derivation of Equation (1-29).

The average SNR in SC systems is computed as:

$$\bar{\gamma}_{SC} = \mathbb{E}[\gamma_j] \sum_{j=1}^{R} \frac{1}{j} \qquad (1\text{-}30)$$

The increase of $\sum_{j=1}^{R} \frac{1}{j}$ is the average of the output SNR that can be achieved (See Jake 1994).

Hybrid Combination

A mix of two combining methods results in a system shown in the block diagram of Figure 1-9.

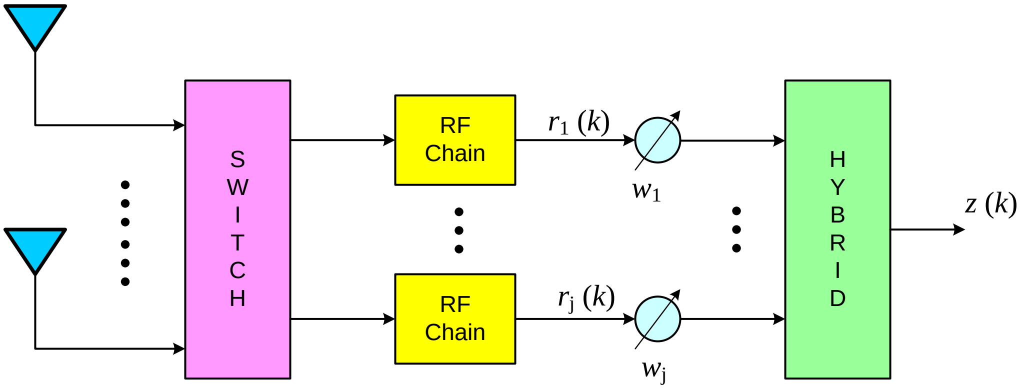

Figure 1-9 Hybrid diversity combination method

With similar assumptions, the average output SNR is computed by:

$$\bar{\gamma}_H = \mathbb{E}[\gamma_i]\, J \left[1 + \sum_{i=R-J}^{R} \frac{1}{i}\right] \qquad (1\text{-}31)$$

Spatial Multiplexing

In MIMO systems, diversity gain can be obtained by using multiple antennas at the transmitter and the receiver. These systems increase diversity and the capacity of the channels. If the number of the antennas at the transmitter is specified by T and the number of the antennas at the receiver by R, then the spatial multiplexing is possible by transmitting up to min $\{T, R\}$ symbols per time slot. The MIMO system's advantages can be used to increase the diversity to the highest spatial diversity of $T \times R$ or to increase the capacity by sending more symbols per time slot while maintaining the same level of diversity.

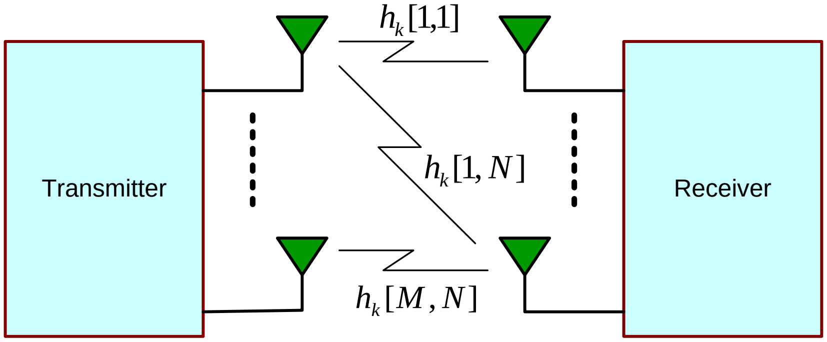

Figure 1-10 MIMO system basic configuration

A measure for spatial diversity gain has been defined as follows.

$$G_{SD} = \lim_{\gamma \to \infty} \frac{K}{\log \gamma} \qquad (1\text{-}32)$$

In Equation (1-32), K represents the code rate given in bits/s and is equal to the number of bits per symbol times the number of symbols spatially multiplexed per time slot.

In conclusion, we specify two major types of MIMO systems. The systems in which the transmitter has no information about the channel are called *open-loop* systems. However, the receiver may estimate the channel information for equalization and decoding. In many systems, the receiver shares the channel information acquired by estimation with the transmitter through a special feedback channel. This second type of system is known as *closed loop.* The channel information can be used by the transmitter in closed-loop systems to improve the overall performance.

1.7 References

[1] Biglieri, E., et al., “MIMO Wireless Communications”, Cambridge University Press, Cambridge, 2007.

[2] Clarke, R.H., “A Statistical Theory of Mobile-Radio Reception”, Bell System Technical Journal, Vol. 47, 1968.

[3] Durgin, G.D., Rappaport, T.S., de Wolf, D.A., “New Analytical Models and Probability Density Functions for Fading in Wireless Communications”, IEEE Trans. On Communications, Vol. 50, No. 6, 2002.

[4] Hanzo, L., et al., “OFDM and MC-COMA for Broadband Multi-user Communications”, *WLANs and Broadcasting”,* Wiley-Interscience/IEEE Press, New Jersey, 2003.

[5] Igbal, R., Abhayapala, J.D., Lamahewa, T.A., “Generalized Clarke Model for Mobile Radio Receptio”, IET Communications, Vol. 3, No. 4, 2008.

[6] Jakes, W.C., Editor, “Microwave Mobile Communications”, Wiley-Interscience/IEEE Press, 1994.

[7] Rappaport, T.S., “Wireless Communication, Principle and Practice”, 2nd Edition, Prentice-Hall, New Jersey, 2000.

[8] Sood, N., Sharma, A.K., Uddin, M., “BER Performance of OFDM-BPSK and –QPSK over Generalized Gamma Fading Channel”, International Journal of Computer Applications, Vol. 3, No. 6, June 2010.

[9] Tang, L., Hongbo, Z. “Analysis and Simulation of Nakagami Fading Channel with MATLAB”, Asia-Pacific Conference on Environmental Electromagnetics, CEEM, 2003.

[10] Yousef, N., Munakata, T., Takeda, M., “Fade Statistics in Nakagami Fading Environments”, IEEE Press, New Jersey, 1996.

Chapter 2: Adaptive Algorithms and Channel Equalization

2.1 Introduction

The application of adaptive algorithms is widespread among various scientific and engineering disciplines and has created an enormous amount of literature, both theoretical and applied. The common applications include topics such as system identification, channel equalization, adaptive control, adaptive filtering for signal processing, and pattern recognition. References [9] and [11] discuss numerous cases in medical and other scientific applications.

Rapid development of computer technology in the second half of the last century has generated a great deal of interest in the applications of iterative adaptive procedures that potentially lead to desired solutions in reasonable time.

Historically, Robbins and Monro (1951) introduced the basic concept of stochastic approximation. About the same time, Kiefer and Wolfowitz (1952) published a formal mathematical treatment of this new area of applied mathematics. The methodology can be further traced back to the work by Hotelling (1941) in “Experimental Determination of the Maximum of a Function”.

- *Stochastic approximation* is the general method by which the value of a vector, known as the *state* or *parameter* vector, is iteratively adjusted through a stochastic difference equation[2]:

  $$\boldsymbol{\theta}[k+1] = \boldsymbol{\theta}[k] + \mu \boldsymbol{Y}[k] \qquad (2\text{-}1)$$

  In the difference equation (also called the update equation) $\boldsymbol{\theta}[k]$ is the state vector at k^{th} step of the adaptation from which only an observation function $\boldsymbol{Y}[k]$ is available. The observation is usually contaminated by random noise. The *step size* or *learning rate* is denoted by μ and it can be a small positive value or it can decrease as the procedure progresses and might go to zero as

[2] We use bold characters to denote a vector, e.g., $\boldsymbol{w}$; the subscripts are used for vector indexing, e.g., w_i and time steps are denoted by [.], as in $\boldsymbol{w}[k]$.

$k \to \infty$. The process continues until some goal is met (or at least is asymptotically met). In most of the optimization cases, there is a scalar function denoted by $\mathcal{J}(.)$ called *objective* or *cost* function.

The common goal of recursive approximations is to find an optimum parameter vector $\boldsymbol{\theta}^*$ so that $\mathcal{J}(\boldsymbol{\theta}^*) = C$ (C is a known constant). For convenience and without loss of generality, one can try to minimize $\mathcal{J}(\boldsymbol{\theta})$; that is equivalent to maximizing $-\mathcal{J}(\boldsymbol{\theta})$.

Considering the target to be $\mathcal{J} = C$, the error at each step is given by $e[k] = C - \mathcal{J}(\boldsymbol{\theta}[k])$. The adjustment term in the update equation, $\mu\boldsymbol{Y}[k]$ must be proportional to the error $e[k]$ when the step size (or learning rate) μ can be kept as a small constant or decrease as the process gets closer to the desired solution $\boldsymbol{\theta}^*$.

Different algorithms that have been devised to preform stochastic approximations are diverse in the way the error in the update equation is computed. In some interesting problems, the objective function is not completely known (or is heavily corrupted by noise) and perhaps has to be estimated, perhaps in an iterative way.

- The *quantized parameters* or up-and-down method updates the parameter vector only by a constant-valued vector $\boldsymbol{d}$ that is not proportional to the error but aligns with its direction. The update equations are $\boldsymbol{\theta}[k+1] = \boldsymbol{\theta}[k] + \boldsymbol{d}$ or $\boldsymbol{\theta}[k+1] = \boldsymbol{\theta}[k] - \boldsymbol{d}$ at each step.

  The decision of which way (up or down) to go is based on some logical condition. This method simplifies the update operations in spite of the fact that in some experimental situations it is possible to change the parameter vector by only a fixed discrete amount. Quantized parameter algorithms have shown to be superior in the trade-off between computational simplicity and convergence speed. (See references [8] and [9] for examples.)
- The *Newton-Raphson* method, rooted in numerical analysis, strives for the same goal as other algorithms of stochastic approximation, namely to find the solution state or weight factor $\boldsymbol{\theta}^*$ for

the objective function to attain the desired value $\mathcal{J}(\boldsymbol{\theta}^{*}) = C$.

The update equation in this method includes the inverse of the objective function derivative with respect to the state vector, denoted by $\left[\frac{\partial \mathcal{J}(\boldsymbol{\theta})}{\partial \boldsymbol{\theta}}\right]^{-1}$, also known as inverse of the gradient vector.

$$\boldsymbol{\theta}[k+1] = \boldsymbol{\theta}[k] - \left[\frac{\partial \mathcal{J}(\boldsymbol{\theta}[k])}{\partial \boldsymbol{\theta}[k]}\right]^{-1} e[k] \qquad (2\text{-}2)$$

Similar to the case of finding roots of a function in numerical analysis, the inverse of the gradient, if it exists, substatially speeds up the convergence of the adaptation towards the solution.

- The *recursive least-squares* method has been characterized by superior performance in comparison to general stochastic approximation methods. The required computational cost of each iteration, however, is significantly higher as the covariance matrix of the target process is being used to accelerate the algorithm convergence.

  In fact, the inverse of the covariance matrix, denoted here by R_X^{-1} is used in the update equation ($x[k]$ denotes the discrete output of the target process for which covariance is being computed). R_X^{-1} is itself iteratively computed and updated at each step. Moreover, a constant parameter slightly less than unity, $\lambda < 1$, is often used as a *forgetting factor* that serves to reduce the dependence of the adaptation on extremely old observations.

There also are other adaptive algorithms applied to variety of problems including, but not limited to, *Quantized State* that can obtain increased convergence speed with reduced computation efforts, *simulated annealing* with interesting historical background (see chapter 5), *hidden Markov modeling*, and definitely the algorithms based on *neural networks* architecture.

Wasan (1969) has given important hints from Kushner quoted as: “Kushner has concluded that the least-squares method is superior to the stochastic approximation after discussing the efficiency of the two methods. The main advantage with the stochastic-approximation method is that one does not know about the input of the system, all one needs to know is the output which is easily available in practice. Furthermore, it is unnecessary to know the form of the regression function or to estimate unknown parameters. Thus, stochastic approximation is a non-parametric technique which quite often generates a non-Markov stochastic process."

Wasan continues on the main problems associated with stochastic approximation procedures:

"First, one will be interested in the convergence and mode of convergence of the sequence generated by the method to the desired solution of the equation. Secondly, one would like to know the asymptotic distribution of the sequence. Finally, since stochastic approximation is a sequential procedure, one will be interested to know an optimum stopping rule for a given situation."

Benveniste, et al., (1990) has asserted, "It would be foolish to try to present a general theory of adaptive systems which created a framework sufficiently broad to encompass all models and algorithms simultaneously. These problems have a major common component: namely, the use of adaptive algorithms. This topic, which we shall now study more specifically, is the counterpart of the notion of stochastic approximation as found in statistical literature."

The last quotation to some extent clarifies the relation between stochastic approximation and adaptive algorithms.

2.2 Channel Equalization

Dispersive channels with slow time-variation can be approximated by transversal (non-recursive) filters. It is also possible to approximate a recursive model by a relatively large transversal filter with controlled approximation error. As was mentioned, the Inter-Symbol-Interference (ISI) created by multiple channels is far more destructive compared to channel and/or receiver noise so that efforts are aimed at the goal of eliminating or at least mitigating the distortion caused by ISI. The distortion obviously begets some bit or symbol errors in digital communication systems.

In addition to the slow time-varying assumption, we assume that the Channel Impulse Response (CIR) is a real-valued function with compact support. As it was shown in Chapter 1, the real and imaginary components of the channel fading model are independent and hence can be equalized independently. This justifies the real-valued assumption. The CIRs corresponding to recursive channel models are infinite (hence the name Infinite Impulse Response, IIR). However, when they are also stable, their CIR decays in time and the truncation used to keep only a finite support of CIR is technically justified.

The models and approximations formed for multipath wireless channels are based on the equivalent *baseband* model of the communication system. The baseband equivalent assumption remains as the case for the rest of our discussion.

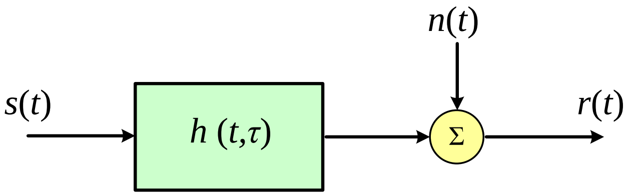

Figure 2-1 Continuous time channel method

In general, we start with a continuous-time channel and corresponding CIR denoted by $h(t,\tau)$ as shown in Figure 2-1 in which $n(t)$ represents channel noise. Let us denote the CIR compact support time or duration by T_c and the continuous-time symbol duration by T_s, then the received signal is determined by a convolution and additive noise:

$$r(t) = h(t) \circledast s(t) + n(t) = s(t) \circledast h(t) + n(t) \qquad (2\text{-}3)$$

$$r(t) = \int_{0}^{T_s} h(t-\tau)s(\tau)d\tau + n(t) = \int_{0}^{T_c} s(t-\tau)h(\tau)d\tau + n(t) \qquad (2\text{-}4)$$

The convolution is symbolized by $\circledast$ in the above equation. The time duration of the received signal is $T = T_c + T_s$. We can adjust our derivation for digital communication in which signals are appropriately sampled and the baseband equivalent system is assumed to generate signal samples at each sample time $t = kT_s$, where T_s is the sampling period. In digital communication systems the samples are taken at each symbol time (occasionally called baud rate or symbol rate systems) that is, the sampling period and the symbol time are equal. Consequently, the CIR can be written as a discrete-time impulse response $\boldsymbol{h} = \left(h_0, h_1, , \dots, h_{N_c-1}\right)^T,\ k = 0,1, \dots, N_C - 1$. It is noteworthy that there are two main assumptions about CIR, that it can be considered constant relative to equalization time (slow-varying), and causal (the matter of the choice for the time reference). Furthermore, the transmitted and received signals are shown in discrete-time by their samples at the k^{th} time step, $s[k] = s(kT_S)$ and $r[k] = r(kT_S)$.

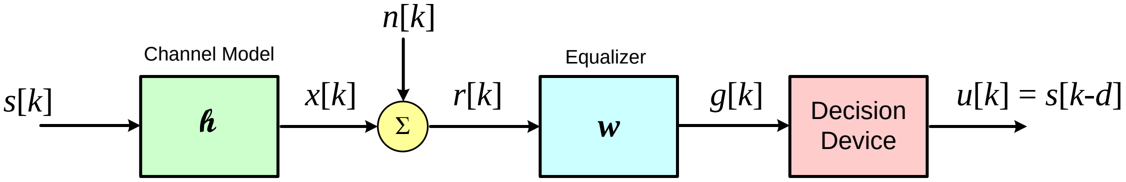

Figure 2-2 Discrete-time model of channel

The channel transfer function is consequently denoted by $H(z)$ that in general can be of Infinite Impulse Response (IIR) when the model is recursive and of Finite Impulse Response when the model is non-recursive. In either case, the discrete-time channel is approximated by a transversal filter with finite length N_C.

The ideal equalization, or channel inversion, is to estimate the weight vector of a transversal filter of finite length N_E denoted by $\boldsymbol{w}$ so that it approximately realizes the transfer function $W(z) \approx H^{-1}(z)$.

As was mentioned earlier, a perfect equalization requires a doubly-infinite equalizer. The ideal transfer function, or at least an approximation of it, is achieved when the weight or state vector of the equalizer attains some optimum value $\boldsymbol{w}^*$. This means that $W(\omega) \approx H^{-1}(\omega)$ when $H(\omega) = H(z)|_{z=\exp(i\omega)}$ and $W(\omega) = W(z)|_{z=\exp(i\omega)}$ are the frequency responses of the channel and the equalizer respectively. It is obvious that a non-minimum phase channel transfer function cannot be satisfactorily equalized with sufficient equalizer delay as its inverse is unstable. Even with the help of stable linear transversal equalizers, a successful inversion by any possible measure might be far from the desired response. Even the channel transfer functions with zeros near the unit circle demonstrate deep-nulls (very low values close to zero) in their frequency response and are hard to equalize. The *Zero-Forcing* equalizer can be computed for the minimum phase channels if its transfer function or equivalently CIR is known in the MS (Minimum Squares) sense (see Chi, et.al. (2006), pp. 188, Ding (2001), pp. 39):

$$W_{MS}(\omega) = \frac{\sigma_s^2 H^*(\omega)}{\sigma_s^2 |H(\omega)|^2 + \sigma_n^2}\,, \qquad -\pi \leq \omega \leq \pi \qquad \text{(2-5)}$$

In Equation (2-5), σ_s^2 represents the zero-mean input data variance that is also assumed to be WSS (Wide Sense Stationary), σ_n^2 is the variance of the zero-mean channel noise process that is independent of the input data. The channel should be stable.

The channel and the linear equalizer system functions $G_S(z)$ and $G_N(z)$; for the input signal and the channel noise can be expressed by:

$$G_S(z) = H(z)W(z),\ G_N(z) = W(z) \qquad \text{(2-6)}$$

In Equation (2-6) it has been assumed that the channel noise samples are *iid* and white. The ideal equalization can be symbolized by $H(z)W(z) = c_o z^{-d}$ for some positive integer delay d. In the time domain the equivalent of the channel (CIR) and the equalizer together is a convolution:

$$\boldsymbol{c} = \boldsymbol{\hbar} \circledast \boldsymbol{w} \qquad (2\text{-}7)$$

The result of the convolution in Equation (2-7) has $M = N_C + N_E$ components computed as:

$$c_k = \sum_{j=0}^{N_C} w_{k-j} h_j = \sum_{j=0}^{N_C} h_{k-j} w_j\,, \qquad k = 0, 1, \dots, M-1 \quad (2\text{-}8)$$

The time-domain equivalent of the ideal equalization is therefore given by the desired response $\boldsymbol{c} = c_o \delta_d$. It means that the effect of the channel and the equalizer together generates $c_k = 0$ for $k \neq d$ and $c_d = c_o$. The only non-zero component is also known as the *cursor*.

The ideal target of the inversion cannot be achieved with finite-length equalizer filters, so instead of seeking perfectly zero components, c_k has many non-zero but hopefully very small weights other than the main delayed weight or the cursor.

The operation of such inversion also has been known as s*eismic deconvolution* (see Clarckson (1993, pp. 112), Chi, et.al. (2006, pp.188)). In seismic deconvolution, an acoustic waveform called seismic wavelet is applied at a shot point using special transducers, and then propagated through the terrain sub-layers. The collected seismic traces are carefully aligned and recorded in seismograms. The seismograms are then processed in an offline mode to discover the sub-layer's structure. Seismic deconvolution is very similar to channel equalization in concept and provides a rich background of research literature. Kumar and Lau [31] have successfully applied the deconvolution technique to very important and commonly used Global Positioning Systems (GPS). Their work has been followed by other researchers in the GPS application that appeared in [29], [30].

The common algorithm in seismic application is Minimum Entropy Deconvolution (MED). The process is based on a new vector norm called *variamax* (see Wiggins (1977), Oldenburg (1981)), which was followed by Cabrelli's (1984) studies on a different norm he called *D-norm*. In fact, MED methods belong to the class of solutions that utilize Higher-Order Statistics (HOS) implicitly.

However since MED is performed offline (performed on recorded seismic waveform traces), it is different in nature from the real-time and adaptive methods.

Finally, similar to Equation (1-21), the common measure of equalization performance is called residual ISI, denoted here by ISI_R. Proakis (2001) has also applied what is called *Peak Distortion* as the worst-case residual ISI for the purpose of equalization quality measure.

2.3 Deconvolution of A-Priori Known Systems

This is a general problem pertaining to any system that can be modeled by a linear transversal filter having a tap-weight vector of finite length. The important point in this case is the fact that the system impulse response is known given by $\boldsymbol{\hbar}$. We seek the best (optimum in the sense of ISI_R reduction) equalizer weight vector $\boldsymbol{w}^*$ so that:

$$\boldsymbol{\hbar} \circledast \boldsymbol{w}^* = \boldsymbol{e}_d \qquad (2\text{-}9)$$

The vector $\boldsymbol{e}_d$ here represents d^{th} standard basis, that is:

$$\boldsymbol{e}_d = (0, 0, \dots 0, 1_d, 0, \dots 0)^T \qquad (2\text{-}10)$$

One can expect the main component or cursor value to be one as compared to c_o because the system impulse response is usually normalized to unit power, that is $\boldsymbol{\hbar} = \boldsymbol{\hbar}_o / \|\boldsymbol{\hbar}_o\|_2$ where $\boldsymbol{\hbar}_o$ represents the response before normalization.

A better formulation of the deconvolution problem can be obtained by the detailed expansion of Equation (2-9) as follows (assuming that $N_C > N_E$):

$$\begin{bmatrix} h_0 & 0 & 0 & . & . & . & 0 \\ h_1 & h_0 & 0 & . & . & . & 0 \\ h_2 & h_1 & h_0 & 0 & . & . & 0 \\ . & . & . & . & . & . & . \\ . & . & . & . & . & . & . \\ h_{N_E-1} & h_{N_E-2} & . & . & h_1 & h_0 & 0 \\ h_{N_E} & h_{N_E-1} & . & . & . & h_1 & h_0 \\ . & . & . & . & . & . & h_1 \\ 0 & . & . & . & . & . & . \\ 0 & 0 & . & . & . & h_{N_C-1} & h_{N_C-2} \\ 0 & 0 & 0 & . & . & 0 & h_{N_C-1} \end{bmatrix} \begin{bmatrix} w_0^* \\ w_1^* \\ . \\ . \\ . \\ . \\ . \\ w_{N_E-1}^* \end{bmatrix} = \begin{bmatrix} 0 \\ 0 \\ . \\ 0 \\ 1 \\ 0 \\ . \\ 0 \end{bmatrix} \qquad (2\text{-}11)$$

Let us denote the matrix in Equation (2-9) by $\boldsymbol{\mathcal{H}}$ (This matrix is often known as a *filtering matrix*). The filtering matrix has dimensions of $(N_C + N_E - 1) \times (N_E)$ that renders Equation (2-9) as an *over-determined* system of equations. The solution in Least Square (LS) sense is simply given by the *normal* equation, symbolically:

$$\boldsymbol{w}^* = (\boldsymbol{\mathcal{H}}^T\boldsymbol{\mathcal{H}})^{-1}\boldsymbol{\mathcal{H}}^T\boldsymbol{e}_d \qquad (2\text{-}12)$$

By inspecting Equation (2-11) for the filtering matrix, it is obvious that it has complete rank of N_E order and hence the matrix $\boldsymbol{\mathcal{H}}^T\boldsymbol{\mathcal{H}}$ of the size $N_E \times N_E$ is positive-definite and has complete rank, consequently $(\boldsymbol{\mathcal{H}}^T\boldsymbol{\mathcal{H}})^{-1}$ exists, and the normal equation in (2-12) has a solution (It is well-known in linear algebra that positive definite matrixes are invertible with positive-definite inverses).

Although the matrix inversion is computationally costly, for the case of knowing the impulse response it will be done once, and most likely, in an offline mode.

Efficient algorithms are available for numerical computation of the solution to the normal equations (see Golub (1996), pp. 237, 545) for numerical methods and analysis).

In most of the practical cases, the system is not a priori-known; in our case for wireless channels that means the CIR is not known.

2.4 Adaptive Algorithm for Equalization of A Priori-Unknown Channels

Although knowledge of the channel is necessary for reliable communication in most modern systems, this information is not a-priori known and has to be acquired usually by some recursive adaptation algorithm. One might try to discover, at the least, important channel characteristics by the application of an adaptive identification algorithm and subsequently apply one of the solutions for the equalizer filter if necessary.

A more efficient and direct approach is to search for the best possible equalizer weight vector adaptively, without identifying the channel in advance. The equalization algorithms for unknown channels are divided into the supervised mode in which a training or pilot sequence known by the receiver is transmitted. Training period apparently takes part of the available air time and bandwidth, and it might be very inefficient or even unfeasible in multi-user environments. In spite of wasting resources, supervised techniques are simple and have guaranteed success in convergence. Qureshi (1982, 1985) has provided excellent references and tutorials on supervised adaptive equalization. The general concept of supervised algorithms is depicted in Figure 2-3, in which a linear (transversal) equalizer filter is adaptively trained for best possible weight or state vector $\boldsymbol{w}^*$.

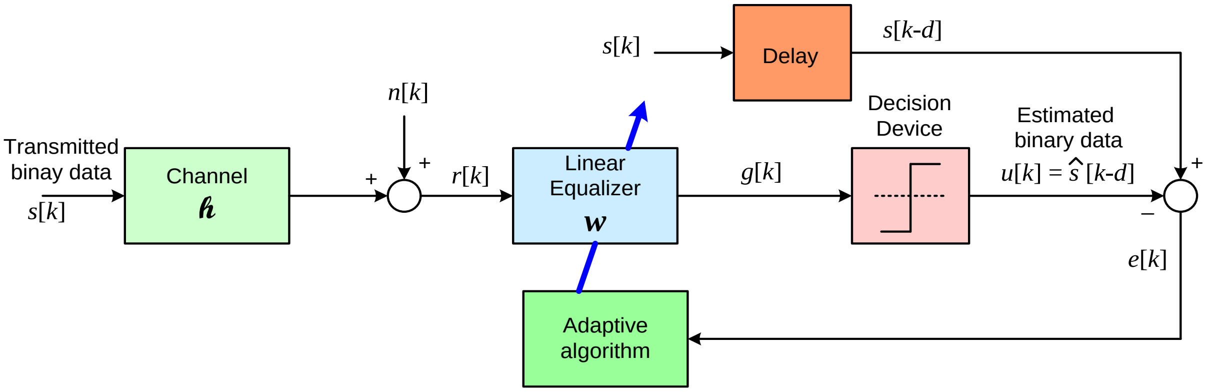

Figure 2-3 General diagram of supervised equalization system

Most cellular standards incorporate some kind of training signal. The training sequence in this case is used to estimate the CIR, then the inverse of the estimated CIR is determined in order to correct the distortion caused by ISI. Once the equalization is performed to attain a sufficiently low residual channel ISI, the receiver detected data replaces the training signal in the adaption process to correct for slow time-variation of the wireless multipath channel.

In blind equalization techniques, the channel equalization or estimation is based solelyon the received signal samples. It is also assumed that statistical properties of the input data to the channel are known and incorporated in the corresponding computations.

2.5 Blind Equalization Algorithms

There are several families of algorithms applied to the problem of blind (unsupervised) system identification or equalization. Here we concentrate on a large family of *Bussgang* algorithms. These algorithms implicitly use the Bussgang theorem stochastic processes. The theorem says (Papoulis (2002), pp. 397): “If the input to a memory-less possibly nonlinear system $y = f(x)$ is a zero-mean normal process $X(t)$, the cross-correlation of $X(t)$ with the resulting output $Y(t) = f\left(x(t)\right)$ is proportional to the input correlation, namely:

$$\mathbb{E}[X(t)X(t-\tau)] = K\mathbb{E}[X(t)Y(t-\tau)] \qquad \text{(2-13)}$$

where the constant is given by $K = \mathbb{E}\left[f^1\left(x(t)\right)\right]$.”

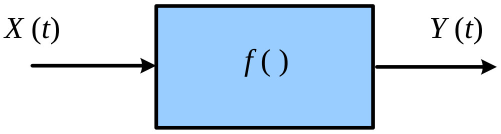

Figure 2-4 Bussgang Theorem

The Bussgang algorithms are named such since all of them use a non-linear (memory-less) function as a decision device to properly estimate the channel input data. In the case of binary data, the decision device is simply a slicer that is $u[k] = \mathrm{sgn}(x[k])$ where $\mathrm{sgn}(.)$ represents signum or sign function (see Figure 2-4). The estimated data is often used instead of any a-priori known training sequence.

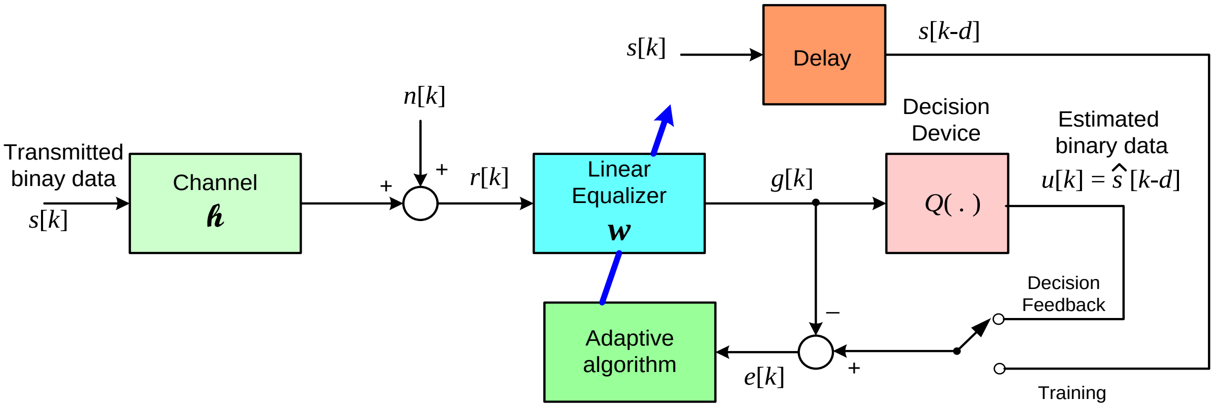

Figure 2-5 Basic linear equalization system

In Figure 2-5, a switch is available to change the mode of the algorithm from supervised (training) to blind mode, or the other way around. We continue to assume that channel variation in time is slow and, for the purpose of the following discussion, constant. The received signal samples are computed as follows:

$$r[k] = \sum_{j=0}^{N_C-1} h_j s[k-j] + n[k] \qquad (2\text{-}14)$$

$$r[k] = \boldsymbol{h}^T \boldsymbol{s}[k] + n[k] \qquad (2\text{-}15)$$

In Equation (2-15), $\boldsymbol{s}[k] = (s[k], s[k-1], \dots, s[k-N_C+1])^T$ is the vector of the input symbols, or data to the channel in the size of the CIR. The equalizer output can be similarly computed by the received signals:

$$g[k] = \sum_{j=0}^{N_C-1} w_j[k] r[k-j]\,. \qquad (2\text{-}16)$$

Or, in the short form:

$$g[k] = \boldsymbol{w}^T[k]\,\boldsymbol{r}[k] \qquad (2\text{-}17)$$

In Equation (2-15), $\boldsymbol{w}[k] = \left(w_0[k], w_1[k], \dots, w_{N_E-1}[k]\right)^T$represents linear equalizer weight vector at k$^{\text{th}}$ step of the adaptation, and $\boldsymbol{r}[k] = (r[k], r[k-1], \dots, r[k-N_E+1])^T$, the vector of the input signal samples with the size of the equalizer. Finally, the estimate of the binary data is determined by the slicer, that is:

$$u[k] = \hat{s}[k-d] = sgn(g[k]) \qquad (2\text{-}18)$$

Similar to any optimization problem, one needs to define an objective or cost function. The common Mean Square Error (MSE) objective function, which implicitly depends on the equalizer weight vector, is defined as follows:

$$\mathcal{J}(\boldsymbol{w}[k]) = \mathbb{E}\{e^2[k]\} = \mathbb{E}\{(s[k-d] - g[k])^2\} \qquad (2\text{-}19)$$

In the blind mode when the actual channel input is not available its estimate is used instead. This mode is called *decision-directed* mode.

$$\mathcal{J}(\boldsymbol{w}[k]) = \mathbb{E}\{(\hat{s}[k-d] - g[k])^2\} \qquad (2\text{-}20)$$

A class of equalizers starts the process in the training mode and switches to decision-directed mode after the channels are approximately equalized in order to track the small variation of the channel adaptively.

One important feature of blind methods in the Bussgang class is the relatively simple procedures. They can use the well-known Least Mean Squares (LMS) method that is probably the simplest technique among the recursive adaptation for optimization (Widrow, 1985).

The basic gradient method of LMS offers a simple update equation as follows:

$$\boldsymbol{w}[k+1] = \boldsymbol{w}[k] - \mu \boldsymbol{\nabla}[k] \qquad (2\text{-}21)$$

The step size or learning rate is denoted by μ in this equation. The gradient of the cost function is specified by $\frac{\partial \mathcal{J}}{\partial \boldsymbol{w}[k]} = \boldsymbol{\nabla}\mathcal{J}(\boldsymbol{w}[k])$, when the dependence on the equalizer weight vector is explicitly shown.

$$\boldsymbol{\nabla}\mathcal{J}(\boldsymbol{w}[k]) = \frac{\partial \mathcal{J}}{\partial \boldsymbol{w}[k]} = \frac{\partial}{\partial \boldsymbol{w}[k]} \mathbb{E}\{e^2[k]\} = \frac{\partial}{\partial \boldsymbol{w}[k]} \mathbb{E}\{(u[k] - g[k]^2\}$$

$$= \mathbb{E}\left\{\frac{\partial}{\partial \boldsymbol{w}[k]} (u[k] - g[k])^2\right\} \qquad (2\text{-}22)$$

The derivative of the error is computed as:

$$\frac{\partial}{\partial \boldsymbol{w}[k]} e[k] = \frac{\partial}{\partial \boldsymbol{w}[k]} (u[k] - g[k]) = \frac{\partial}{\partial \boldsymbol{w}[k]} u[k] - \frac{\partial}{\partial \boldsymbol{w}[k]} g[k] \qquad (2\text{-}23)$$

$$\frac{\partial}{\partial \boldsymbol{w}[k]} sgn(g[k]) = 2\delta[k] \qquad (2\text{-}24)$$

$$\frac{\partial}{\partial \boldsymbol{w}[k]} g[k] = \frac{\partial}{\partial \boldsymbol{w}[k]} (\boldsymbol{w}^T[k]\, \boldsymbol{r}[k]) = \boldsymbol{r}[k]. \qquad (2\text{-}25)$$

The result of Equation (2-24) is valid when $g[k]$ is extremely close to zero (this is unlikely as $g[k]$ has to be close to $+1$ or -1 when the equalizer has converged) and can be ignored. Consequently, the gradient of the objective function is given by:

$$\boldsymbol{\nabla}\mathcal{J}(\boldsymbol{w}[k]) = -2\mathbb{E}\{e[k]\boldsymbol{r}[k]\} = -2\mathbb{E}\{(u[k] - g[k])\boldsymbol{r}[k]\} = -2\mathbb{E}\{\hat{s}[k-d] - g[k])\boldsymbol{r}[k]\} \qquad (2\text{-}26)$$

The simplicity of the LMS technique lies in the fact that it takes the simplest possible estimate (and probably not quite accurate gradient by just removing the expectation operator. That is

$$\mathbb{E}\left\{\frac{\partial}{\partial \boldsymbol{w}[k]} e^2[k]\right\} \approx \frac{\partial}{\partial \boldsymbol{w}[k]} e^2[k] = -2e[k]\boldsymbol{r}[k]. \qquad (2\text{-}27)$$

Consequently, updating the equalizer weight vector simplifies to the following one (the coefficient 2 in (2-27) is absorbed in the step size μ:)

$$\boldsymbol{w}[k+1] = \boldsymbol{w}[k] - \mu \boldsymbol{\nabla} \mathcal{J}(\boldsymbol{w}[k]) = \boldsymbol{w}[k] + \mu e[k]\boldsymbol{r}[k] \qquad (2\text{-}28)$$

2.6 Bussgang Algorithms

We consider the overall channel and the equalizer system for which a transversal filter with finite number of taps is used as the linear equalizer in Figure 2-6.

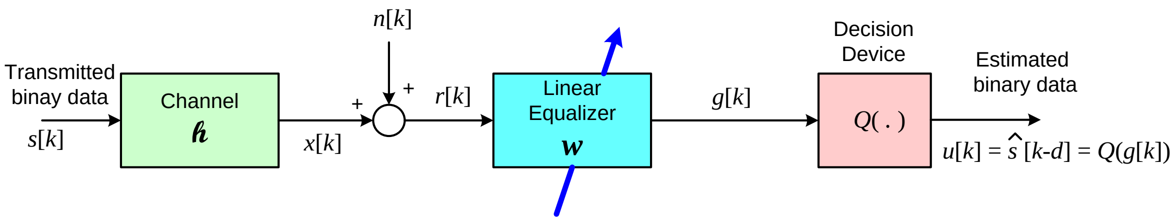

Figure 2-6 Basic equalization system

As was mentioned earlier, the channel noise sample $n[k]$ is relatively small compared to ISI measure and its effects are not considerable until most of ISI has been removed. Consequently, one may ignore the channel noise: that means $\tilde{r}[k] \approx r[k]$, where $\tilde{r}[k]$ is the noise-free signal at the receiver. Once again, we assume that the CIR (Channel Impulse Response) represents the transmitter filter, multipath channel, and the receiver filter together.

$$\tilde{r}[k] = \boldsymbol{h} \circledast \boldsymbol{s}[k] = \sum_{i=0}^{N_C-1} h[i]s[k-i] \approx r[k] \qquad (2-29)$$

$$\tilde{g}[k] = \boldsymbol{w}[k] \circledast \boldsymbol{r}[k] = \sum_{i=0}^{N_E-1} w_i[k]r[k-i] \approx g[k] \qquad (2-30)$$

In the above equations the subscript *k* indicates the vector values at the *k*-th step. The subscript *k* in the equalizer weight vector w_k could be dropped for convenience and be considered as implied when it simplifies the equations. Equation (2-30) can be expanded as

$$\tilde{g}[k] = \boldsymbol{w}[k] \circledast \boldsymbol{h} \circledast \boldsymbol{s}[k] = \sum_{j=0}^{N_E-1} w_j[k] \sum_{i=0}^{N_C-1} h[i]s[k-j-i] \qquad (2-31)$$

Let $\boldsymbol{w}^*$denote the best (optimal) weight vector of the linear equalizer. Equation (2-30) can be written including the optimum weight vector.

$$\tilde{g}[k] = \sum_{i=0}^{N_E-1} w_i[k]r[k-i] = \sum_{i=0}^{N_E-1} w_i^* r[k-i] + \sum_{i=0}^{N_E-1} (w_i[k] - w_i^*)r[k-i] \qquad (2-32)$$

The first term on the right-hand side in (2-32) is the optimum equalized signal representing the correct estimate of $s[k-d]$, the appropriately delayed input signal to the channel.

$$\sum_{i=0}^{N_E-1} w_i^* r[k-i] = c_o \hat{s}[k-d] \qquad (2-33)$$

The constant coefficient c_o in (2-33) is the cursor value (see Equation (2-7)). The second term in (2-32) is the undesired remainder and is known as *convolution error*.

$$I[k] = \sum_{i=0}^{N_E-1} (w_i[k] - w_i^*)r[k-i] = \sum_{i=0}^{N_E-1} e_i[k]r[k-i] \qquad (2-34)$$

The convolution error is approximated to be zero-mean, Gaussian, and independent of the input sequence $s[k]$ (See Nandi 1999).

The final block in Figure 2-5 in most of the implementations is a memoryless (zero-memory) nonlinear device, whose function is denoted by $Q(.)$. As will be discussed the choice of nonlinear function has a major impact on the performance of the algorithm to which it belongs. In the case of the system with binary input data we used a slicer ($sgn(.)$ Function) for the zero-memory nonlinearity.

Having explained the general setup for linear equalizers, we turn our attention to the Bussgang family of algorithms. Haykin (2002) and Ding, et.al. (2001) have provided great expositions of the general Bussgang algorithms as the foundation for most of the known techniques in linear equalization. Let us reconsider the effect of the channel and the equalizer together by their convolution denoted by $\boldsymbol{c}[k] = \boldsymbol{h} \circledast \boldsymbol{w}[k]$:

$$c_i[k] = \sum_{j=0}^{N_C-1} h_j w_{i-j}[k], \qquad i = 0, 1, 2, \dots M-1 \quad (2-35)$$

$$\tilde{g}[k] = \sum_{j=0}^{M-1} c_j[k] s[k-j] = c_d[k] s[k-d] + I[k], \qquad M = N_E + N_C \quad (2-36)$$

In (2-7) and (2-33) we have denoted the cursor value after the algorithm has converged by $c_k[d] = c_o$ and then the convolution error is as follows:

$$I[k] = \sum_{\substack{j=0, \\ j \neq d}}^{M-1} c_j[k] s[k-j]. \qquad (2-37)$$

Equation (2-37) is just a reformulation of (2-34) in terms of the convolution samples $c_j[k]$.

When the equalizer has converged to the final point, Equation (2-36) should become $\tilde{g}[k] = c_o s[k-d] + I[k]$ with the minimum possible value for the convolution error. When the distribution (pdf) of $I[k]$ is known the decision device is a Maximum A-Posteriori (MAP) estimator as defined in the following equation.

$$\hat{s}[k-d]_{MAP} = \underset{s}{\operatorname{argmax}} P_{g[k]|s[k-d]}(g[k]|s) \qquad (2-38)$$

When the distribution of $I[k]$ is not available, in particular the conditional probability in (2-38) is not known, the same approximations are made based on the assumptions that the input sequence $s[k]$ is zero-mean iid. Consequently the $c_j[k]s[k-j]$ terms in $I[k]$ (Equation 2-38) are independent and have finite variance so that the application of the central limit theorem implies that the $I[k]$ distribution is approximately Gaussian and is independent of $s[k-d]$. The $I[k]$ process is also assumed to be zero-mean and its variance can be computed with the knowledge of the variance of the input data sequence (namely σ_s^2) as follows.

$$\sigma_I^2 = \sigma_s^2 \sum_{j=0}^{M-1} \left|c_j[k]\right|^2 \qquad (2-39)$$

By considering $I[k]$ as the equalizer output noise with the variance given by (2-39), the optimum memoryless nonlinearity in the sense of MAP will be the minimum variance estimation as in Equation (2-40) (see Ding (2001), pp. 48):

$$Q(g[k]) = \hat{s}[k-d]_{MAP} = \mathbb{E}\{s[k-d]|g[k]\}. \qquad (2-40)$$

The signal-to-noise ratio at the output of the equalizer can now be computed easily by:

$$\frac{c_o^2 \mathbb{E}\{|s[k]|^2\}}{\sigma_I^2}. \qquad (2-41)$$

$\mathbb{E}\{|s[k]|^2\}$ in (2-41) represents the input sequence power. The information in Equation (2-41) must be known in order to find the nonlinearity function $Q(.)$ and when such information is not available or difficult to estimate, the Bussgang algorithms are no longer optimum (for detailed ZNL determination see Ding (2001), pp. 49). Finally when the nonlinearity has been determined, one can iteratively solve for the equalizer weights in the *Least Squares* (LS) sense using the following update equation:

$$\boldsymbol{w}[k+1] = (\mathbb{E}\{\boldsymbol{r}[k]\boldsymbol{r}^T[k]\})^{-1}\mathbb{E}\{\boldsymbol{r}[k]Q(\boldsymbol{r}^T[k].\boldsymbol{w}[k])\} \qquad (2-42)$$

The simple and popular adaptive method is the *gradient descent* algorithm that can be employed for finding the optimal weight vector with the following update equation.

$$\boldsymbol{w}[k+1] = \boldsymbol{w}[k] + \mu(Q(g[k]) - g[k])\boldsymbol{r}[k] \qquad (2-43)$$

In the recursive methods of Equations (2-42) and (2-43) $\boldsymbol{r}_k$ is assumed to be the noise-free signal at the receiver.

It has been shown that when the equalizer is converged, the output satisfies the Bussgang condition

$$\mathbb{E}\{g[k]g[k-\ell]\} = \mathbb{E}\{g[k]Q(g[k-\ell])\}, \forall \ell. \qquad (2-44)$$

A final point to be made is that the convergence of the Bussgang algorithm is mostly unknown. Godfrey (1981) has proved the local convergence of the Bussgang algorithms.

Almost all of the linear equalization techniques that we review in this section are based on the same basic concept except for the choice of zero-memory nonlinearity device. They are similar in the use of gradient descent and LMS (Least Mean Square) algorithm for their iterative adaptation process.

The Sato Algorithm

The Sato algorithm is perhaps the simplest technique used for the problem of blind equalization and was introduced early in the rich research history. It is also among the algorithms categorized as Decision-Directed Equalizers (see Figure 2-7.)

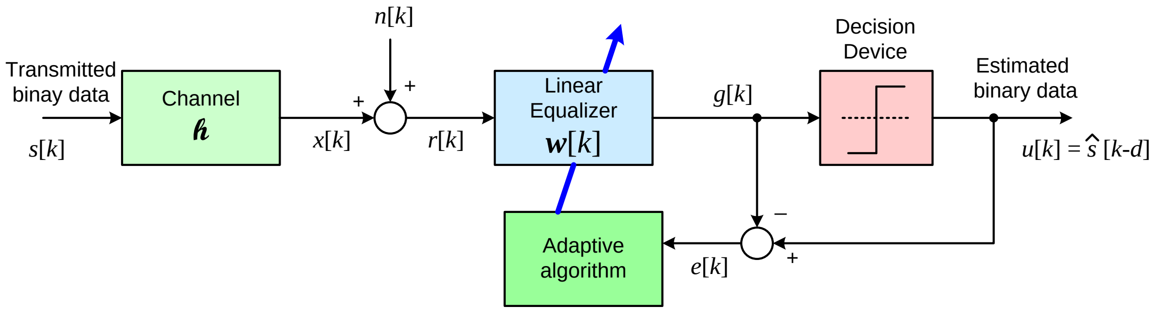

Figure 2-7 Basic Decision Feedback Equalizer diagram

This algorithm and some improved versions of it that are mentioned here are appropriate for PAM (Pulse Amplitude Modulation), including the simple binary case (2-PAM) for which the nonlinearity is simply $Q(.) = sgn(.)$. The cost function that was chosen by Sato without any theoretical justification was:

$$\mathcal{J}(\boldsymbol{w}[k]) = \mathbb{E}\left\{\left(g[k] - \gamma_1 sgn(g[k])\right)^2\right\} \qquad (2-45)$$

The important parameter in (2-45) is the choice of γ_1 that is given in Equation (2-47). The update equation, based on gradient descent method will therefore be given by the following equation:

$$\boldsymbol{w}[k+1] = \boldsymbol{w}[k] - \mu\left(g[k] - \gamma_1 sgn(g[k])\right)\boldsymbol{r}[k] \qquad (2-46)$$

In the update equation the coefficient of ½ of the gradient is absorbed in the step size μ. The Sato choice for γ_1 was intuitively selected as:

$$\gamma_1 = \frac{\mathbb{E}\{|s[k]|^2\}}{\mathbb{E}\{|s[k]|\}}. \qquad (2-47)$$

The only information necessary for this choice is the input data statistics that are assumed to be known in advance. The Sato algorithm can be compared to the simple LMS algorithm:

$$\boldsymbol{w}[k+1] = \boldsymbol{w}[k] - \mu(g[k] - \hat{s}[k-d])\boldsymbol{r}[k] \qquad (2-48)$$

where the delayed input estimate is determined as $\hat{s}[k-d] = sgn(g[k])$. Consequently, the only difference is that $\gamma_1 = 1$ in the LMS algorithm. In fact, the success (convergence) of the Sato algorithm has been attributed to the choice of γ_1. Hence, it is clear that the convergence of the Sato algorithm depends on the probability of the event when the sign of the real error $g[k] - s[k-d]$ and its estimate $g[k] - \gamma_1 sgn(g[k])$ agree. Sato's method was intended for one-dimensional multi-level PAM, in particular for the case of binary 2-level signaling. The Benveniste-Goursat-Ruget theorem for convergence (Haykin (2002), pp 716, 717) with the assumption of doubly-infinite filter size applies to Sato's method. The theorem states that the global convergence of the Sato can be gained for the input distributions of continuous non-Gaussian or sub-Gaussian in particular uniformly distributed input sequences. Macchi (1985) and Mazo (1980) have shown that the Sato algorithm converges to local minima for QAM (Quadratic Amplitude Modulation) input signals instead of the optimum global minimum. Moreover, Ding, et.al. (1989) have shown the possible convergence to any local minima for multi-level signaling as well.

The Godard Algorithm

Godard (1980) proposed a family of Constant-Modulus Algorithms (CMA) for blind equalization in general M-ary QAM systems. The QAM systems are collectively known as two-dimensional digital communications. The main idea is to use a cost function that depends only on the magnitude of the equalizer output, that is to say that the cost function is independent of the equalizer output phase. The *p*-th order cost function (where *p* is a positive integer) is defined by:

$$\mathcal{J}(\boldsymbol{w}[k]) = \frac{1}{p}\mathbb{E}\left\{\left(|g[k]|^p - \gamma_p\right)^2\right\}. \qquad (2-49)$$

The new Godard parameter γ_p is a positive and real constant.

$$\gamma_p = \frac{\mathbb{E}\{|g[k]|^{2p}\}}{\mathbb{E}\{|g[k]|^p\}} \qquad (2-50)$$

It seems that the unavailable input sequence $s[k]$ in the error samples is replaced by the constant γ_p, which contains the information about the input data distribution. In other words, the Godard algorithm is designed to measure the deviation of the equalizer output $g[k]$ from a constant modulus γ_p and use it for adaption.

The error signal for the general *p*-th order is given by

$$e[k] = \left(|g[k]|^p - \gamma_p\right)|g[k]|^{p-2}g[k]. \qquad (2-51)$$

The corresponding update equation will be written as

$$\boldsymbol{w}[k+1] = \boldsymbol{w}[k] - \mu e[k]\boldsymbol{r}[k]. \qquad (2-52)$$

In the case of $p = 1$, the cost function reduces to one that can be considered as a modified Sato algorithm.

$$\mathcal{J}(\boldsymbol{w}[k]) = \mathbb{E}\{(|g[k]| - \gamma_1)\}, \qquad \gamma_1 = \frac{\mathbb{E}\{|g[k]|^2\}}{\mathbb{E}\{|g[k]|\}} \qquad (2-53)$$

The cost function for the case of $p = 2$ is CMA (Constant-Modulus Algorithm), which is well-known in the literature. Equation (2-54) is the corresponding cost function and the modulus parameter for this important case:

$$\mathcal{J}(\boldsymbol{w}[k]) = \mathbb{E}\{(|g[k]|^2 - \gamma_2)\}, \qquad \gamma_2 = \frac{\mathbb{E}\{|g[k]|^4\}}{\mathbb{E}\{|g[k]|^2\}} \qquad (2-54)$$

The CMA algorithm is intended for systems in which the symbols have the same amplitude (constant) with different phases in the corresponding constellation of the QAM system and cannot be used for multi-level PAM cases. In conclusion, we remark that the Godard algorithm performs better than the other Bussgang algorithms in the MSE sense. The algorithm can equalize a dispersive channel even when the eye (of eye-pattern) is not initially open (Haykin (2002), pp 724).

Many researchers have challenged the problem of blind equalization or of the system identification, and their effects have culminated in many algorithms, each with some advantages. Of these algorithms, many belong to the family of Bussgang algorithms in which the zero-memory nonlinearity has the Bussgang property.

BGR (Benveniste-Goursat-Ruget) is an extension to the Sato algorithm with the goal of pushing the start-up adaptation from the local (that is near) of the optimal tap weights (it was mentioned that the Sato algorithm has sure convergence when the initial weights are close to the global optimum point.)

Stop-and-Go algorithm by Picchi and Prati (1987) basically implements the same adaptation as Sato's and the following technique except that the adaptation at each iteration can be skipped (no change to the state vector) based on the examination of some condition that flags possible incorrect estimates. This, for instance, can be done by comparing the sign of two different errors each belonging to a different algorithm of this family.

2.7 References

[1] Benveniste, A., Goursat, M., Ruget, G., “Robust Identification of Nonminimum Phase Systems: Blind Adjustment of Linear Equalizer in data Communications”, IEEE Transactions on Automatic Control, Vol. AC-25, No. 3, 1980.

[2] Bussgang, J.J., “Cross-correlation function of amplitude distorted Gaussian signals”, Tech. Rep. 216, MIT, 1992.

[3] Cabrelli, C.A., “Minimum Entropy Deconvolution and Simplicity: A Noniterative Algorithm”, geophysics, Vol. 50, No. 3, March 1984.

[4] Chi, et.al., “Blind Equalization and System Identification”, Springer-Verlag, London, 2006.

[5] Ding, Z., Li, Y., “Blind Equalization and Identification”, Marcel Dekker, 2001.

[6] Diniz, P.S.R., “Adaptive Filtering Algorithms and Practical Implementation”, Springer, New York, 2010.

[7] Friedman, M., Savage, L.J., “Experimental determination of the maximum of a function”, Selected Techniques of Statistical Analysis, McGraw-Hill, New York, 1947.

[8] Freidman, S. “On stochastic approximation”, Ann. Math. Stat. 34, 1963.

[9] Godfrey, R., Rocca, F., “Zero-memory nonlinear deconvolution”, geophysical Prospecting, No. 29, 1981.

[10] Godard, D.N., “Self-Recovering Equalization and Carrier Tracking in Two-Dimensional Data Communication Systems”, IEEE Transactions on Communications, Vol. COM-28, No. 11, November 1980.

[11] Haykin, S., “Adaptive Filtering Theory”, 4th Edition, Prentice-Hall, New Jersey, 2002.

[12] Hotelling, H., “Experimental determination of the maximum of a function”, Ann. Math. Stat. 12, 1941.

[13] Kiefer, J., Wolfowitz, J., “Stochastic estimation of the maximum of a regression function”, Ann. Math. Stat. 23, 1952.

[14] Kumar, R., Moore, J.B., “Adaptive Equalization via Fast Quantized State Method”, IEEE Transactions on Communications, Vol. COM-29, No. 10, October 1981.

[15] Kumar, R., Moore, J.B., “State Inverse and Decorrelated State Stochastic Approximating”, Automatica, Vol. 16, may 1980.

[16] Kushner, H.J., “Adaptive technique for the optimization of binary detection systems”, 22G-2 Lincoln Laboratories, MIT 1962.

[17] Kushner H.J., Yin, G.G., “Stochastic Approximation and Recursive Algorithms and Application”’ 2nd Edition, Springer-Verlag, New York, 2010.

[18] Macchi, O., Eweda, E., “Convergence Analysis of Self-Adaptive Equalizers”, IEEE Transaction on Information Theory”, Vol. IT-30, No. 2, March 1984.

[19] Mazo, J.E., “Analysis of decision-directed convergence”, Bell Systems Tech., Vol. 59, pp. 1857-1876.

[20] Nandi, A.K., “Blind Estimation using Higer-Order Statistics”, Kluwer, 1999.

[21] Oldenburg, D.W., Levy, S., Whittall, K.P., “wavelet Estimation and Deconvolution”, Geophysics, Vol. 46, No. 11, Nov. 1981.

[22] Papoulis, A., Unnikrishna Pillai, S., “Probability, random Variables, and Stochastic Processes”, McGraw-Hill Higher Education, 2002.

[23] Picchi, G., Prati, G., “Blind Equalization and carrier Recovery using a “Stop-And-Go” Decision-Directed Algorithm”, IEEE Trans. on Comm., Vol. COM-25, No. 99, Sept. 1987.

[24] Proakis, J.G., “Digital Communications”, 4th Edition, McGraw-Hill Higher Education, 2001.

[25] Robbins, H., Monro, S., “A Stochastic approximation method”’ Ann. Math. Stat. 22 (1951).

[26] Wasan, M.T., “Stochastic Approximation”’ Cambridge University Press, Cambridge, 1969.

[27] Widrow, B., Stearns, S.D., “Adaptive Signal Processing”, Prentice-Hall, New Jersey, 1985.

[28] Wiggins, R.A., “Minimum Entropy Deconvolution”, Geoexploration, Vol. 16, 1978.

Additional References:

[29] Dragunas, K., Borre K, “Multipath Mitigation Based on Deconvolution,” Journal of Global Positioning Systems, Vol. 10, No. 1, 2011.

[30] Dragunas, K., Borre K, “Indoor Multipath Mitigation,” Ubiquitous Positioning Indoor Navigation and Location Based Services (UPINLBS), 2010, pp. 1-8.

[31] Kumar, R., Lau, K., “Deconvolution Approach to Carrier and Code Multipath Error Elimination in High Precision GPS,” Proceedings of the 1996 National Technical Meeting of the Institute of Navigation, Santa Monica, CA., pp. 729-737,.

Chapter 3: Blind Channel Equalization using Diversified Algorithms

3.1 Introduction

Blind techniques in wireless channel equalization are diversified and abundant; nonetheless, a robust and fast convergent technique with reasonably efficient computations remains as an open problem. We have briefly reviewed most of these techniques but not all of them in Chapter 2. In particular Fractionally-Spaced Equalization (FSE) and the algorithms using Higher Order Statistics (HOS) were not visited. The reason of such negligence is the fact that various techniques of FSE and HOS are computationally costly and our target systems with multiple algorithms need to employ relatively simple methods to keep overall computational cost of the system affordable. Our new conception in the blind or unsupervised equalization is to employ two or more of the simple algorithms in a cooperative scheme[3] to increase the probability of convergence of the overall system comprising multiple of algorithms. Figure 3-1 shows the proposed arrangement that includes three separate equalizers generating and sharing one final estimate of binary data.

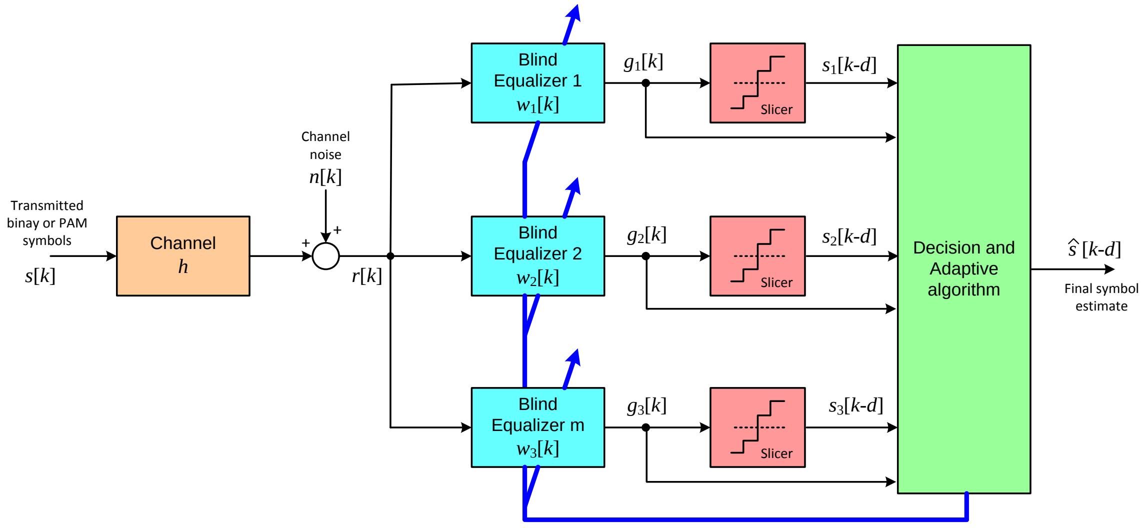

Figure 3-1 Blind equalizer system with diversified algorithms

[3] The multiple algorithm architecture for adaptive signal processing was invented by Dr Rajendra Kumar, and is in the process of being patented. Here the performance analysis of one of the various possible forms of this architecture for the blind mode equalizer is presented.

3.2 Recursive Least Squares Adaptive Algorithms

In this section we give a brief introduction to a family of algorithms known as Recursive Least Squares (RLS). RLS algorithms incorporate the inverse of the covariance matrix of the process (wireless channel in our case) in the update equation that resembles the Wiener optimum filter solution, or Newton-like algorithms in adaptive techniques. Its final performance measures are often poor as we will explore in sections 3.4 and 3.5 of this chapter. RLS techniques and the resulting ramifications are well-known and long lasting. The references [1, 3, and 6] give comprehensive origin and proofs of the methods. A closely-related application of RLS in the area of digital communications is given in [2].

Consider the problem of iteratively adjusting the weight vector of a transversal filter used to equalize a wireless channel. Figure 3-2 depicts a general system setup in which the received signals are generated by a process that could be the unknown wireless communication channel.

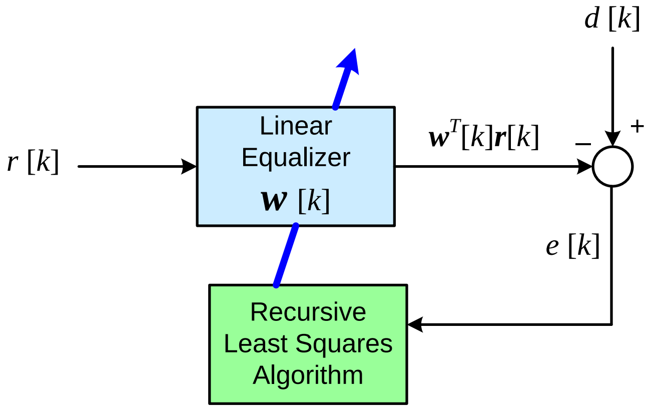
$d\,[k]$
Linear Equalizer
$\boldsymbol{w}\,[k]$
$r\,[k]$
$\boldsymbol{w}^T[k]\boldsymbol{r}[k]$
$-$
$+$
$e\,[k]$
Recursive Least Squares Algorithm

Figure 3-2 General Recursive Least Squares algorithm

The inputs to the transversal filter are collected in a vector of the size of the filter S denoted by $\boldsymbol{r}[k] = (r[k], r[k-1], \dots, r[k-S+1])^T$. We have used exactly the same vector as the baseband samples of the received signals input to the channel equalizer in Chapter 2.

An approximate estimate of the auto-covariance matrix of the process generating the input vector $\boldsymbol{r}[k]$ at step k is computed by

$$\boldsymbol{R}_k = \frac{1}{k}\sum_{i=1}^{k} \boldsymbol{r}[k]\boldsymbol{r}^T[k]. \qquad (3-1)$$

The computation of the running estimate of $\boldsymbol{R}_{k+1}$ is simplified, commonly as follows.

$$\boldsymbol{R}_{k+1} = \left(\frac{k}{k+1}\right)\boldsymbol{R}_k + \left(\frac{1}{k+1}\right)\boldsymbol{r}[k+1]\boldsymbol{r}^T[k+1] \qquad (3-2)$$

The basic weight vector update equation for the RLS type of algorithm includes the inverse of the covariance matrix. This equation for advancing to the next step from step k can be written as:

$$\boldsymbol{w}_{k+1} = \boldsymbol{w}_k + \mu e[k]\boldsymbol{R}_k^{-1}\boldsymbol{r}[k]. \qquad (3-3)$$

In Equation (3-3), μ is the step size and in common RLS implementations is usually equal to one, and the error is computed as the difference of the desired output $d[k]$ and the filter output.

$$e[k] = d[k] - \boldsymbol{w}^T[k]\boldsymbol{r}[k] \qquad (3-4)$$

The inverse covariance matrix required for the weight vector update equation needs to be updated in each step using the running update Equation (3-2).

$$\boldsymbol{R}_{k+1}^{-1} = (\boldsymbol{R}_k + \boldsymbol{r}[k+1]\boldsymbol{r}^T[k+1])^{-1} \qquad (3-5)$$

To avoid costly matrix inversion at each step of adaptation the famous Woodbury's matrix inversion identity is used to obtain

$$\boldsymbol{R}_{k+1}^{-1} = \boldsymbol{R}_k^{-1} - \frac{\boldsymbol{R}_k^{-1}\boldsymbol{r}[k+1]\boldsymbol{r}^T[k+1]\boldsymbol{R}_k^{-1}}{1 + \boldsymbol{r}^T[k+1]\boldsymbol{R}_k^{-1}\boldsymbol{r}[k+1]}. \qquad (3-6)$$

For simplicity the inverse matrix is denoted by $\boldsymbol{Q}_k = \boldsymbol{R}_k^{-1}$ and the last equation simplifies to the following.

$$\boldsymbol{Q}_{k+1} = \boldsymbol{Q}_k - \frac{\boldsymbol{Q}_k \boldsymbol{r}[k+1]\boldsymbol{r}^T[k+1]\boldsymbol{Q}_k}{1 + \boldsymbol{r}^T[k+1]\boldsymbol{Q}_k \boldsymbol{r}[k+1]} \qquad (3-7)$$

The update equation becomes

$$\boldsymbol{w}_{k+1} = \boldsymbol{w}_k + \mu e[k]\boldsymbol{Q}_k \boldsymbol{r}[k]. \qquad (3-8)$$

It has been recommended (See Clarkson [1]) to initialize the weight vector to a zero vector $\boldsymbol{w}_0 = \boldsymbol{0}$ and the inverse covariance matrix to a large diagonal matrix $\boldsymbol{Q}_o = \delta^{-1}\boldsymbol{I}$ where δ is a small constant .

Exponentially Weighted Recursive Least Squares

A popular variation of the RLS algorithm is the Exponentially Weighted version (EWRLS) in which a forgetting factor usually close to one is used to reduce the effects of relatively old received information. Specifically in the channels that are modeled by limited-size transversal filters the correlation between the recently received signals and the ones belonging to many steps backward is trivial if not zero, hence the application of forgetting factors in Exponentially Weighted RLS of the range of $\lambda = 0.99$ to $\lambda = 0.999$ has been shown to have favorable results, in particular n case of time-varying channels. The EWRLS algorithm equations incorporating the forgetting factor λ are similar to those for regular RLS and are summarized in the following ($\boldsymbol{Q}_k = \boldsymbol{R}_k^{-1}$).

$$\boldsymbol{R}_{k+1} = \lambda \boldsymbol{R}_k + \boldsymbol{r}[k+1]\boldsymbol{r}^T[k+1] \qquad (3-9)$$

$$\boldsymbol{Q}_{k+1}^{-1} = \lambda \boldsymbol{Q}_k^{-1} + \boldsymbol{r}[k+1]\boldsymbol{r}^T[k+1] \qquad (3-10)$$

$$\boldsymbol{Q}_{k+1} = \frac{1}{\lambda}\left(\boldsymbol{Q}_k - \frac{\boldsymbol{Q}_k \boldsymbol{r}[k+1]\boldsymbol{r}^T[k+1]\boldsymbol{Q}_k}{\lambda + \boldsymbol{r}^T[k+1]\boldsymbol{Q}_k \boldsymbol{r}[k+1]}\right) \qquad (3-11)$$

$$\boldsymbol{w}_{k+1} = \boldsymbol{w}_k + \mu e[k]\boldsymbol{Q}_{k+1}\boldsymbol{r}[k]. \qquad (3-12)$$

Quantized-State Recursive Least Squares

Kumar and Moore in their 1981 paper [4] proposed four different algorithms that are similar in structure as the RLS algorithms to simplify the computational effort and speed up the convergence. These Quantized-State (QS) algorithms have been successfully applied to some problems ever since (for example see Kumar and Khor [5]).

The first two of the QS algorithms are based on a sliced version of the input signal vector $\hat{\boldsymbol{r}}[k]$, in which each element is determined by $\hat{r}_j[k] = sgn\big(r_j[k]\big)$. Consequently all elements of the input vector (also known as state) belong to the binary field of $\{+1, -1\}$, and together as a vector they are called the quantized state. The differences between the two proposed Quantized-State algorithms are easily seen in the following summary of the sets of recursive equations.

Quantized-State 1 (QS-1):

$$\boldsymbol{Q}_{k+1}^{-1} = \lambda\boldsymbol{Q}_k^{-1} + \boldsymbol{r}[k+1]\boldsymbol{r}^T[k+1]\,,\ \boldsymbol{Q}_k = \boldsymbol{R}_k^{-1} \qquad (3-13)$$

$$\boldsymbol{Q}_{k+1} = \frac{1}{\lambda}\left(\boldsymbol{Q}_k - \frac{\boldsymbol{Q}_k\hat{\boldsymbol{r}}[k+1]\boldsymbol{r}^T[k+1]\boldsymbol{Q}_k}{\lambda + \hat{\boldsymbol{r}}^T[k+1]\boldsymbol{Q}_k\boldsymbol{r}[k+1]}\right) \qquad (3-14)$$

$$\boldsymbol{w}_{k+1} = \boldsymbol{w}_k + \mu e[k]\boldsymbol{Q}_{k+1}\hat{\boldsymbol{r}}[k]. \qquad (3-15)$$

Quantized-State 2 (QS-2):

$$\boldsymbol{Q}_{k+1}^{-1} = \lambda\boldsymbol{Q}_k^{-1} + \hat{\boldsymbol{r}}[k+1]\hat{\boldsymbol{r}}^T[k+1]\,,\ \boldsymbol{Q}_k = \boldsymbol{R}_k^{-1} \qquad (3-16)$$

$$\boldsymbol{Q}_{k+1} = \frac{1}{\lambda}\left(\boldsymbol{Q}_k - \frac{\boldsymbol{Q}_k\hat{\boldsymbol{r}}[k+1]\hat{\boldsymbol{r}}^T[k+1]\boldsymbol{Q}_k}{\lambda + \hat{\boldsymbol{r}}^T[k+1]\boldsymbol{Q}_k\hat{\boldsymbol{r}}[k+1]}\right) \qquad (3-17)$$

$$\boldsymbol{w}_{k+1} = \boldsymbol{w}_k + \mu e[k]\boldsymbol{Q}_{k+1}\hat{\boldsymbol{r}}[k]. \qquad (3-18)$$

In all of the above equations the error at k^{th} step is $e[k] = d[k] - \boldsymbol{w}^T[k]\boldsymbol{r}[k]$. It should be clarified that the learning rate μ in QS algorithms has different effect and purpose compared to the LMS, and RLS algorithms. The learning rate or as often called step size in the LMS algorithm determines the stability (see Widrow [7] or [8]).

It is well-known that for stationary processes the covariance matrix is symmetric and Toeplitz. The inverse of the covariance matrix however is symmetric but not completely Toeplitz. Kumar and Moore have used this fact to further speed up the required computation. This method leads to another two algorithms in their paper [4] that are not being applied in this chapter.

The concentration of this chapter is not to evaluate the performance of the individual algorithms, which have their own distinguished advantages exemplified and documented in the corresponding literature.

A good example is QS algorithms, form which the QS-2 is used in cooperation with other algorithms. In practice for QS algorithms the step size μ should be adjusted and the number of taps in the equalizer be increased to achieve quality performance, however QS-2 has been used for cooperation and no particular adjustment to corresponding parameters is made.

3.3 General Cooperative Adaptive System with Diversified Algorithms

The concept of devising multiple-algorithm system to solve the problem of wireless channel equalization or other related problems that can be tackled by adaptive algorithms seeks carefully crafted plans for using the outcome of the contributing algorithms. Since we need to use two or more techniques, the participating algorithms should not be computationally intensive. Good candidates having the desired simplicity are LMS, RLS and Quantized-State techniques. The principle idea for cooperating algorithms is to use majority vote system; however this can only be done for the system having 3 or more methods involved. Moreover, we have to keep the number of algorithms small to avoid excessive computation at each step of adaptation. Since the system of having only two algorithms is attractive in terms of required computations, we need to design a different plan for such systems (see section 3.4).

First we consider the case of 3 algorithms for a binary data system (field of $\{+1, -1\}$): if 2 out of 3 or more of the adaptive processes agree on the estimate of the data in step k, the majority wins and the wining estimate is used for computing the error at that step. Let us denote the probability of correct data estimate of each algorithm by p_i , $i = 1, 2, 3$. The total probability of correct data estimate of the system based on the majority vote and denoted by $P_{s3}$is determined as follows.

$$P_{s3} = p_1 p_2 (1 - p_3) + p_1 \, (1 - p_2) p_3 + (1 - p_1) p_2 p_3 + p_1 p_2 p_3 \qquad (3 - 19)$$

To see how this technique improves the overall performance of the system we need to have a reasonable estimate for p_i , $i = 1, 2, 3$. We argue that if one does not make any effort one can estimate the correct binary data with 0.5 probability, say using a uniform random number generator. We fairly assume that when one makes some effort by signal processing to perform better, the probability of a correct estimate goes up by a very small amount, say 0.5%. Now for simplicity we assume that the probability of the algorithms are equal and $p_1 = p_2 = p_3 = 0.505 = p$.

$$P_{s3} = 3p^2 - 2p^3 \qquad (3 - 20)$$

We further assume that in theory the correct estimate of the data at step k leads to the correct error calculation used for updating the weight vector that in turn results in a slightly better estimation probability in next step $k + 1$. Using this assumption we can run the system for a few steps and compute the probability of the correct performance as shown in Figure 3-3. As it can be seen in Figure 3-3 at least in theory we can achieve a fast improving system. In fact this needs to be evaluated by simulations (see section 3.5).

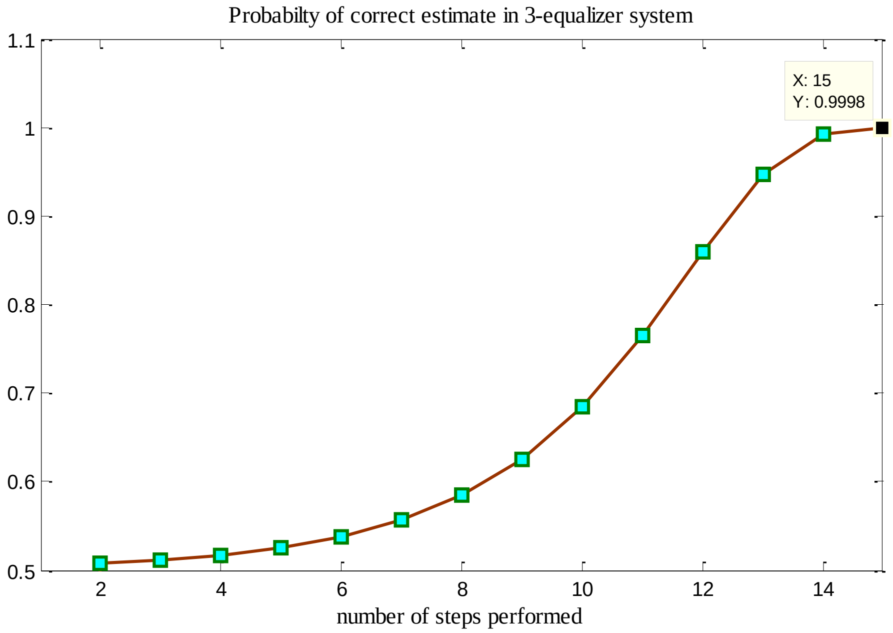

Figure 3-3 The improvement of the probability of correct estimate in 3-algorithm equalizer

The case of 4-algorithm is not promising, first because it requires at least a vote of 3 to 1 (a ratio of 3/1) when compared to the 3-algorithm system (it is only 2 to 1, a ratio of 2/1). Second, the simulation result (see Figure 3-4) indicates that the performance of the system deteriorates quickly. Applying the same convenient assumption of $p_1 = p_2 = p_3 = p_4 = 0.505 = p$, the system performance probability of correct estimation is computed as

$$P_{s4} = 4p^3 - 3p^4. \qquad (3-21)$$

Running the system for a few steps and computing the probability of the correct performance for the case of 4 algorithms is shown in Figure 3-4. Consequently the system of 4 different algorithms is not appealing for further work and investigation.

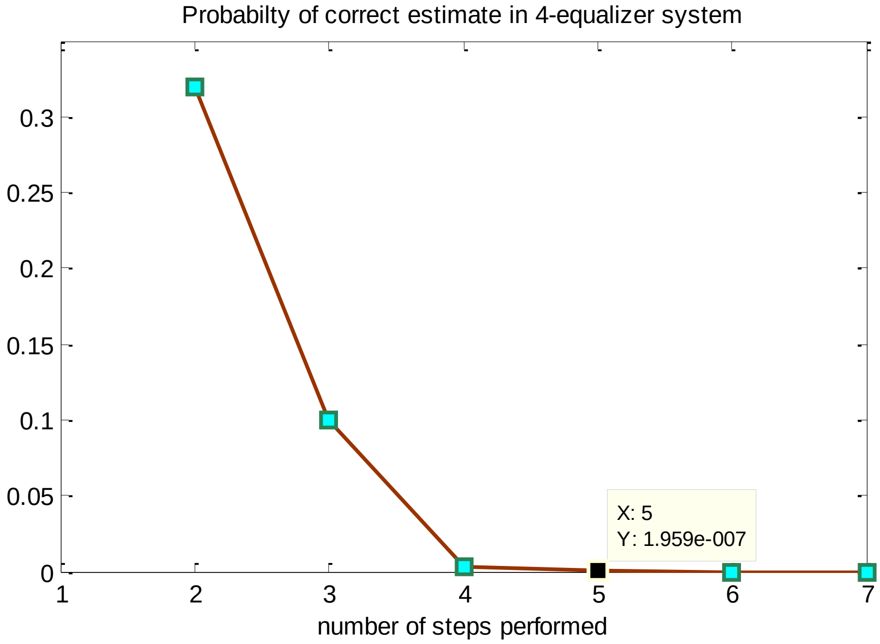

Figure 3-4 The degradation of the probability of correct estimate in 4-algorithm equalizer

Contrary to the 4-algorithm case, the system composed of 5 different algorithms has the benefit of even lower minimum ratio of 3 to 2 (3/2) vote for majority. Using similar assumptions as in the other cases, $p_1 = p_2 = p_3 = p_4 = p_5 = 0.505 = p$, the system correct estimate probability becomes

$$P_s = 10p^3 - 15p^4 + 6p^5 \qquad (3-22)$$

The improvement of the estimation, illustrated in Figure 3-5, grows faster with the number of steps compared to the 3-algorithm case. The drawback of the system with 5 algorithms is the increase in the amount of computation required, which may significantly reduce its practical application.

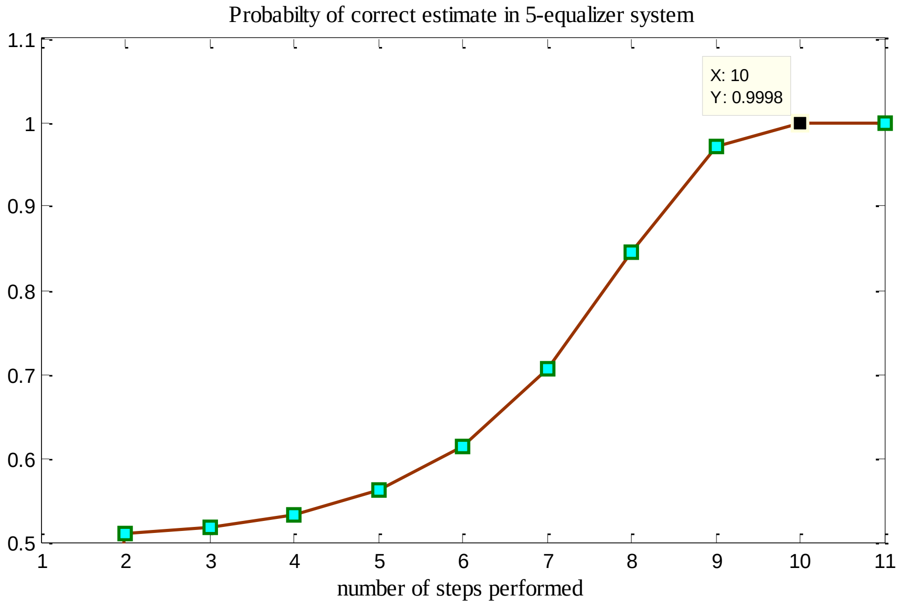

Figure 3-5 The improvement of the probability of correct estimate in 5-algorithm equalizer

3.4 Adaptive Systems with Two Algorithms

As was mentioned in section 3.3 the majority vote approach cannot be applied to a system of two algorithms (Notice that the similar approach as for 3 and more algorithms of $p_1 = p_2 = 0.505 = p$ leads to $P_s = p^2 = 0.255$ that is disappointing). Hence we need to create a different configuration. The proposed configuration w chooses the equalizer output with larger absolute value (g_1 or g_2) to be applied to the slicer that generates the final system estimate of the binary data by $sgn(\max(|g_1|, |g_2|))$. The corresponding system configuration is shown in Figure 3-6.

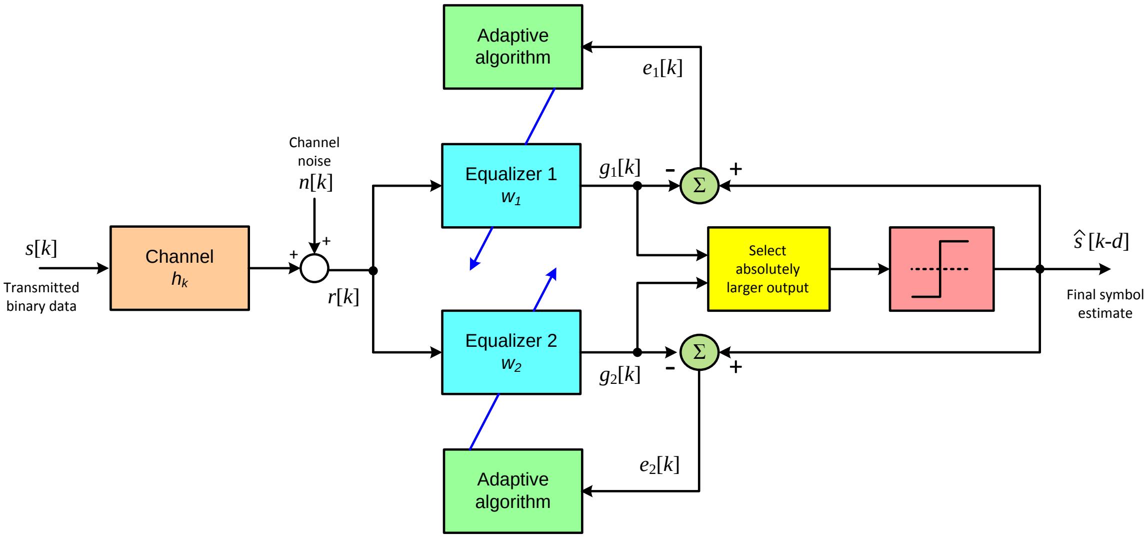

Figure 3-6 The configuration for cooperative 2-algorithm equalizer system

The algorithms selected to be used here are: a very simple LMS algorithm specified in chapter 2 by Equation (2-21) and (2-28), repeated here for convenience and the computationally more intensive but faster EWRLS algorithm specified by Equation (3-11) and (3-12) in section 3.2.

$$\boldsymbol{w}[k+1] = \boldsymbol{w}[k] - \mu\boldsymbol{\nabla}[k] \qquad (2\text{-}21)$$

$$\boldsymbol{w}[k+1] = \boldsymbol{w}[k] - \mu\boldsymbol{\nabla}\mathcal{J}(\boldsymbol{w}[k]) = \boldsymbol{w}[k] + \mu e[k]\boldsymbol{r}[k] \qquad (2\text{-}28)$$

We have examined the proposed configuration on different channels with the equalizers of equal channel-size (number of taps) in each algorithm. The equalizer can be larger in size, and the size equal to the length of the channel impulse response. The equalizers of larger size are frequently designed and used to get better performance (lower residual ISI for example).

Channel 1

The first channel is symmetric with five taps (non-minimum phase) specified by the following impulse response and the corresponding transfer function

$$h = -0.2287\delta[k] + 0.3964\delta[k-1] + 0.7623\delta[k-2] + 0.3964\delta[k-3] - 0.2287\delta[k-4].$$

$$H(z) = -0.2287 + 0.3964z^{-1} + 0.7623z^{-2} + 0.3964z^{-3} - 0.2287z^{-4}.$$

The four channel zeros are located at: $3, -0.8 \pm j0.6$, and $1/3$, the complex zeros being on the unit circle.

When the LMS (with $\mu = 0.004$) and EWRLS (with $\mu = 1$) are adapting independently, the corresponding residual ISI for two algorithms is given in Figure 3-7.

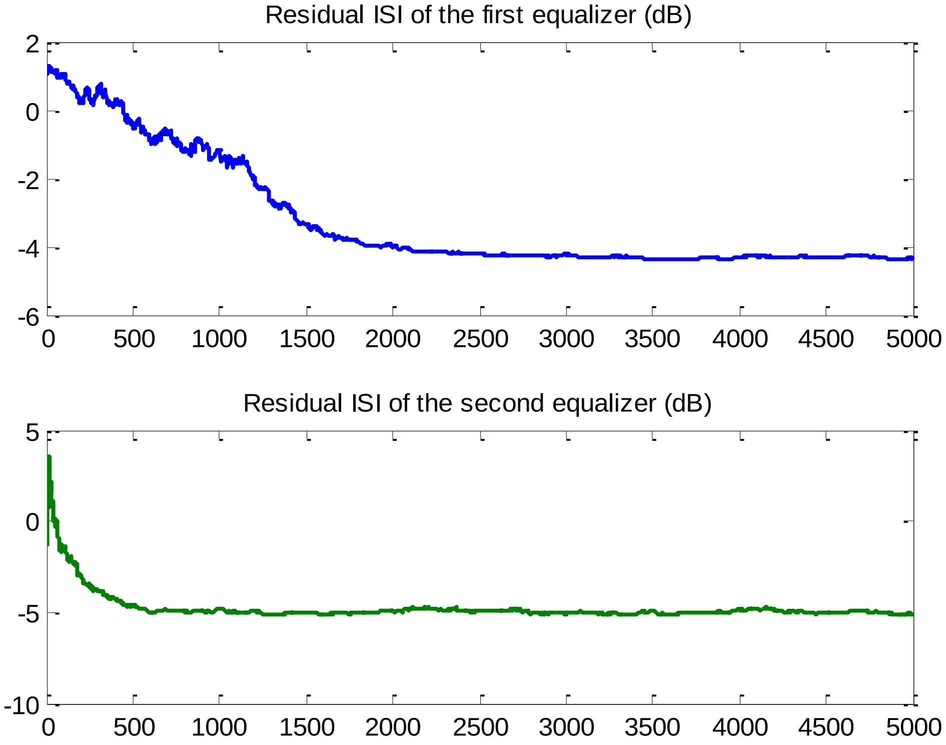

Figure 3-7 Independent residual ISI of LMS (top) and EWRLS (bottom) algorithms

It can be seen from Figure 3-7 that EWRLS converges faster; however neither one achieves a residual ISI of better that -5 dB (the optimum LS equalizer for known CIR achieves the residual ISI of only -3.22 dB).

The resulting residual ISI of the proposed configuration when the algorithms are sharing their equalizer outputs in this case are given in Figure 3-8.

It is clearly shown that LMS algorithm has become faster, which to the contrary the EWRLS algorithm is relatively slower in convergence. Final residual ISI of the algorithms have not improved in value for this case.

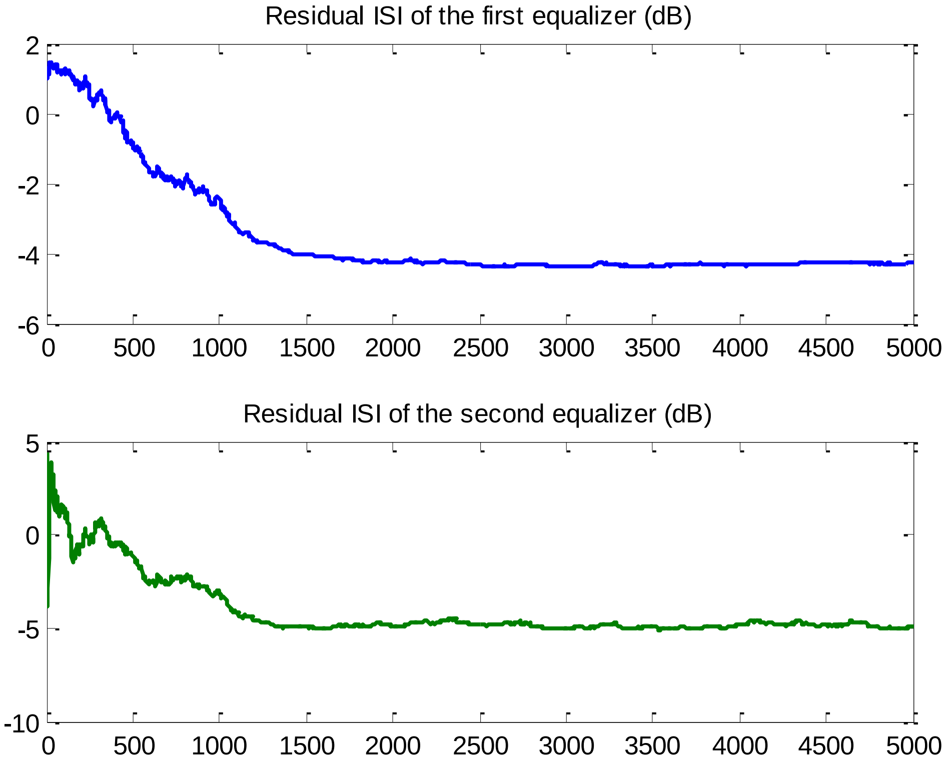

Figure 3-8 Cooperative residual ISI of LMS (top) and EWRLS (bottom) algorithms

The comparison of the results of the LMS and EWRLS algorithms of independent and cooperative processing of channel 1 are given in Figure 3-9 and 3-10 respectively.

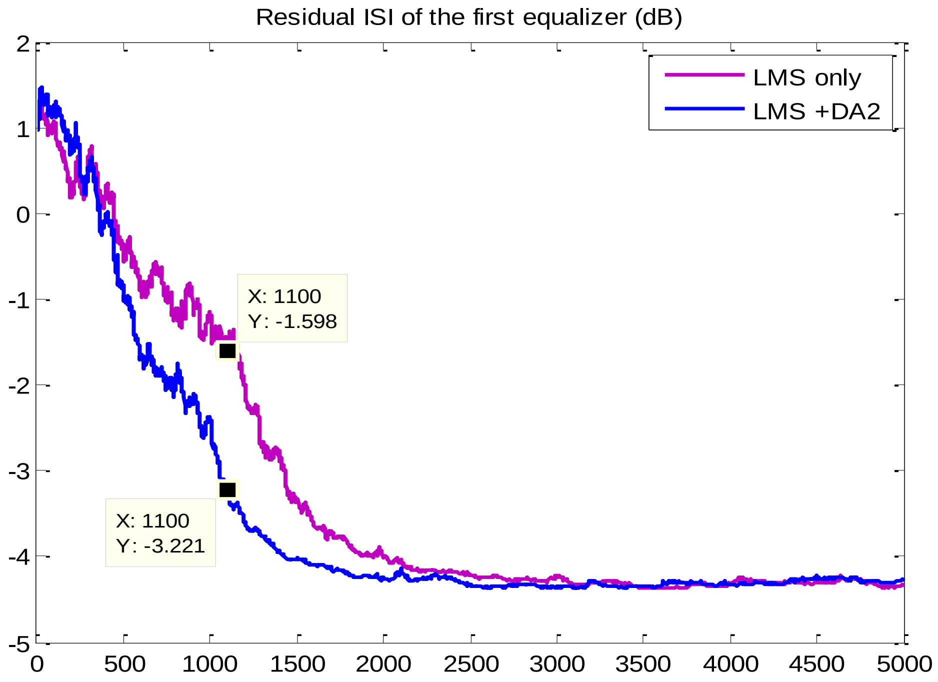

Figure 3-9 Comparison of LMS algorithm residual ISI for independent (magenta) and cooperative (blue) modes

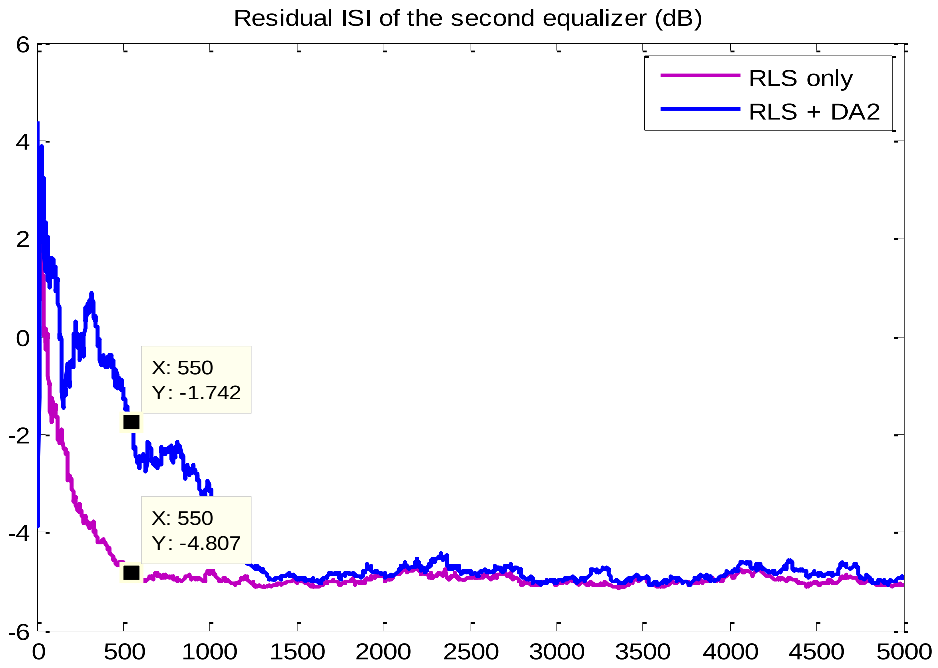

Figure 3-10 Comparison of EWRLS algorithm residual ISI for independent (magenta) and cooperative (blue) modes

Channel 2

The second channel with eleven taps is specified by the impulse response of

$$h = 0.04\delta[k] - 0.05\delta[k-1] + 0.07\delta[k-2] - 0.21\delta[k-3] - 0.5\delta[k-4] + 0.72\delta[k-5] + 0.36\delta[k-6] + 0.21\delta[k-8] + 0.03\delta[k-9] + 0.07\delta[k-10].$$

The corresponding transfer function is:

$$H(z) = 0.04 - 0.5z^{-1} + 0.07z^{-2} - 0.21z^{-3} - 0.5z^{-4} + 0.72z^{-5} + 0.36z^{-6} + 0.21z^{-8} + 0.03z^{-9} + 0.07z^{-10}.$$

The ten channel zeros are located at :

$-0.1419 \pm j2.259, 1.7503 \pm j0.1045, -1.4449, -0.832, 0.3358 \pm j0.5055,$ and $- 0.1808 \pm j0.4672$. This channel is also non-minimum phase.

We let the LMS and EWRLS (with $\mu = 1$) algorithms adapt separately and the corresponding residual ISI of each algorithm in this case is shown in Figure 3-11.

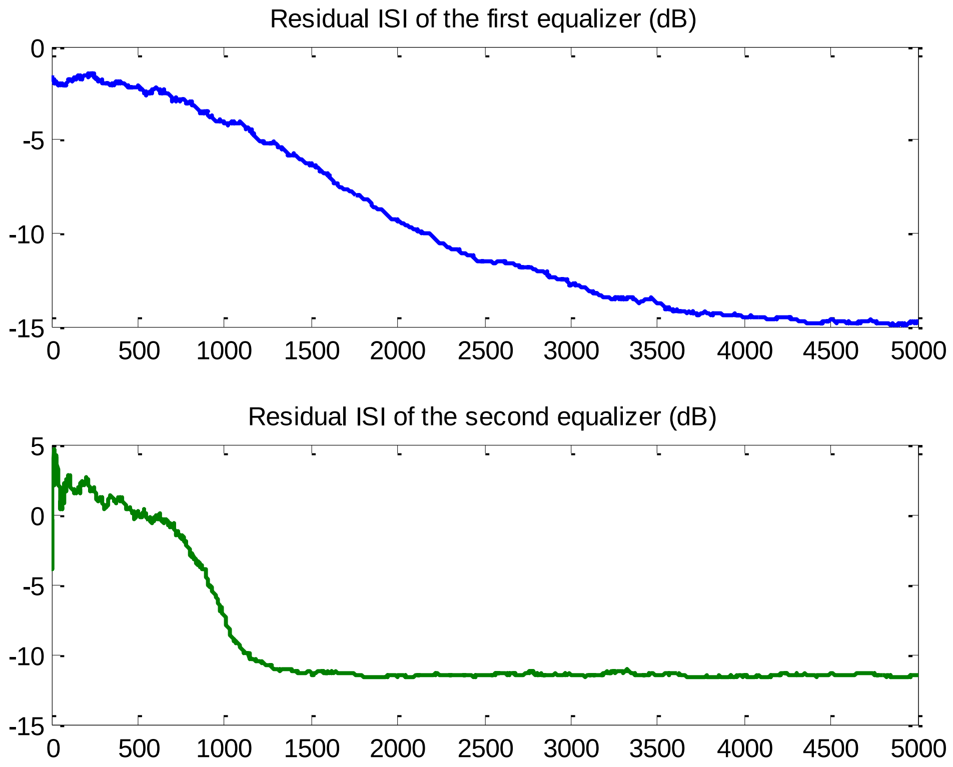

Figure 3-11 Independent residual ISI of LMS (top) and EWRLS (bottom) algorithms

It can be seen from Figure 3-11 that EWRLS converges relatively faster, however LMS achieves a better residual ISI of about -15 dB (the optimum LS equalizer residual ISI of -15.7 dB).

The residual ISI of the proposed configuration with the cooperating algorithms in this case are given in Figure 3-12. It can be seen that LMS algorithm has become slightly faster with the same final residual ISI and so does the EWRLS algorithm that also converges faster with about the same final residual ISI.

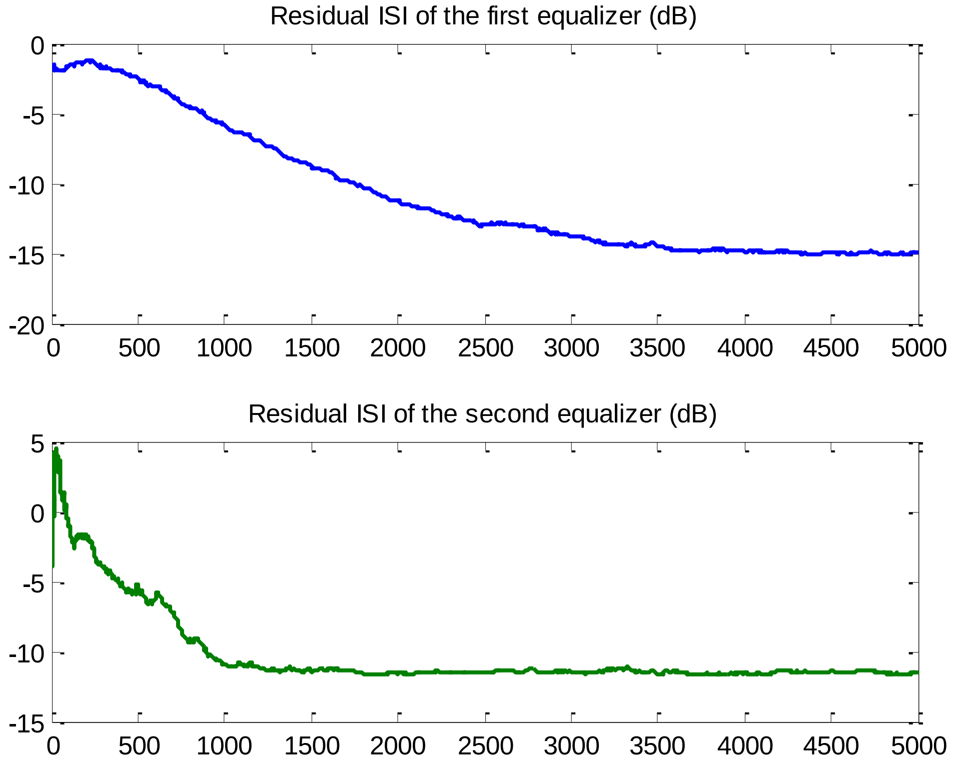

Figure 3-12 Cooperative residual ISI of LMS (top) and EWRLS (bottom) algorithms

The comparison of the results of LMS and EWRLS algorithms in the independent and the cooperative processing for channel 2 are given in Figure 3-13 and 3-14 respectively.

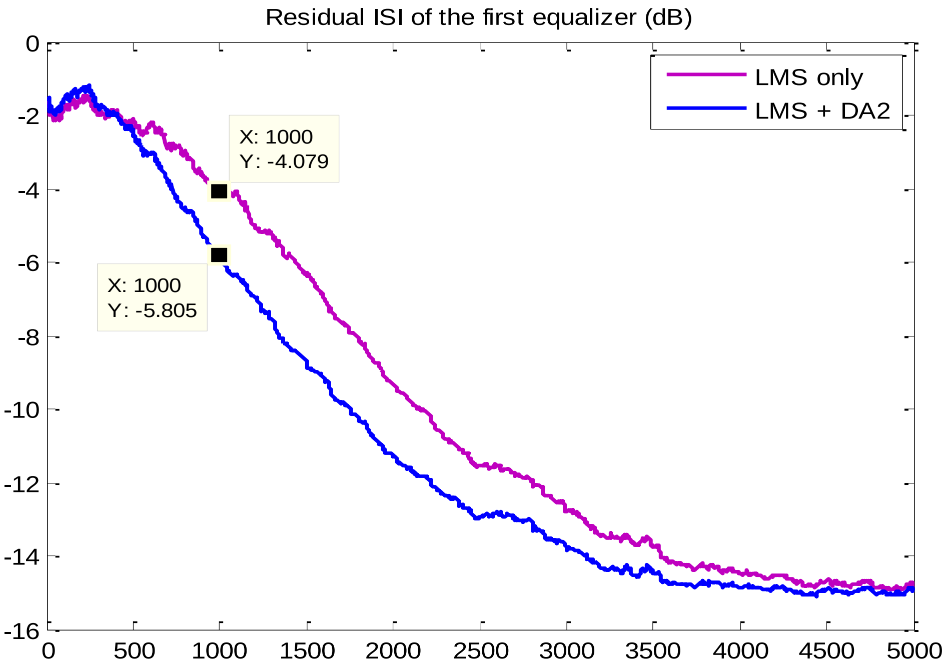

Figure 3-13 Comparison of LMS algorithm residual ISI for independent (magenta) and cooperative (blue) modes

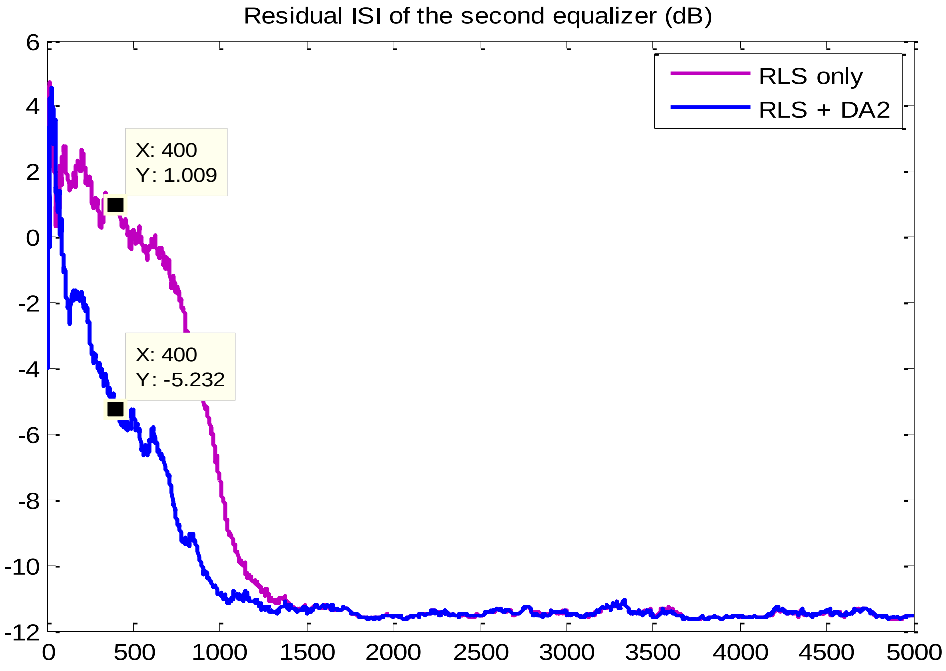

Figure 3-14 Comparison of EWRLS algorithm residual ISI for independent (magenta) and cooperative (blue) modes

3.5 Adaptive Systems with Three Algorithms

With a system including 3 different cooperating algorithms the majority vote determines the final system estimate of the transmitted data and therefore the error for each algorithm is computed based on this estimate. The equalizer outputs are first applied to a hard-limiter before the votes are sensed and a minimum ratio of 2 to 1 suffices to win. We have shown with some optimistic assumptions that it can improve the overall system performance in terms of the probability by which the system attains the correct estimate (see Figure 3-3). The general set up for the systems employing 3 algorithms is illustrated in Figure 3-15.

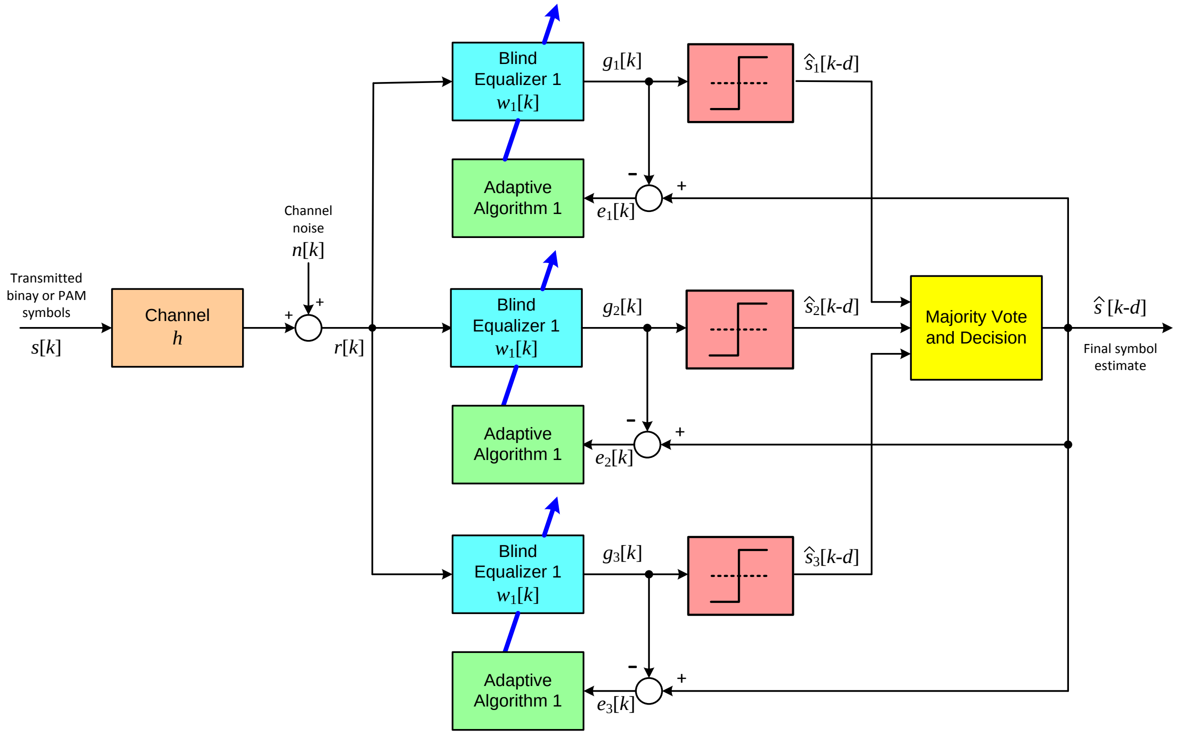

Figure 3-15 The configuration for cooperative 3-algorithm equalizer system

The algorithms selected to be used here are the same simple LMS algorithm specified in chapter 2 by Equation (2-21) and (2-28), repeated here for convenience.

$$\boldsymbol{w}[k+1] = \boldsymbol{w}[k] - \mu\boldsymbol{\nabla}[k] \qquad (2\text{-}21)$$

$$\boldsymbol{w}[k+1] = \boldsymbol{w}[k] - \mu \boldsymbol{\nabla} \mathcal{J}(\boldsymbol{w}[k]) = \boldsymbol{w}[k] + \mu e[k]\boldsymbol{r}[k] \qquad \text{(2-28)}$$

The second algorithm is the computationally more intensive but faster EWRLS specified by equations (3-11) and (3-12), and finally the third algorithm is the Quantized State-2 of the RLS type that is given by equation (3-17) and (3-18) both explained in section 3.2. The latter was selected based on more satisfactory results observed by simulations.

Three different channels are examined by the proposed system and the results are summarized in the following. Each algorithm uses an equalizer of the size of the channel impulse response (CIR).

Channel 1

The first channel is symmetric with five taps and non-minimum phase specified by the impulse response of

$$h = -0.2287\delta[k] + 0.3964\delta[k-1] + 0.7623\delta[k-2] + 0.3964\delta[k-3] - 0.2287\delta[k-4].$$

The corresponding transfer function is:

$$H(z) = -0.2287 + 0.3964z^{-1} + 0.7623z^{-2} + 0.3964z^{-3} - 0.2287z^{-4}.$$

The four channel zeros are located at: $3, -0.8 \pm j0.6,$ and $1/3$, the complex zeros being on the unit circle that make the equalization hard and questionable, if not impossible; hence one may try only to equalize the channel to a possible low residual ISI.

When the LMS, EWRLS, and QS-2 are adapting separately the corresponding residual ISI of each algorithm is given in Figure 3-16. It can be seen that QS-2 is fastest to converge with the poorest final residual ISI. LMS and EWRLS achieve -4 dB and -5 dB residual ISI respectively when the EWRLS is faster in convergence.

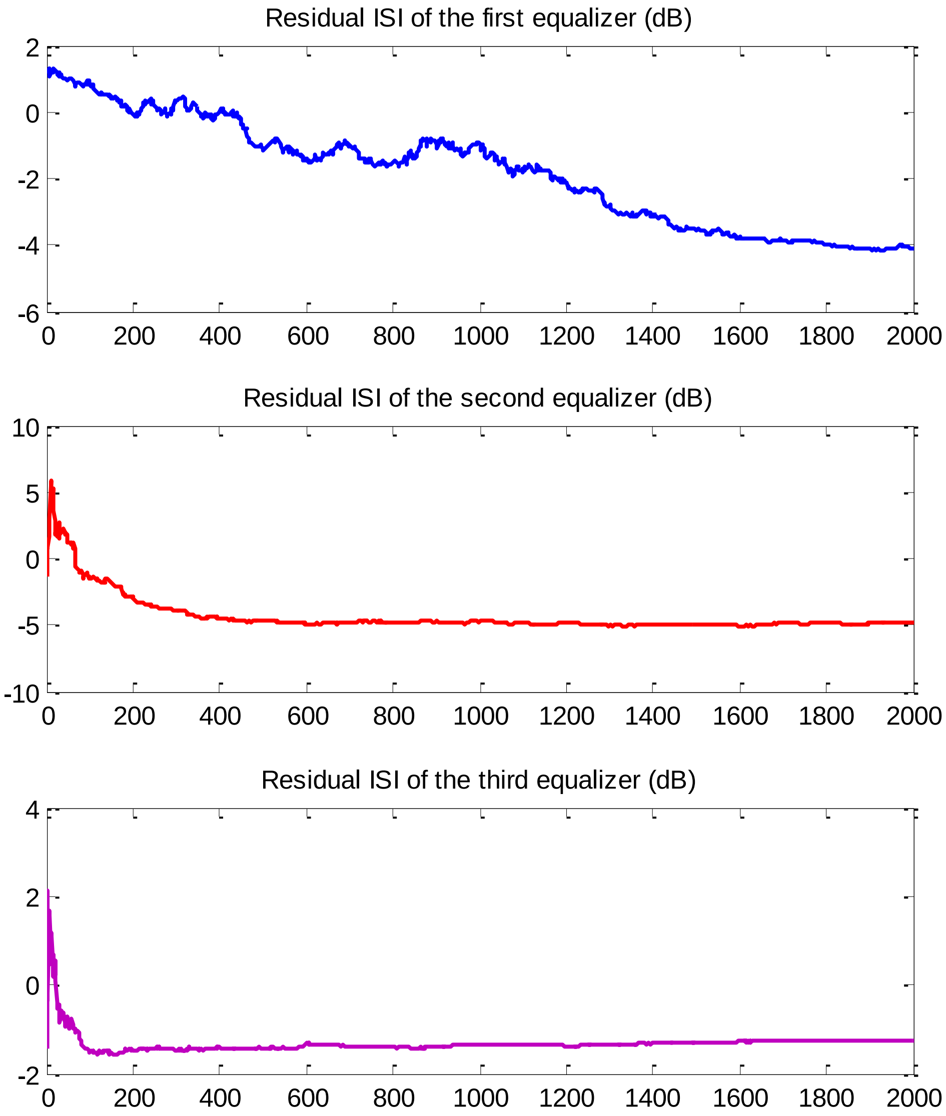

Figure 3-16 Independent residual ISI of LMS (top), EWRLS (middle), and QS-2 (bottom) algorithms

When all three algorithms work cooperatively based on a majority vote strategy the resulting residual ISI graphs are varied in behavior as shown in Figure 3-17. It is clearly shown that LMS algorithm has become faster when the EWRLS and QS-2 algorithms have been steady in both convergence and performance. It is important to bear in mind that the channel 1 transfer function has two zeros on the unit circle that makes quality blind mode equalization nearly impossible.

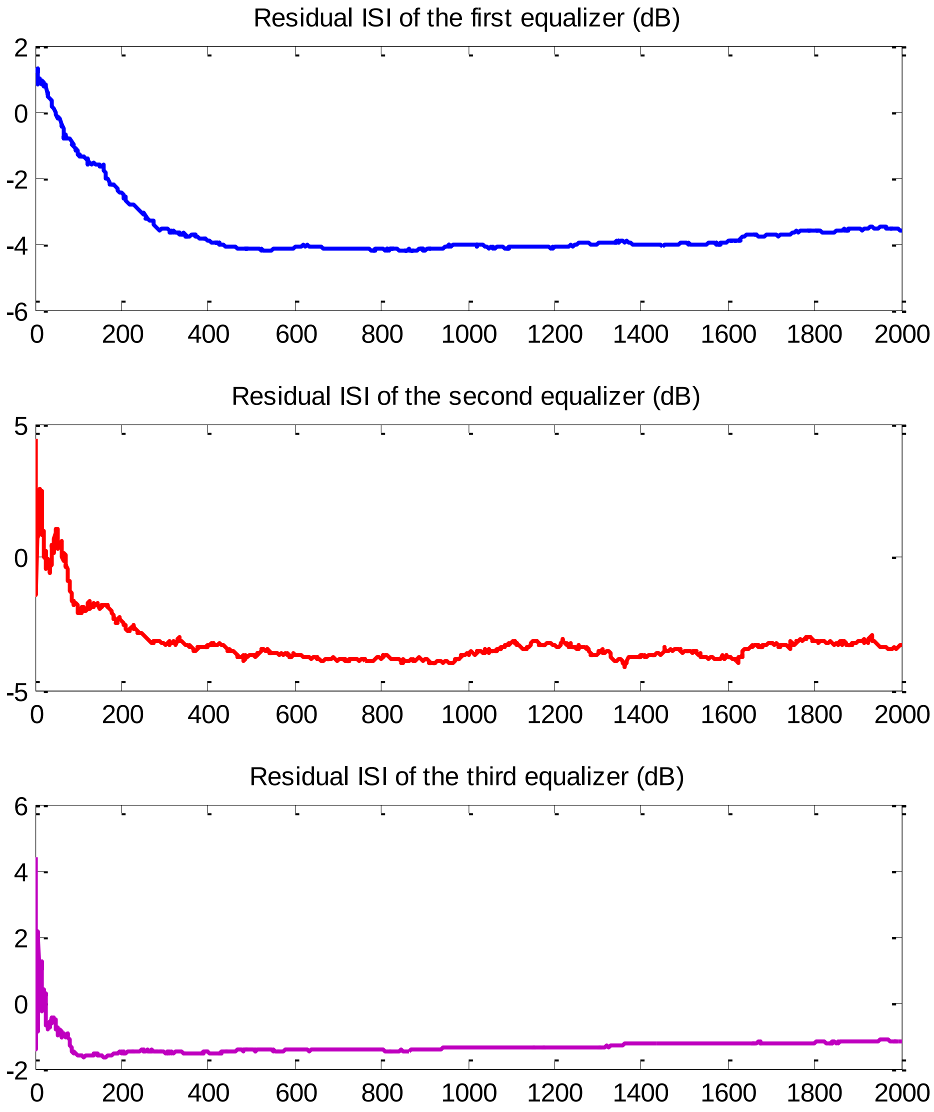

Figure 3-17 Cooperative residual ISI of LMS (top), EWRLS (middle), and QS-2 (bottom) algorithms

Considering that the optimum Least-Squares equalizer when the CIR is known achieves only a residual ISI of -3.22 dB, reaching -4 dB in about 400 steps by the LMS algorithm is a significant improvement both in performance measure and convergence speed that is gained by cooperation of the other different algorithms. This result is better seen in the comparison made in Figure 3-18.

There is also a minor degradation in the final residual ISI when the adaptation process is allowed to carry on after 1500 steps. (DA3 stands for Diversified 3-Algorithm.)

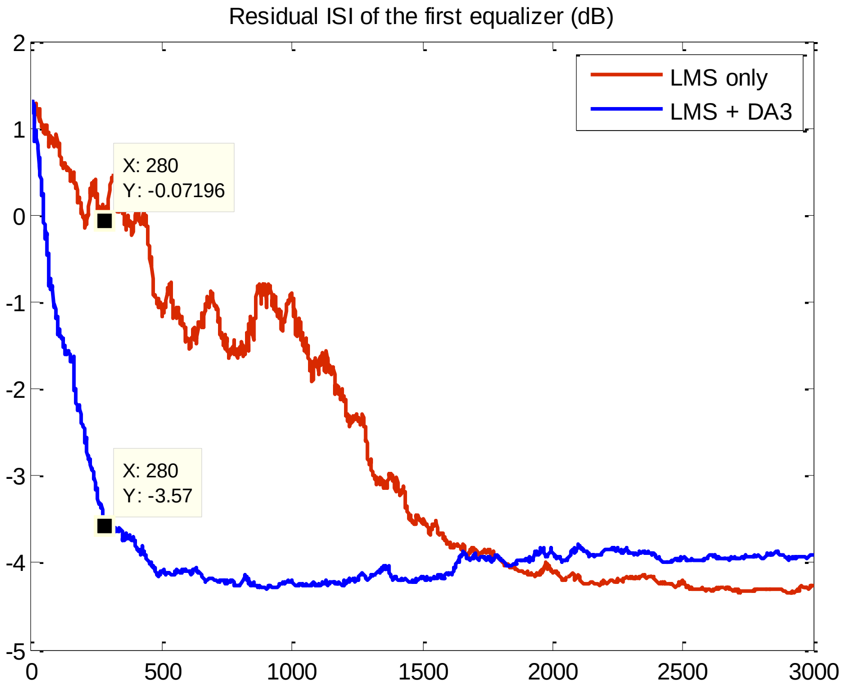

Figure 3-18 Comparison of LMS algorithm residual ISI for independent mode (red) and cooperative mode (blue)

Channel 2

The second channel with seven taps is specified by the impulse response of

$$h = 0.017\delta[k] + 0.083\delta[k-1] + 0.19\delta[k-2] + 0.42\delta[k-3] + 0.21\delta[k-4] + 0.036\delta[k-5] + 0.01\delta[k-6].$$

The corresponding transfer function is:

$$H(z) = 0.017 + 0.083z^{-1} + 0.19z^{-2} + 0.42z^{-3} + 0.21z^{-4} + 0.036z^{-5} + 0.01z^{-6}.$$

The six channel zeros are located at: $-3.4318, -0.4284 \pm j2.3258, -521,$ and $-\ 0.0364 \pm j0.2398$.

The channel is also non-minimum phase.

First we let the LMS, EWRLS, and QS-2 algorithms adapt separately and the corresponding residual ISI of each algorithm is given in Figure 3-19. It can be seen that QS-2 is fastest to converge with the poorest final residual ISI. The LMS and EWRLS achieve -8 dB and -4 dB residual ISI respectively when the latter converges much faster.

It is our desire to make LMS convergence faster while maintaining the same final residual ISI as in the independent mode.

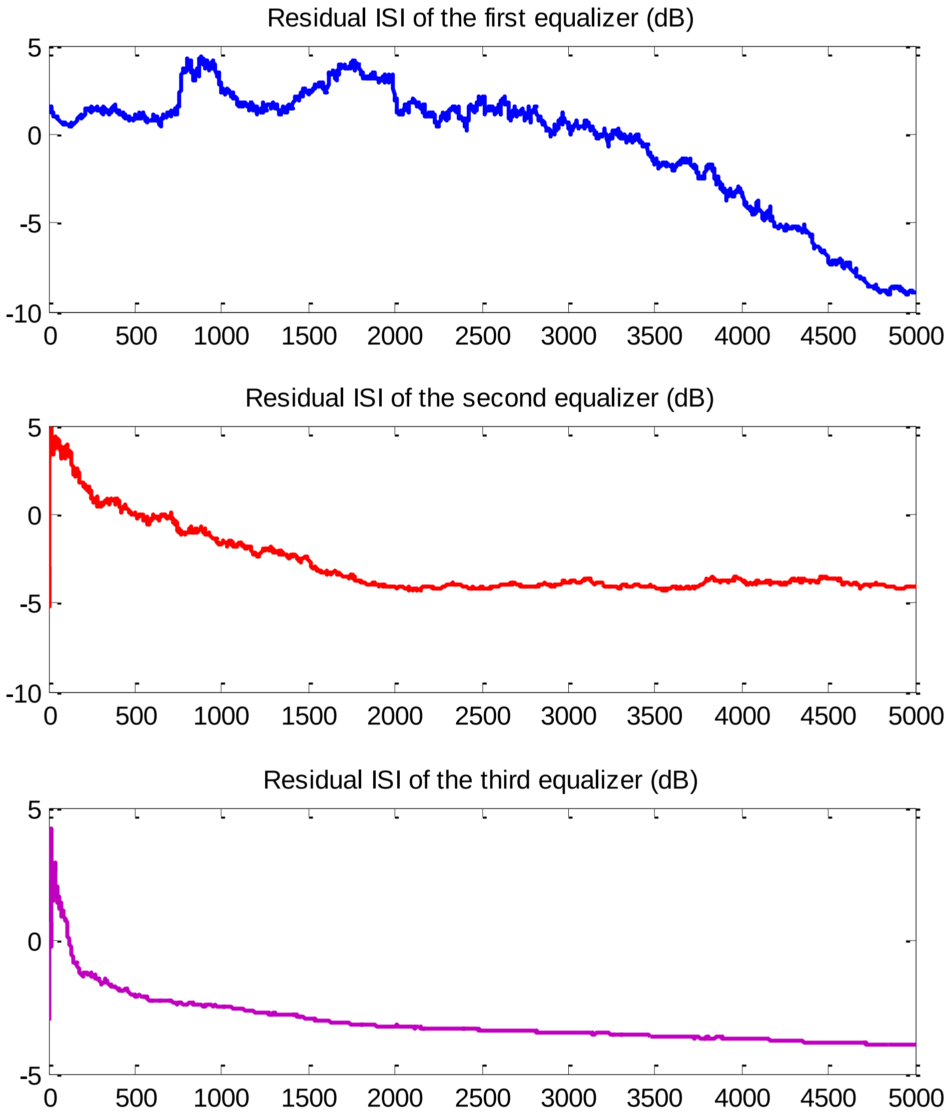

Residual ISI of the first equalizer (dB)

Residual ISI of the second equalizer (dB)

Residual ISI of the third equalizer (dB)

Figure 3-19 Independent residual ISI of LMS (top), EWRLS (middle), and QS-2 (bottom) algorithms

When all three algorithms work cooperatively based on a majority vote strategy the resulting residual ISI graphs are changed as shown in Figure 3-20.

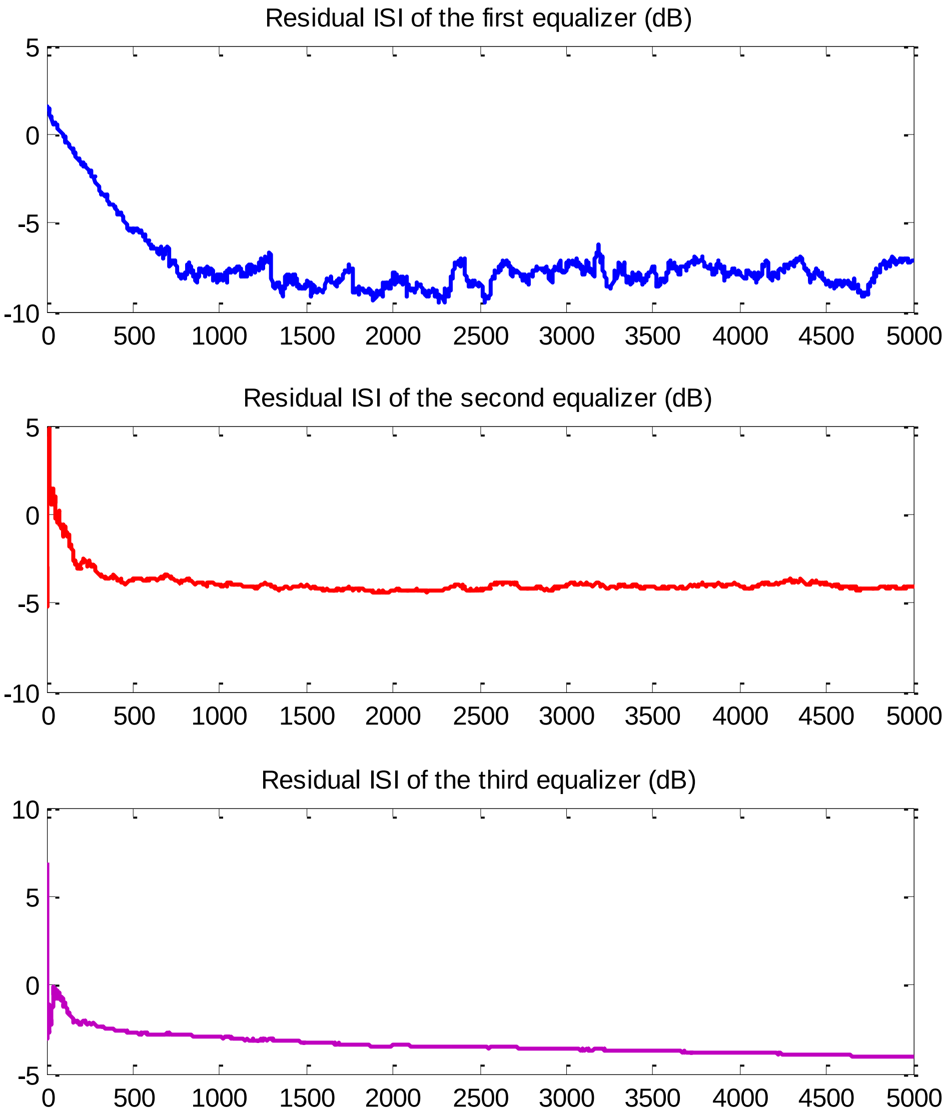

Figure 3-20 Cooperative residual ISI of LMS (top), EWRLS (middle), and QS-2 (bottom) algorithms

It is clearly shown that LMS algorithm has gained relatively great speed in convergence while the other algorithms have also improved when the EWRLS achieves higher speed than QS-2. In the channels examined during this research the author has observed that LMS algorithm usually outperforms other algorithms in spite of its slower convergence. The comparison of the residual ISI performance of each algorithm in independent and cooperative modes are given by Figure 3-21, 3-22, and 3-23 for LMS, RLS, and QS-2 respectively.

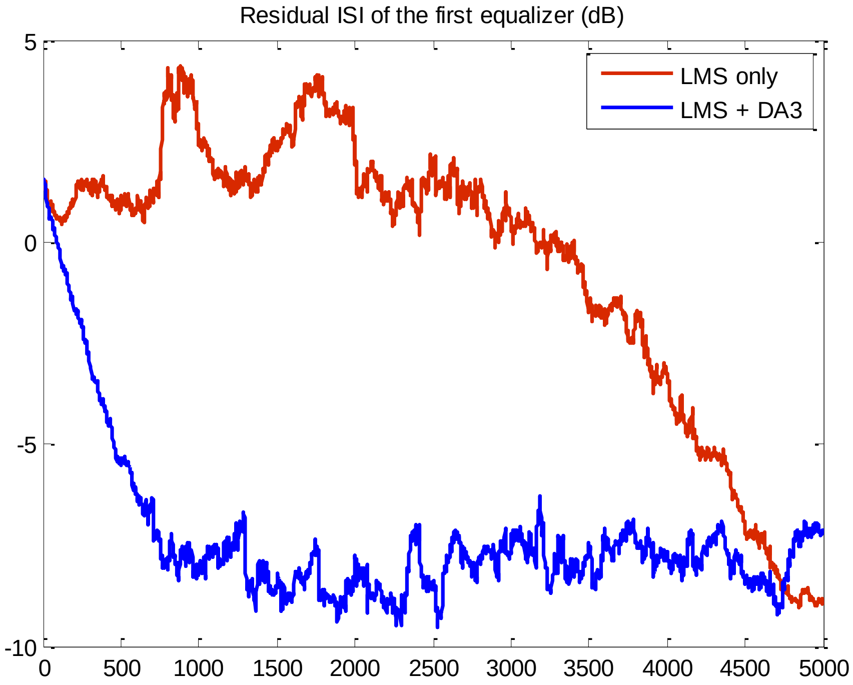

Figure 3-21 Comparison of LMS algorithm residual ISI for independent mode (red) and cooperative mode (blue)

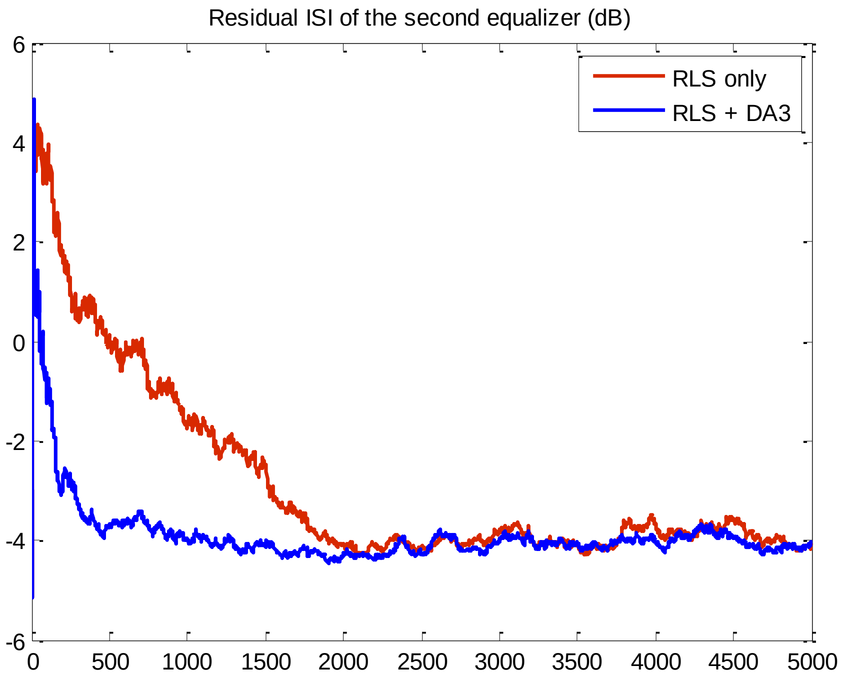

Figure 3-22 Comparison of RLS algorithm residual ISI for independent mode (red) and cooperative mode (blue)

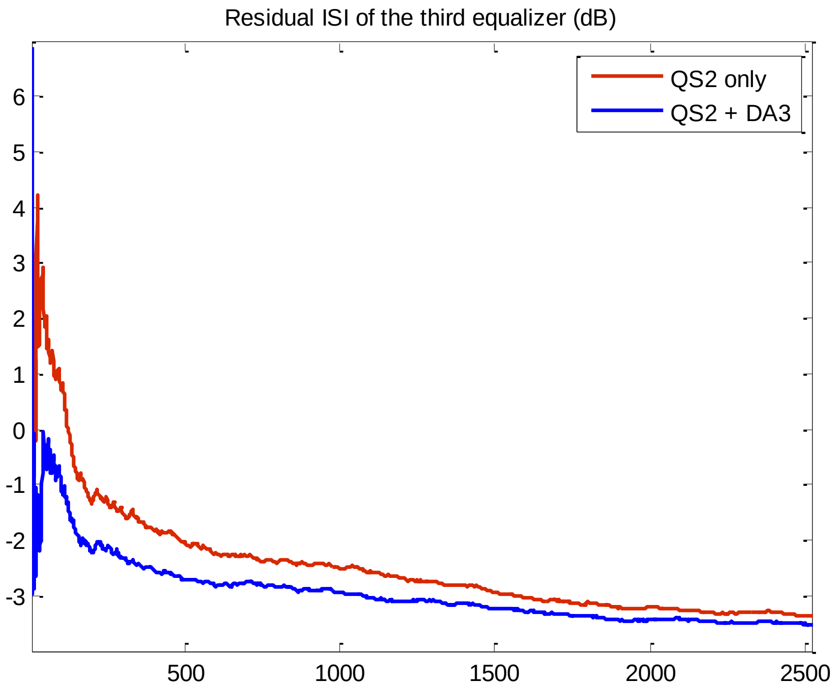

Figure 3-23 Comparison of QS-2 algorithm residual ISI for independent mode (red) and cooperative mode (blue)

Channel 3

The third channel with eleven taps is specified by the impulse response of

$$h = 0.04\delta[k] - 0.05\delta[k-1] + 0.07\delta[k-2] - 0.21\delta[k-3] - 0.5\delta[k-4] + 0.72\delta[k-5] + 0.36\delta[k-6] + 0.21\delta[k-8] + 0.03\delta[k-9] + 0.07\delta[k-10].$$

The corresponding transfer function is:

$$H(z) = 0.04 - 0.5z^{-1} + 0.07z^{-2} - 0.21z^{-3} - 0.5z^{-4} + 0.72z^{-5} + 0.36z^{-6} + 0.21z^{-8} + 0.03z^{-9} + 0.07z^{-10}.$$

The ten channel zeros are located at:

$-0.1419 \pm j2.259, 1.7503 \pm j0.1045, -1.4449, -0.832, 0.3358 \pm j0.5055,$ and $-0.1808 \pm j0.4672$. This channel is also non-minimum phase because the first five zeros are located outside of the unit circle.

When all of the algorithms adapt independently from each other they achieve the residual ISI trends of Figure 3-23. The final ISI for LMS, RLS, and QS-2 are about -14 dB, -11.5 dB, and -1 dB respectively. The latter performance measure is of course not satisfactory compared to the others.

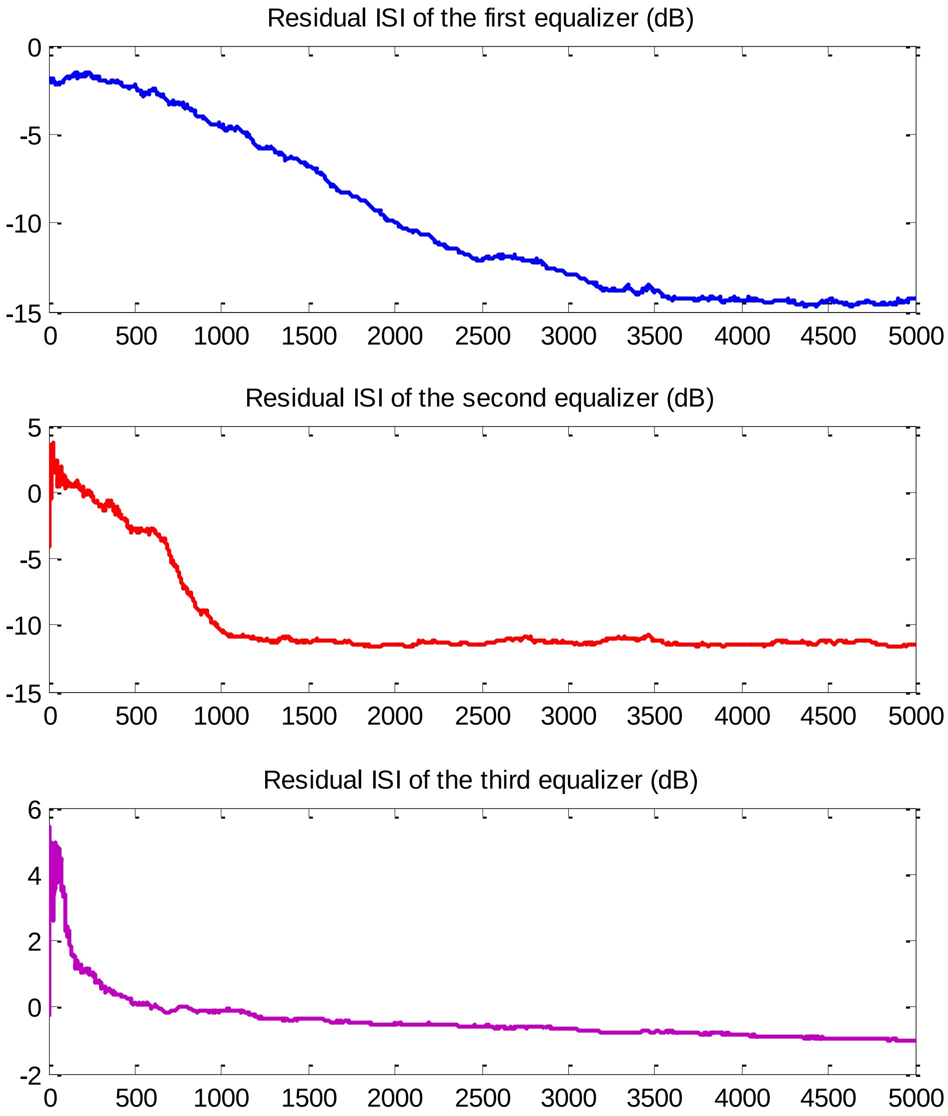

Figure 3-23 Independent residual ISI of LMS (top), EWRLS (middle), and QS-2 (bottom) algorithms

The results of cooperative adaptation based on majority vote for this channel in graphs of residual ISI are shown in Figure 3-24.

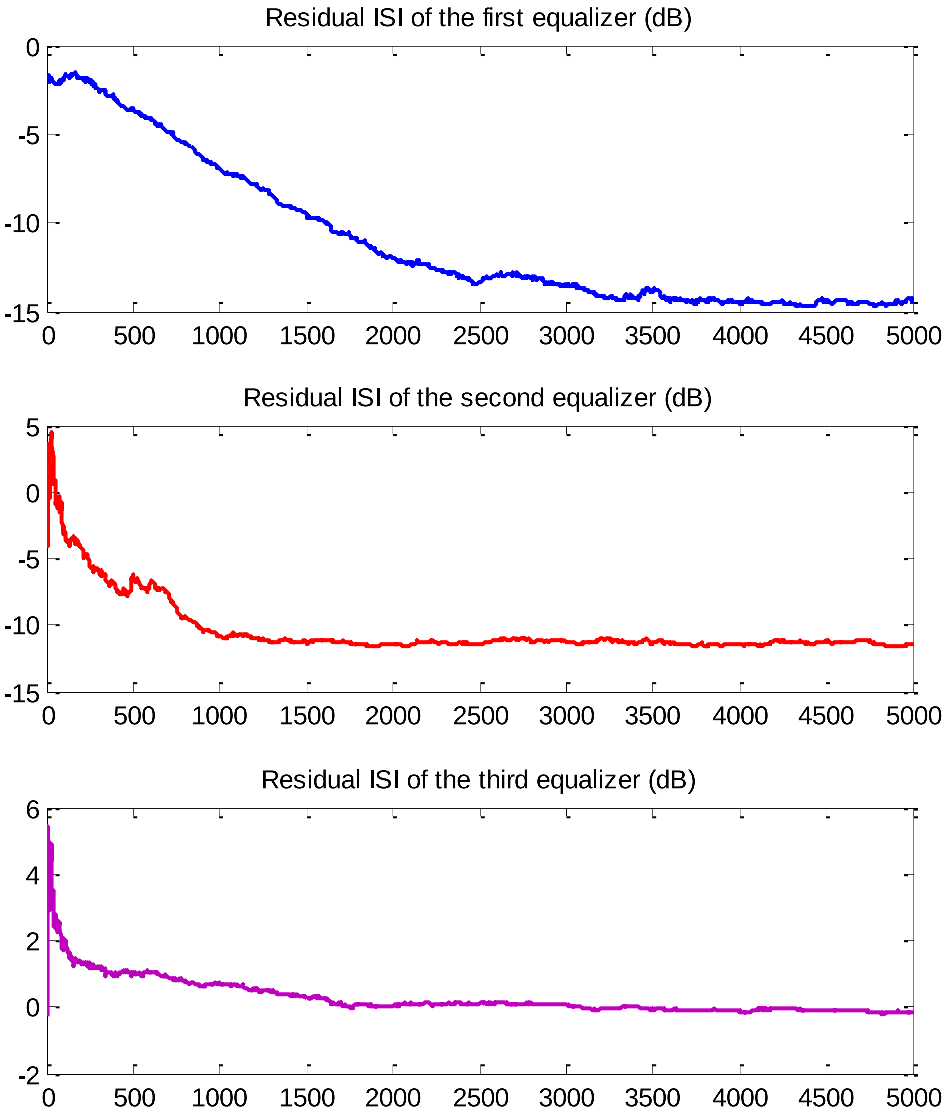

Figure 3-24 Cooperative residual ISI of LMS (top), EWRLS (middle), and QS-2 (bottom) algorithms

In order to inspect the improvements gained by using the proposed diversified method we compare the independent and cooperative residual ISI trend for each algorithm in Figure 3-25, 3-26, and 3-27 for the LMS, RLS, and QS-2 respectively.

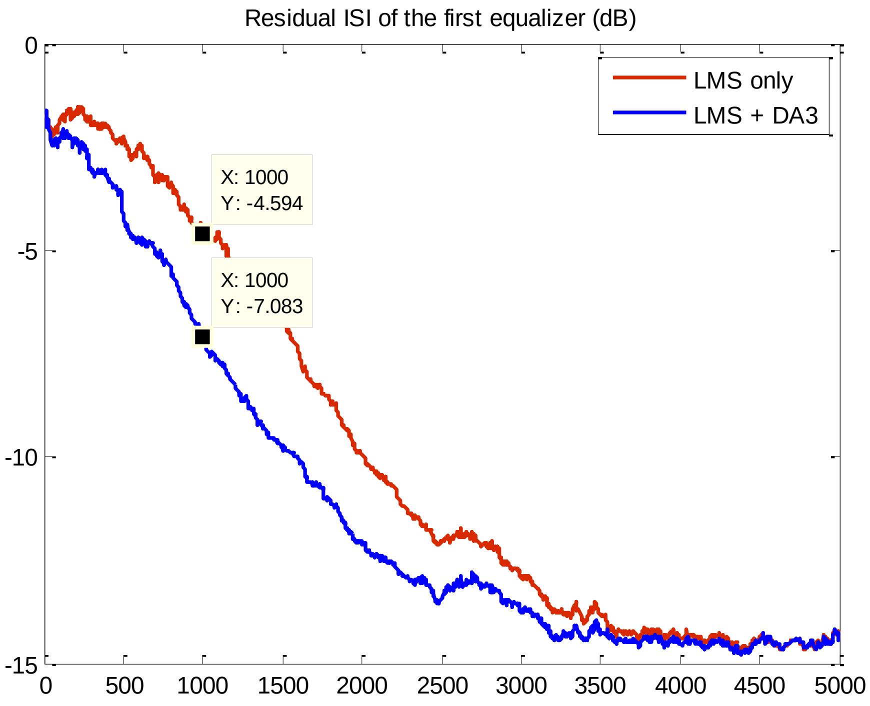

Figure 3-25 Comparison of LMS algorithm residual ISI for independent mode (red) and cooperative mode (blue)

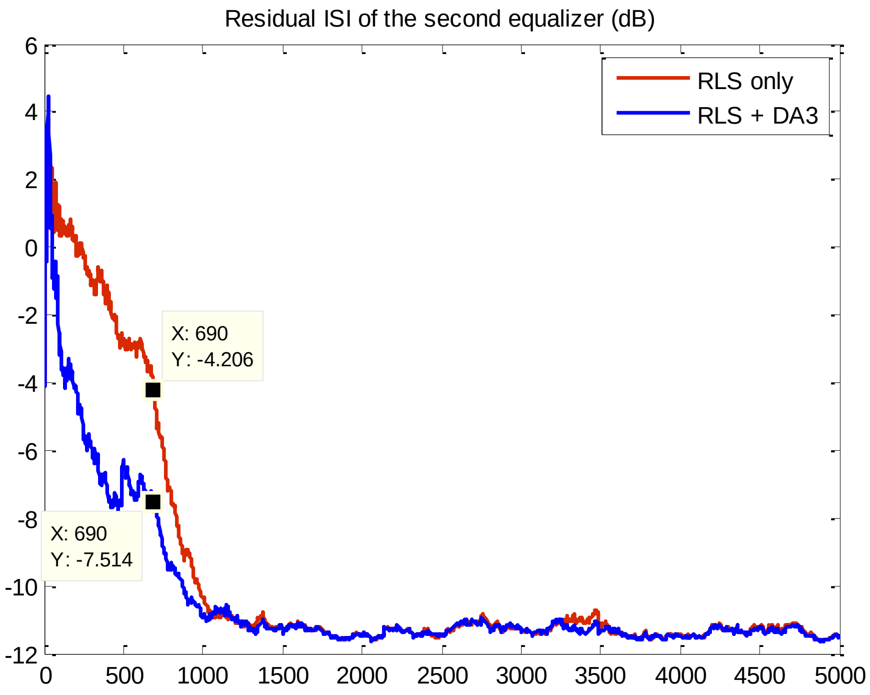

Figure 3-26 Comparison of RLS algorithm residual ISI for independent mode (red) and cooperative mode (blue)

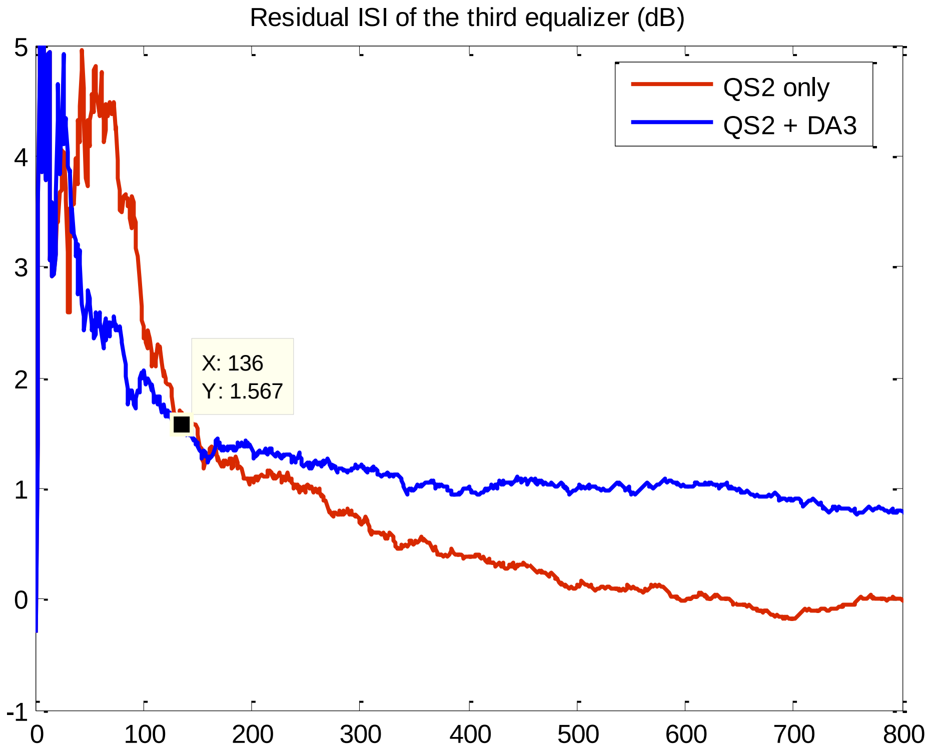

Figure 3-27 Comparison of QS-2 algorithm residual ISI for independent mode (red) and cooperative mode (blue)

The improvements in performance for the convergence speed of the LMS and EWRLS algorithms are clearly observed in Figure 3-25 and 3-26 when some initial acceleration is noticeable for QS-2 algorithm in Figure 3-27.

3.6 Chapter Conclusion

In summary, we have shown that the proposed majority vote algorithm achieves variable improvements based on wireless channel models being examined and different algorithms being measured. Since the majority vote cannot be applied to the case of 2-algorithm system, this case requires a different approach. One proposed methodology that has been used in section 3.4 with variable results in terms of the amount of the gain in convergence speed. This case requires future work to guarantee robust benefits in the general channel model and incorporating algorithms.

We have not examined the 5-algorithm system due to the fact that excessive simultaneous computations for the adaptation of five different algorithms may not be justified unless for very hard channels that resist any other existing blind mode equalization technique.

The 3-algortihm system is computationally acceptable, in particular when the participating algorithms are relatively simple such as LMS, EWRLS, and QS-2 techniques used in section 3.5. As shown by the simulation results this case is promising with variable improvement rates. It is the author’s intention to augment the proposed methodology to accomplish more consistent performance benefit by adding the possible option of choosing different cooperative and congruent algorithms.

In a practical application includes 3 cooperating algorithms, say forcing the LMS to converge faster to its final residual ISI, and the other two algorithms are stopped. Slow variations of the channel can be tracked by continuing LMS adaptation.

Finally, very high speed signal processors with low power consumption warrant the use of multiple algorithms in diversified systems even in case of using 5 or more algorithms in one system.

3.7 References

[1] Clarkson, P.M., “Optimal and Adaptive Signal Processing,” CRC Press LLC, 1993.

[2] Ding, Z.Z., Zhang, X.D., Su, Y.T., “Performance Analysis of Nested RLS-Type Interference Suppression Algorithm for CDMA System in Dispersive Channels,” IEEE Signal Processing Letters, Vol. 14, No. 1, January 2007.

[3] Hayes, M.H., “Statistical Digital Signal Processing and Modeling,” John Wiley & Sons,1996.

[4] Kumar, R., Moore, J.B., “Adaptive Equalization via Fast Quantized State Method”, IEEE Transactions on Communications, Vol. COM-29, No. 10, October 1981.

[5] Kumar, R., Khor, K. “Adaptive Decision-Directed Quantized-State Algorithms for Multi-user Detection of CDMA Signals,” IEEE Aerospace Conference, 2007.

[6] Therrien, C.W., “Discrete Random Signals and Statistical Signal Processing,” Prentice-Hall, 1992.

[7] Widrow, B., Stearns, S.D., “Adaptive Signal Processing”, Prentice-Hall, New Jersey, 1985.

[8] Widrow, B, Walach, E., “Adaptive Inverse Control: A Signal Processing Approach,” Wiley-IEEE Press, Nov. 2007.

Chapter 4: Neural Networks, a Novel Back Propagation Configuration for Wireless Channel Equalization

4.1 Introduction

Neural networks are viewed as dense interconnections of elementary computational elements known as perceptrons that are simplified models of neurons in the human brain. This model is based on our perception and understanding of the biological nervous system. Neural networks also have been considered as massively parallel networks composed of many computational elements organized in parallel to each other and in turn cascaded to other elements in different layers. Almost every introduction to neural networks includes a simplified nervous anatomy to demonstrate the resemblance to the human brain.

Neural nets have great potential applications in the area of speech processing and pattern recognition and multi-dimensional signal processing. These applications usually seek high parallelism and high computational costs. In recent years the technique of neural nets has been applied to other engineering problems including, but not limited to, wireless channel equalization and adaptive control.

Although there are early traces of neural nets in the literature by Widrow (1962) and Stark, et.al. (1962), the pioneering works by Rosenblatt (1962) deserve the distinction of being the first formal analysis of what was called perceptron analysis. These are actually adaptive linear combiners augmented by a nonlinear function block (See Figure 4-1.) Grossberg (1976) and later Carpenter and Grossberg (1983) developed adaptive resonance theory and the architecture that became known as self-organizing neural nets for pattern recognition. Hopfield (1982) created Hopfield models for the class of recurrent (feedback) networks, which in combination of an algorithm called back propagation demonstrated significant success in some applications. The development of the early neural network systems was taking place at the same time that other adaptive signal processing algorithms, in particular the attractive LMS algorithm, were successfully applied to many scientific and engineering problems (See Widrow and Stearns (1985)). Some disappointing experiences with this new concept (in addition to the fact that efforts to develop learning rules for neural networks with multiple layers were not successful) led to a conundrum in the research of this area for about a decade. Particularly, Minsky and Selfridge (1961) showed the inadequacy of perceptron methods, or more generally the single-layer network in cases where linear classifications were not possible. They suggested the use of Multi-Layer Perceptrons (MLP) that has nonlinear behavior. Minsky also gave a treatment of the subject in his 1969 textbook.

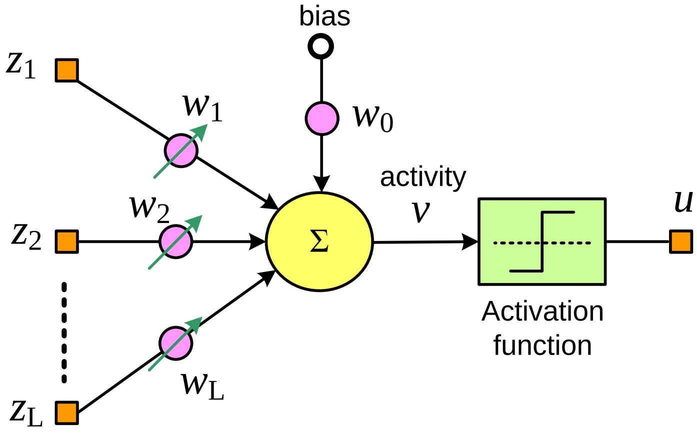

Figure 4-1 Basic perceptron architecture

So far, most neural nets have *feed forward* classifier architecture. A major advancement was made by Werbos (1974). Werbos proposed a *back propagation* learning algorithm which has become the most applied algorithm in many applications of neural nets including the signal processing application. His work remained unknown until Parker (1985) revitalized the back propagation algorithm in his MIT report. After the works by Parker and many others, the multilayer neural nets with some modifications to the architecture and the choice of activation function using back propagation have gained momentum in the research community. Specially, it has been employed for problems of channel equalization and system identification (see Botoca and Budura (2006), Chang, et.al. (2010), Chen and Mars (1991), Fang and Chow (1999), Feng, et.al. (2003), Kechriotis, et.al. (1994), Lee and Kim (2003), Li and Er (2008), Mo and Shafai (1994), Rui, et.al. (1999), Sarajedini and Hecht-Nielson (1992), Satapathy and Subhushini (2009), Xie and Leung (2005), and Zhang, et.al. (2010)).

Rumelhart, et.al. (1985, 1986) introduced the use of *sigmoid* function $\varphi(x) = \frac{1}{1+e^{-ax}}$ in place of the signum function ($sgn(.)$) that also was known as slicer or hard-limiter to modify the nonlinear activation. Overall, the idea of the combination of this back propagation learning algorithm with multilayer architecture has demonstrated great achievements in many applications.

We conclude this section by briefly mentioning some of the salient advantages of neural nets as compared to general linear adaptive filtering.

The first advantage of neural nets is obviously their massive parallel distributed structure that affords the network strong computing power. The second and unique advantage is what is known as generalization by which the neural nets are capable of learning. In simple words, a trained network can generate reasonably correct and expected outputs for the inputs that have not been encountered during the training process. Consequently, neural nets are capable of solving relatively complicated problems. In some large and hard-to-attack problems several networks are deployed, each having a specific task to perform, so that an appropriate structure for each network can be selected and configured.

Haykin (2009) has summarized the important features of common neural networks that are concisely given in the following.

- Nonlinearity: nonlinearity is the prominent feature of neural nets. Although a neural net can also be linear in design; however its distributed nonlinearity is used almost exclusively in most of the applications. In passing, we mention that nonlinear channels cannot be equalized adequately by a linear equalizer, and the neural net has becomes an essential option.

- Input-output mapping: supervised learning that is performed in adjusting the synaptic connection weights by applying a set of training inputs or examples, and computing the network error using the knowledge of the desired (expected) response. If a sufficient number of training inputs is exploited, and if the synaptic weights have reached stable and stationary values, we can say that the network has created an input-output mapping for the problem under investigation. It is an outstanding feature that unlike almost all other channel equalization methods no statistical assumptions about the possible input set are made.
- Adaptivity: neural nets have the capability to adapt their synaptic weights according to changes in the environment or inputs. Specifically, they can be retrained to perform an ongoing adaptation to respond to minor changes encountered.

There are other features such as fault tolerance and many more that will not fit in a concise introduction.

4.2 Fundamental Theory of Neural Networks

The credit for introducing the neural networks as we know them today goes to McCulloch and Pitts (1943) when they designed a simple model they called “neuron”. Nonetheless, the Rosenblatt perceptron (1958) became the main building block for various classes of neural networks that were designed and investigated in the second half of the last century.

The perceptron is a simple network similar to what is known as a linear combiner except for the addition of a constant input called *bias* and hard-limiter (signum function). The latter was replaced with other nonlinear functions such as sigmoid or hyperbolic tangent, etc. designated here by $\varphi(.)$ in different configurations and applications (see Figure 4-2).

The formulation by which the perceptron output u is computed is a simple summation sometimes referred to as activity v, and the application of a nonlinear function. These are given in the following equations for the k^{th} epoch or step (as the perceptron is being trained adaptively):

$$v[k] = \sum_{j=1}^{L} w_j[k]z_j + w_0 b \qquad (4-1)$$

$$u[k] = \varphi(v[k]) \qquad (4-2)$$

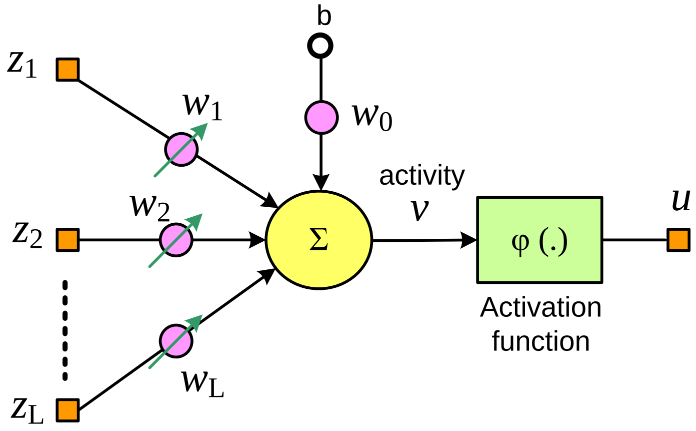

Figure 4-2 The perceptron architecture with general nonlinear activation function

Rosenblatt developed the learning algorithm to adjust (adapt) the free parameters that comprise the weights for what are called synaptic connections $w_j, j = 1, 2, \dots, L$ for a perceptron with L connections. An extra parameter w_0 can be used for the bias input connection that is usually constant with $b = -1$ in many designs. The bias is not always included as it might not be necessary for the perceptron performance and can be eliminated in certain applications.

This model was originally applied to the problem of classification of patterns, and so they were also called classifiers. They were proved to be successful in pattern classification when the sets of different patterns were linearly separable, say by a straight line in two-dimensional space or by a hyperplane in L-dimensional space. Rosenblatt (1962) provided the well-known "perceptron convergence theorem" that is also given by others with minor changes (see Haykin (2009), pp. 50). The simple perceptron equation consists of a linear combination of inputs or stimuli s_j and the bias that together generate activity $v = \sum_{j=1}^{L} w_j[k]z_j + w_0 b$. In the simple form the perceptron separates two classes of the stimuli by a hyperplane with the simple equation:

$$\sum_{j=1}^{L} w_j z_j + w_0 b = 0. \qquad (4-3)$$

The final decision in early perceptron applications was made by using a hard-limiter $u = sgn(v)$. The synaptic weights w_j of the perceptron can be iteratively adapted. The adaptation like any other adaptive algorithms requires first a method of computing the output error and then a method to make an appropriate correction to the weights according to the computed error.

It is the method designed for these two steps that creates many successful advanced network architecture and algorithms. The perceptron created on a single neuron has a very limited performance domain. It can separate only two linearly separable classes and is not capable of implementing more complicated and nonlinear functions. The network should be expanded to comprise more neurons and more layers containing similar neurons.

The natural option for further examination of neural network performance was to expand the network to employ more neurons and more layers comprising many more neurons. Additional neurons bring the capability to separate more classes (more than two) and the additional layers seemingly removes the linear separability constraint. Benefits come with the cost of more computation in addition to the complexity of error and correction formulation. The use of sigmoidal function $\varphi(x) = \frac{1}{1+e^{-ax}}$ and hyperbolic tangent $\varphi(x) = \frac{1-e^{-ax}}{1+e^{-ax}}$ were investigated in literature as the activation functions replacing hard limiter or threshold $\varphi(x) = sgn(x)$.

4.3 Network Architectures and Algorithms

In common neural network architectures, the neurons are grouped in the form of layers. Neurons in the same layer usually share the same set of inputs or stimuli. Networks with only one layer are known as single-layer feed forward (see Figure 4-2). Each neuron in the same layer generates an output, together these outputs can be applied to another layer of neurons as stimuli, and thus creating a two-layer feed forward networks. In general, adding more layers in general creates multilayer feed forward networks (see Figure 4-3). If the final outputs of the network are fed back to the network input layer the new configuration is known as *recurrent* (see Bradley and Mars (1994 and 1995)). It also justifies the ‘feed forward” modifier for non-recurrent networks.

Important parameters and features that distinguish the modern neural net architectures are the choice of activation function $\varphi(.)$, the rule by which the output error in each step or epoch $e[k]$ is determined, and the corresponding correction applied to the weights in each layer in an adaptive method. The networks are divided into two categories based on the output error calculations, *supervised* nets in which the exact required or expected output is available to the network, and *unsupervised* or *blind* nets when this information is not available. The present neural network architectures applied to the channel equalization problem are similar to those typically used in various other applications in the spirit of the theorem by Hecht-Nielson (1987) that states: “Any continuous function in a closed interval can be approximated by back propagation neural network with one hidden layer.”

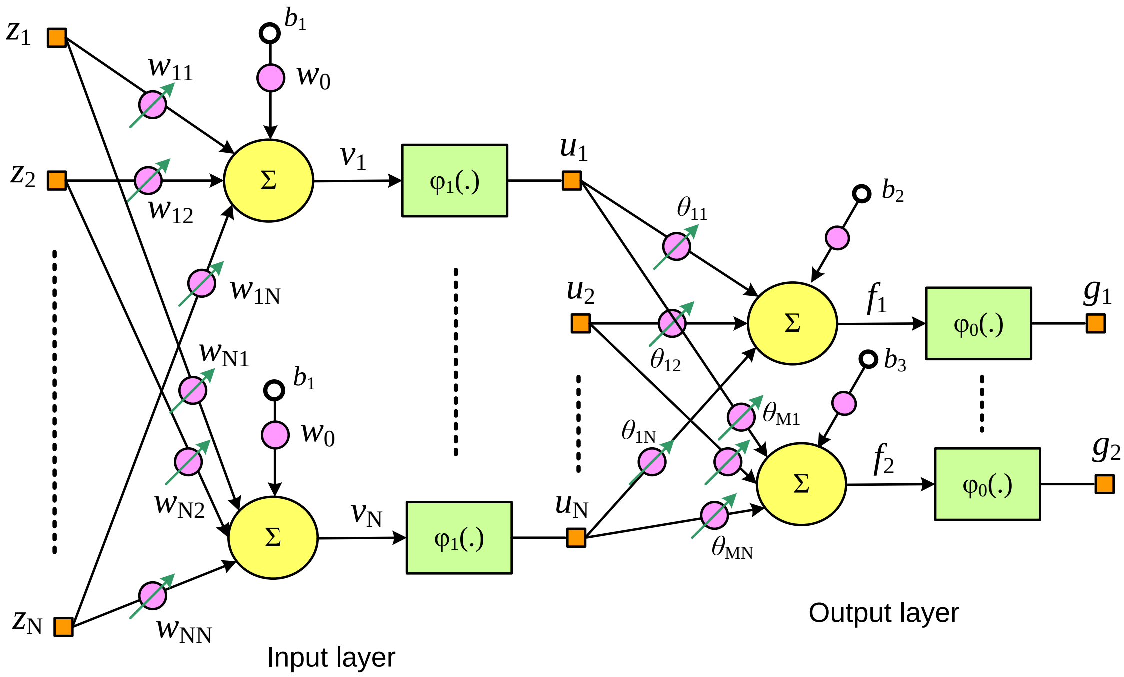

Figure 4-3 A multilayer perceptron example of two layer model with *N* neurons in the input and *M* neurons in the output layer

The Back Propagation Algorithm

One major reason for the popularity of adaptive supervised training of multilayer perceptrons or neural nets in general is the development of back propagation algorithm on recurrent networks. The development of back propagation algorithm is credited to Rumelhart and McClelland (1986) in their book “Parallel Distributed Processing”. Their development has thwarted the Minsky and Papert (1969) argument of multilayer networks deficiency.

Based on the back propagation algorithm the network operates in two major phases. Phase one is forward propagation in which the ultimate output error of the current step is computed based on current synaptic weight values in each layer from the very input of the network layer-by-layer toward the output. In second phase or back propagation the gradient of error surface with respect to weights in each layer is computed from the output of the network backward toward the input layer and is used for updating the weights of each neuron synaptic connections in each layer. This is also the kernel of what we know as stochastic approximation (see chapter 2). It can be said that the success of the back propagation method has revitalized the study and application of neural networks.

Radial-Basis Function Networks

Cover's theorem (1965) is often referred to as the incentive for designing multi-layer neural networks for the case of classes that are not linearly separable. This is in fact a different approach compared to back propagation for solving the classification problem of nonlinearly separable patterns. The two phase operations are modified so that in the first a transformation is adopted to convert a set of nonlinearly separable patterns into a possibly linearly separable set. The justification for this attempt is supported by the Cover's theorem. The second phase is dedicated to find the solution to the problem in the least-squares sense.

The radial-basis functions (RBF) are used for the nonlinear transformation for the sets that possess spherical symmetry in relatively high-dimensional inputs and hidden layer networks.

The RBF are the functions that have spherical symmetry are generally in the form of $\varphi\left(\left\|\boldsymbol{z}-\boldsymbol{z}_j\right\|^2\right)$ for $j = 0, 1, \dots, N-1$, when z_j are the inputs to the network and the corresponding activation function

$$f(\boldsymbol{z}) = \sum_{j=0}^{N-1} w_j \varphi\left(\left\|\boldsymbol{z}-\boldsymbol{z}_j\right\|^2\right). \qquad (4-4)$$

The Gaussian function $\varphi(\boldsymbol{z}) = \exp\left(\left\|\boldsymbol{z}-\boldsymbol{z}_j\right\|^2\right)$ is often tested in many applications (see for examples Botoca and Budura (2006), Sarajedini and Hecht-Nielson (1992)).

Self-Organizing Maps

Like many other advanced neural nets, self-organizing nets are also employed in pattern recognition and image processing. These nets bear some resemblance to the human brain in sensory systems. The self-organizing map is based on a technique known as competitive learning. There is only one winner neuron of the output layer or other groups of neurons in competitive learning. The winner neuron will be relocated topologically in an ordered manner with respect to other neurons in the same layer.

The concept of neural network has explored many regions of adaptive systems and learning processes.

There are more versions of networks that are not mentioned in this chapter, each demonstrating some advantages in certain applications. The use of fuzzy logic in neural nets for example has received special attention and several research documents have been published for this case (see Kosko's book (1992): Neural Networks and Fuzzy Systems).

4.4 A Novel Neural Network as a Wireless Channel Equalizer

There are many research papers that agree on the fact that linear transversal equalizers are not capable of equalizing highly nonlinear channels. Gibson et.al (1989) has explicitly mentioned that: "When the channel is non-minimum phase, the decision boundary of equalizer is highly nonlinear and deviates markedly from any decision boundary which can be formed by a linear transversal equalizer."

In searching for a neural network architecture suitable for equalizing an unknown wireless channel a reasonable choice would be a multi-layer network and the use of the back propagation algorithm in a common gradient descent adaptation.

The baseband binary data channel models with the assumptions in chapter 2 are considered. The hyperbolic tangent activation function is adequate for binary data system and the bias input connection in each neuron is eliminated.

We decided to try supervised training with the hope of obtaining very fast convergence and significant reduction in the training period (see section 4.6), as blind training does not seem promising in speed and simplicity (See Zhang, et.al. (2010), Xie and Leung (2005).)

Figure 4-4 shows the block diagram of the proposed neural network (Kumar and Jalali (2012)). As shown in the figure, the sequence of symbols is input to an unknown channel. The output of the channel is corrupted by noise. The noisy channel output is inputted to the neural network adaptive equalizer through a tapped delay line of length M. The outputs of the tapped delay line are segmented into a number of S groups such that each adjacent group may possibly have some amount of overlap among their elements with each group of the tapped delay line outputs connected to a neuron. Thus the number of neurons S and the total number of synaptic connections is dependent on the length of the delay line, the amount of overlap among the various groups and the number of elements in each group. The computational complexity is determined by the total number of synaptic connections in the network and thus reduced overlap among the various groups' results in relatively reduced computational complexity but may possibly result in relatively reduced convergence rate. Consequently, there may be a trade-off between t computational complexity and the rate of convergence via the length of the tapped delay line M, the number of neurons S, and the number of synaptic connections to each neuron L.

Each group of the delay line outputs along with its associated neuron has a structure similar to that of a linear equalizer except that the nonlinear activation function operating in the neuron replaces the decision function of the linear equalizer.

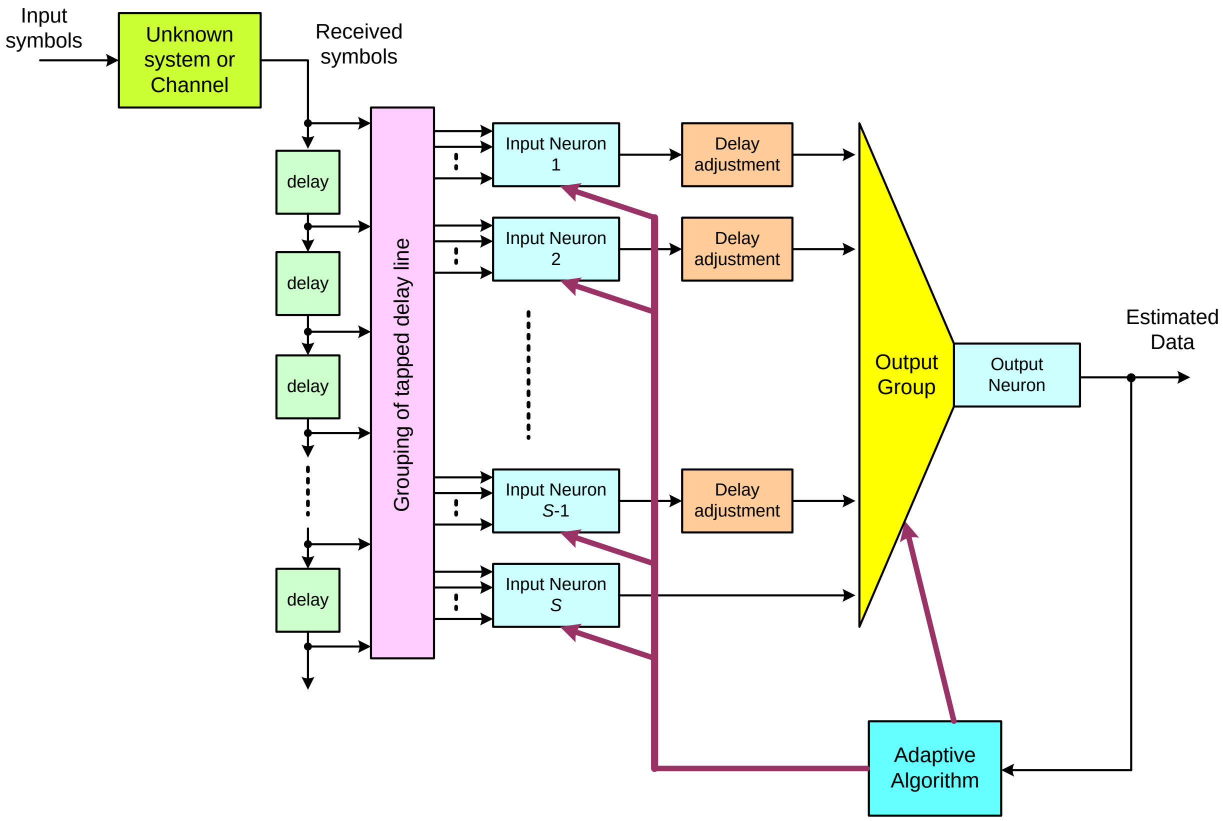

Figure 4-4 Proposed neural network equalizer architecture

Figure 4-5 shows the detailed diagram of the neural network equalizer architecture. In this figure $z[k]$ denotes the sampled noisy channel output that is inputted to the tapped delay line with the number of taps equal to $M = (S-1)\ell + L$ with ℓ denoting the offset in terms of the indices of the tapped delay line outputs connected to the adjacent neurons. The grouping block segments the M outputs of the tapped delay line into a number of S groups such that the adjacent group has some overlap of $(L-\ell)$ elements among its elements with each group of the tapped delay line outputs connected to a neuron. The number of connections to each neuron is equal to L, resulting in $M = (S-1)\ell + L$ total samples fed into the network.

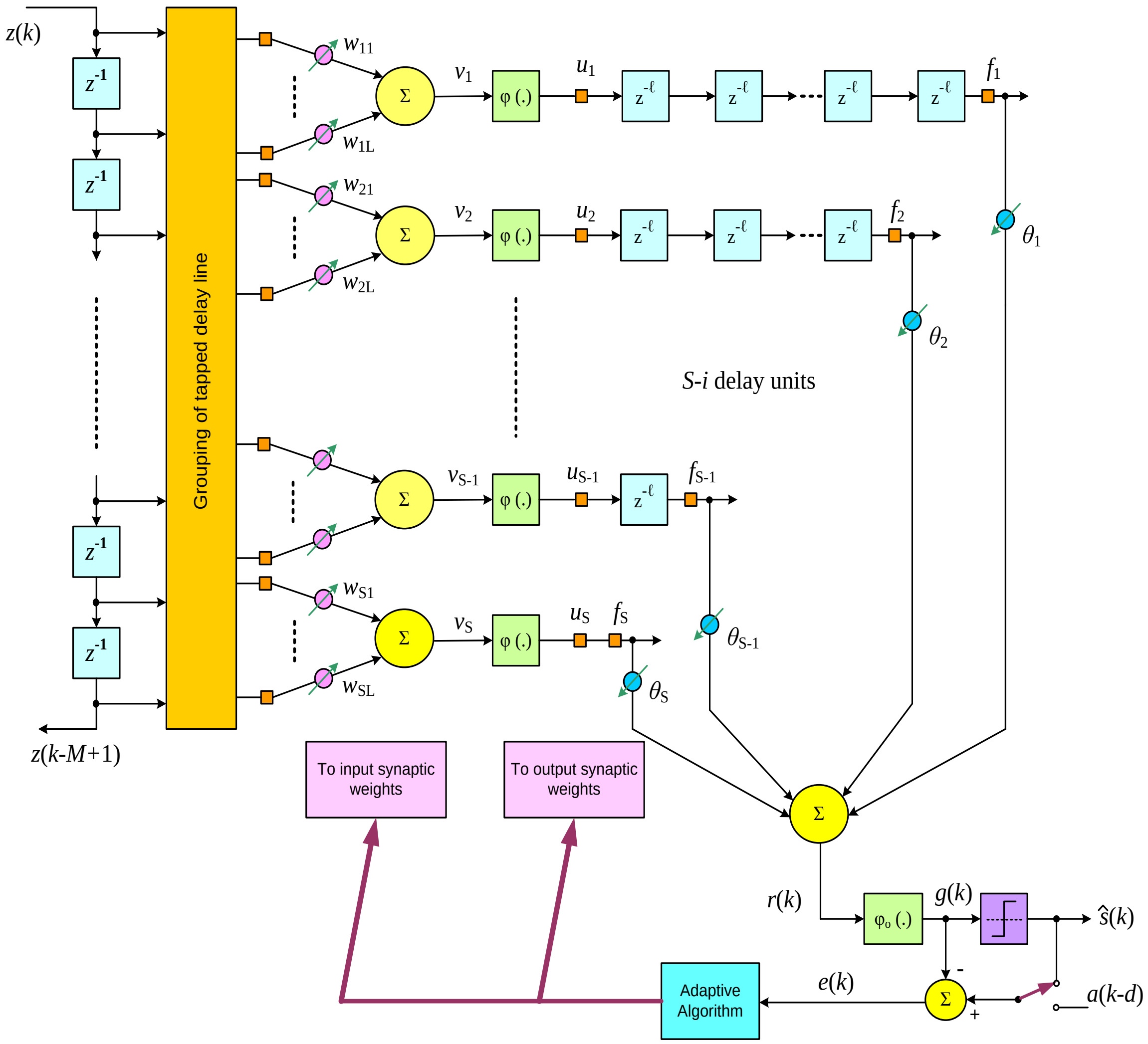

Figure 4-5 Detailed block diagram of the proposed neural network based adaptive equalizer

Thus the first neuron is inputted with $z[k], z[k-1], \ldots, z[k-L+1]$, the second neuron inputs are given by $z[k-\ell], z[k-\ell-1], \ldots, z[k-\ell-L+1]$, with the last neuron input given by $z[k-M+L], z[k-M+L-1], \ldots, z[k-M+1]$. The special case of $L=\ell$ corresponds to no overlap among the inputs to the various neurons while the case of $\ell=0$ corresponds to the case where all of the tapped delay line outputs are connected to each neuron as in the previous architectures.

In terms of the computational complexity of the proposed equalizer, the number of neurons *S* in the input layer is given by $S = \frac{M-L}{\ell} + 1$. Thus, for a selected length of the delay line *M* and the number of inputs L to each neuron, the number of neurons *S* is minimized by maximizing the offset ℓ.

From the results for the linear equalizer it is known that the performance in terms of the residual ISI is increased with an increase in *M*. Thus, intuitively increasing *M* would also result in increased performance of the neural network-based equalizer. Also, it is expected that a higher value of *L* would result in better performance. Although the performance will also depend upon the number of neurons *S*, the dependence of the performance on *S* will be relatively less when every neuron is processing all or most of the inputs. The number of synaptic connections in the first layer is given by $SL = L + (M - L)\left(\frac{L}{\ell}\right)$ and is equal to M for $\ell = L$. In comparison to this, in previous neural network equalizer architectures, the number of neurons S_p is selected independently of *M;* thus the number of synaptic connections is equal to MS_p showing at least in intuitive terms that the proposed architecture can have much less computational requirements for similar level of performance. Moreover, the previous neural network based equalizer architectures also have hidden layers of neurons that further increase the computational requirements. The proposed architecture does not have any hidden layer. In the proposed architecture, the absence of hidden layer is compensated by the introduction of delay adjustments in the outputs of the neurons in the first layer before being connected to the output neuron. The functions $\varphi(.)$ in Figure 4-5 may be the *sigmoidal*, *hyperbolic tangent* or any other similar function.

As shown in Figure 4-5, the i^{th} neuron output u_i is delayed by $(S - i)\ell$ samples for $i = 1, 2, \ldots, S$. Each group of delay line outputs (along with its associated neuron) has a structure similar to that of a linear equalizer, except that the nonlinear function operating in the neuron replaces the decision function of the linear equalizer. Thus the output of the *S* neurons may be considered to be different versions of the equalized output, except that there is a relative delay among the various outputs. This is in view of the fact that the inputs to the other neurons are the delayed versions of each other. Therefore as shown in Figure 4-5, with an introduction of the appropriate delays among the output to various neurons, the relative delays introduced by the input tapped delay line are equalized and the various neuron outputs have a cumulative effect, achieving a similar effect when different neurons all are inputted with exactly the same inputs but with much reduced computational complexity. As shown in Figure 4-5, the delayed versions $f_1, f_2, \dots, f_S$ of the outputs of the neurons $u_1, u_2, \dots, u_S$ in the input layer are inputted to the single neuron in the output layer with weights $\theta_1, \theta_2, \dots, \theta_S$. The output $g[k]$ of the neuron in the output layer is input to the decision device whose output $\hat{s}[k]$ is equal to $\mathrm{sgn}(g[k])$ with $\mathrm{sgn}(.)$ denoting the *signum* function. During the initial training phase, the equalizer error signal is $e[k] = a[k-d] - g[k]$ where $a[k]$ denotes the symbol at the input of the channel and d denotes the sum of delays introduced by the channel and the equalizer. After the initial phase, $a[k-d]$ is replaced by $\hat{s}[k]$, as shown in Figure 4-5. The equalizer error $e[k]$ is input to the adaptive algorithm block that updates the weights of the various neurons in the neural network adaptive equalizer. Section 4.5 describes the adaptive learning algorithm for the neural network.

4.5 Learning Algorithm

For the neural network of Figure 4-5, the nonlinear activity function $\varphi(.)$ is selected to be the hyperbolic tangent function $\tanh(.)$. The equations for the forward propagation of the signal through the network are derived for this activity function. The back propagation algorithm is used to determine the local and complete gradients required for updating the input and output layer synaptic weights as given in the following sections.

Forward propagation

Forward propagation can be performed by starting to compute the S activation functions of the input layer neurons, each having L weighted synaptic connections. At the k^{th} iteration or epoch of the adaptive algorithm, one obtains:

$$v_i[k] = \sum_{j=1}^{L} w_{ij}[k]z[k-(i-1)\ell - j + 1] \quad , i = 1, 2, \dots, S \qquad (4-5)$$

The appropriate activation function employed is the hyperbolic tangent function, thus the outputs $u_i(k)$ of the neurons in the input layer are given by:

$$u_i[k] = \tanh(v_i[k]), \qquad i = 1, 2, \dots, S \qquad (4-6)$$

As may be observed from Figure 4-5 there is no *bias* or *input threshold* present for any neuron in the input and output layers of the network. The outputs of the first layer are delayed so that they convey the information about the channel and the data symbols that belong to the same time slot, in other words they are adjusted to be concurrent with respect to the output of the farthest (most delayed) neuron in the input layer. These delayed outputs are computed as follows.

$$f_i[k] = u_i[k-(S-i)\ell], \qquad i = 1, 2, \dots, S \qquad (4-7)$$

The signals $f_1[k], f_2[k], \dots, f_S[k]$ are inputted to the output layer that possesses only one neuron. It may be observed that no hidden layer is incorporated in the neural network of Figure 4-5. The output layer activity is computed as $r[k] = \sum_{n=1}^{S} \theta_n[k] f_n[k]$ and using the same activation function as for the input layer. Thus the output of the neural network is obtained by $g[k] = \tanh(r[k])$.

The final estimate for the case of binary data $\hat{s}[k] = \text{sgn}(g[k])$ is the estimate of the channel delayed input $a[k]$, i.e., when appropriately converged in supervised mode $\hat{s}[k] = a[k-d]$ and the error $e[k]$ is applied for the learning algorithm and is given by:

$e[k] = a[k-d] - g[k]$ in training mode,

$e[k] = \hat{s}[k] - g[k]$ in decision-feedback mode.

The weights of the various synaptic connections in the network are iteratively adjusted on the basis of the error $e[k]$ using the back propagation algorithm as follows.

Back propagation: Output layer

The objective function for optimization of the equalizer performance is defined as $\mathcal{J}[k] = \frac{1}{2}\mathbb{E}\{e^2[k]\}$ where $e[k] = \hat{s}[k] - g[k]$ is the estimation error and $\mathbb{E}$ represents expectation. Notice that in the short training mode $e_T[k] = a[k-d] - g[k]$ is the actual error.

The computation of the total gradient for the update equations of the output layer weight vector is summarized in the following:

$$\frac{\partial \mathcal{J}[k]}{\partial \theta_i} = \mathbb{E}\left\{e[k]\frac{\partial e[k]}{\partial \theta_i}\right\} \qquad (4-8)$$

The application of the output *local gradient* denoted by δ_o that is defined in the following simplifies the equation for complete gradients:

$$\delta_o[k] = \frac{\partial e[k]}{\partial g[k]}\frac{\partial g[k]}{\partial r[k]} \qquad (4-9)$$

$$\frac{\partial e[k]}{\partial \theta_i} = \frac{\partial e[k]}{\partial g[k]}\frac{\partial g[k]}{\partial r[k]}\frac{\partial r[k]}{\partial \theta_i} = \delta_o(k) f_i(k)\,, \;\; i = 1,2,\ldots,S \qquad (4-10)$$

The local gradient for the output neuron is computed as

$$\delta_o[k] = -(1 - \tanh^2 r[k]) = -(1 - g^2[k])\,. \qquad (4-11)$$

Therefore the stochastic gradient algorithm for updating synaptic weights of the output layer is:

$$\theta_i[k+1] = \theta_i[k] - \eta_1 e[k]\frac{\partial e[k]}{\partial \theta_i} =$$

$$\theta_i[k] + \eta_1 e[k](1 - g^2[k])f_i[k]\,;\, i = 1, 2, \dots, S \quad (4-12)$$

In the last equation η_1 is the step size or learning rate for the output weight vector update equation.

Back propagation: Input layer

In the following, the equations for adaptation of the weights are derived first for the case without the delay adjustment. The adaptations equations pertaining to the case with delay adjustment are presented subsequently.

In the first case of no delay adjustment, the inputs to the output layer neuron are given by $f_i[k] = u_i[k], i = 1, 2, \dots, S$ and the derivatives of the objective function $\mathcal{J}[k]$ with respect to the weights w_{ij} are evaluated as

$$\frac{\partial \mathcal{J}[k]}{\partial w_{i,j}} = \mathbb{E}\left\{e[k]\frac{\partial e[k]}{\partial w_{ij}}\right\} \qquad (4-13)$$

$$\frac{\partial e[k]}{\partial w_{ij}} = \frac{\partial e[k]}{\partial g[k]}\frac{\partial g[k]}{\partial r[k]}\frac{\partial r[k]}{\partial f_i[k]}\frac{\partial f_i[k]}{\partial v_i[k]}\frac{\partial v_i[k]}{\partial w_{ij}} \qquad (4-14)$$

The local gradients for the input layer neurons $\delta_i[k]$ are defined by the equation in (4-14) that makes use of the output layer local gradient $\delta_o[k]$.

$$\delta_i[k] = \frac{\partial e[k]}{\partial g[k]}\frac{\partial g[k]}{\partial r[k]}\frac{\partial r[k]}{\partial f_i[k]}\frac{\partial f_i[k]}{\partial v_i[k]} \qquad (4-15)$$

$$\delta_i[k] = \delta_o[k]\frac{\partial r[k]}{\partial f_i[k]}\frac{\partial f_i[k]}{\partial v_i[k]} \qquad (4-16)$$

In (4-16) $\partial r[k]/\partial f_i[k] = \theta_i[k]$ and $\partial f_i[k]/\partial v_i[k] = \partial u_i[k]/\partial v_i[k]$ with

$$\frac{\partial u_i[k]}{\partial v_i[k]} = 1 - \tanh^2 v_i[k] = 1 - u_i^2[k] \qquad (4-17)$$

Thus

$$\frac{\partial f_i[k]}{\partial v_i[k]} = 1 - f_i^2[k]. \qquad (4-18)$$

Substitution of (4-18) in (4-16) results in

$$\delta_i[k] = \delta_o[k]\theta_i[k]\left(1 - f_i^2[k]\right) \qquad (4-19)$$

The last term in (4-14) is given by

$$\frac{\partial v_i[k]}{\partial w_{ij}} = z[k - (i-1)\ell - j + 1] \qquad (4-20)$$

The Equation (4-20) follows directly from (4-5). With the substitution of (4-16) to (4-20) in (4-14), one obtains the derivative of $e[k]$ with respect to w_{ij} as:

$$\frac{\partial e[k]}{\partial w_{ij}} = \delta_o[k]\theta_i[k]\left(1 - f_i^2[k]\right) z[k - (i-1)\ell - j + 1] \qquad (4-21)$$

For $i = 1, 2, \dots, S$ and $j = 1, 2, \dots, L$.

Further, the output layer local gradient from (4-9) is given as:

$$\delta_o[k] = -(1 - g^2[k]) \qquad (4-22)$$

With the proposed delay adjustments the input signals to the output layer neuron are given by $f_i[k] = u_i[k - (S-i)\ell]$ for $i = 1, 2, \dots, S$. One starts with the following equation:

$$\frac{\partial \mathcal{J}[k]}{\partial w_{ij}} = \delta_o[k]\frac{\partial r[k]}{\partial f_i[k]}\frac{\partial f_i[k]}{\partial v_i[k-k_0]}\frac{\partial v_i[k-k_0]}{\partial w_{ij}} \qquad (4-23)$$

In (4-23) $k_o = (S-i)\ell$. Similar to the first case of no delay adjustments, in this case one also obtains $\partial r[k]/\partial f_i[k] = \theta_i[k]$ for the first partial derivative on the right hand side of (4-23). The other partial derivatives in (4-23) are taken as follows:

$$\frac{\partial f_i[k]}{\partial v_i[k-k_0]} = 1 - \tanh^2 v_i[k-(S-i)\ell] = \ 1 - u_i^2(k-(S-i)\ell) = 1 - f_i^2(k) \qquad (4-24)$$

$$\frac{\partial v_i[k-k_0]}{\partial w_{ij}} = \ z[k-(i-1)\ell - j + 1 - (S-i)\ell] = z[k-(S-1)\ell - j + 1] \qquad (4-25)$$

It may be noted that the last expression in (20) is independent of input layer neuron index i, and this independence can make the computations somewhat faster. Substitution of (4-24) and (4-25) in Equation (4-23) yields:

$$\frac{\partial e[k]}{\partial w_{ij}} = \delta_o[k]\theta_i[k]\big(1 - f_i^2[k]\big)\, z[k-(S-1)\ell - j + 1]. \qquad (4-26)$$

The stochastic gradient based update equations for adjustment of the synaptic weights for the input layer neurons may be generally written as:

$$w_{ij}[k+1] = w_{ij}[k] - \eta_2 e[k]\frac{\partial e[k]}{\partial w_{ij}}. \qquad (4-27)$$

The use of (4-26) in Equation (4-27) results in the following adaptive algorithm for the adjustment of the weights of the synaptic connections of the input layer in the neural network:

$$w_{ij}[k+1] = w_{ij}[k] + \eta_2 e[k](1-g^2[k])\theta_i[k]\big(1-f_i^2[k]\big)z[k-(S-1)\ell - j + 1] \quad (4-28)$$

For $i = 1,2,\dots,S; j = 1,2,\dots,L$. In (4-28) the constant η_2 is the step size or learning rate for input layer neurons.

The simulation results of the following section show that not only the update formula (4-28) is somewhat faster because each update equation includes the same input symbol set due to the independence from the neuron index i, but also it makes a very significant difference in the convergence time for all the channels considered for simulations.

4.6 Performance and Simulation Results for the Proposed Network

In order to evaluate the performance of the neural network equalizer of section 4.4, three different non-minimum phase channels are examined. These channels have been used in the previously published literature and are considered to be more difficult to equalize. The performance is evaluated in terms of the mean square error (MSE) computed by a simple average of the square of the true equalization error $e_T[k] = a[k-d] - g[k]$ over a moving window of size 50.

The first simulated channel has the impulse response:

$$h = [0, 0.0361, -0.0488, 0.0170, 0.8908, 0.4454, 0.0636]$$

with norm $\|h\| = 1$. The corresponding transfer function is given by:

$$H(z) = 0.0361z^{-1} - 0.0488z^{-2} + 0.017z^{-3} + 0.8908z^{-4} + 0.4454z^{-4} + 0.0636z^{-5}$$

The transfer function in this case has zeros located at $3.2672e^{\pm j51}, -2.2635,\ 0.2703e^{\pm j160}$ with the phases shown in degrees. Only 40 steps or epochs are used for training including the delay, the input layer is selected to have $S = 9$ neurons, each having $L = 11$ synaptic connections, the offset $\ell = 1$, and the symbol bit energy to noise spectral density ratio $\frac{E_b}{N_o} = 11$ dB. The step sizes for the input and the output layer adaptations are $\eta_2 = \eta_1 = 0.10$, that are changed to $\eta_2 = \eta_1 = 0.03$ after the initial convergence, the overall network delay between the network estimate and the channel input data is set to $d = 14$.

Figure 3 shows the instantaneous actual error $e_T[k]$ from the very beginning of the transmission. The first 14 network data estimates $\hat{s}[k]$ of the network have not been used due to the overall delay of the channel and the network. Note however that the azimuth axis for Figures 3–6 show the number of symbols including those in the delay period of 14 symbols.

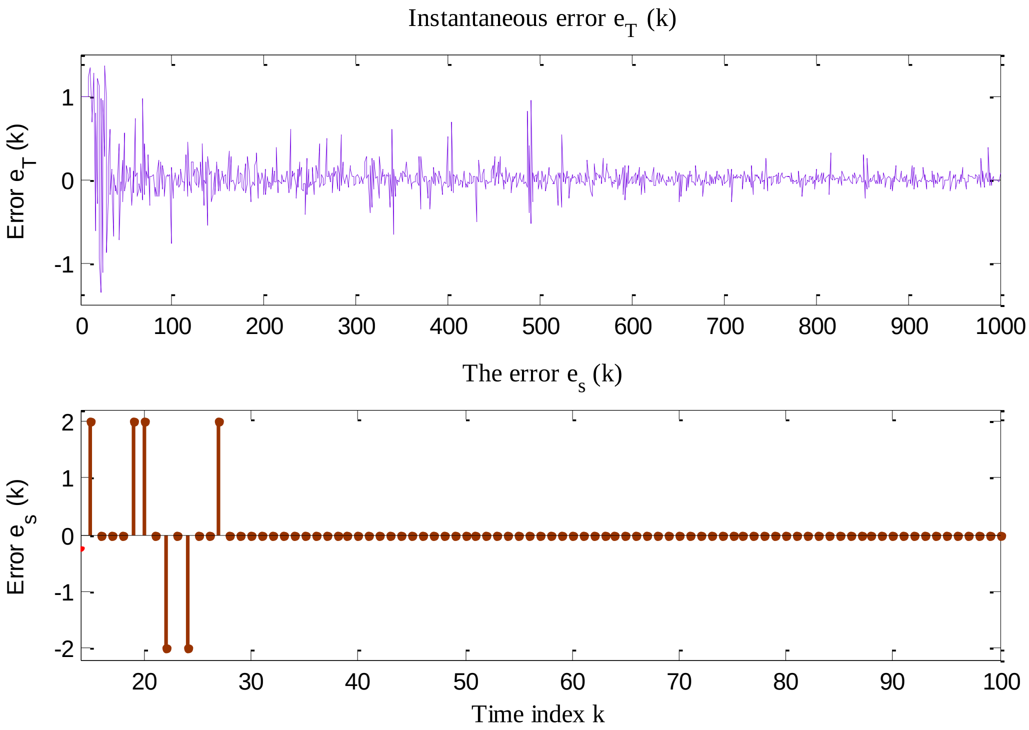

Figure 4-6 Instantaneous error (top) and the bit errors that have occurred during the adaptation process (bottom).

Figure 4-6 indicates the mean square error for this channel simulation over a period of the first 1000 iterations.

There are only a total of 6 bit errors in the whole process. The data bit error figure is zoomed in to the first 100 steps because no further bit error occurs for another 2000 bits of data exchanged. Figure 4-7 plots the mean squared error plotted over a period of first 1000 bits.

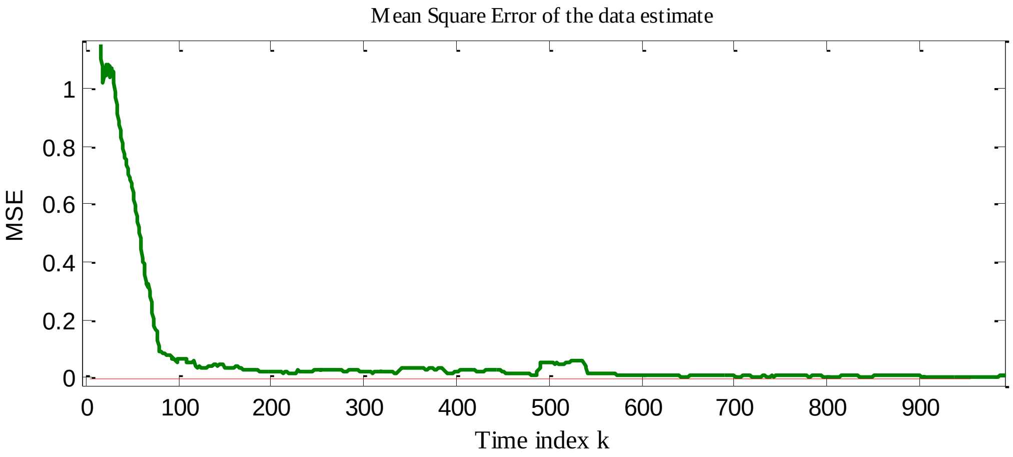

Figure 4-7 Mean Square Error (MSE) averaged over a moving window of 50 steps

The second channel has been taken from Bradley and Mars (1995) and the impulse response of the channel is $h = [-0.2052\,, -0.5131, 0.7183, 0.3695, 0.2052]$ with norm $\|h\| = 1$.

The corresponding transfer function is given by:

$$H(z) = -0.2052 - 0.5131z^{-1} + 0.7183z^{-2} + 0.3695z^{-3} + 0.2052z^{-4}$$

The transfer function has zeros located at $-3.3998,\ 1.3765,\ 0.4623e^{\pm j121}$; and thus the transfer function is of composite minimum and non minimum phase type.

In this case 80 steps or epochs have been used for training including the delay; the input layer is selected to have $S = 9$ neurons, each having $L = 11$ synaptic connection weights, the offset $\ell = 1$, and the symbol bit energy to noise spectral density ratio is $\frac{E_b}{N_o} = 8$ dB. The step sizes for the input and output layer adaptations are $\eta_2 = \eta_1 = 0.15$, that are changed to $\eta_2 = \eta_1 = 0.05$ after convergence; the overall network delay between the network estimate and the channel input data is set to $d = 15$.

Figure 4-8 shows the instantaneous actual error $e_T[k]$ from the start of the transmission and the data error that occurred from the very beginning of the transmission. Obviously the first 15 network data estimates $\hat{s}[k]$ of the network have not been used due to the overall delay. Figure 4-9 plots the mean square error for this case.

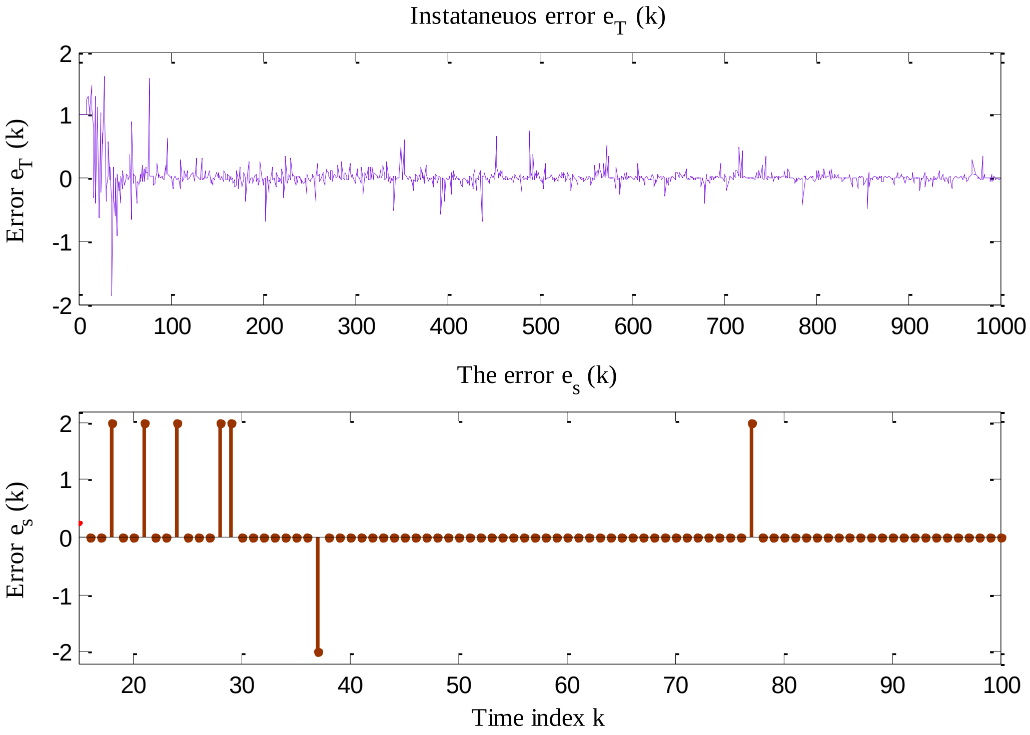

Figure 4-8 Instantaneous error (top) and the only bit errors that have occurred during the adaptation process (bottom).

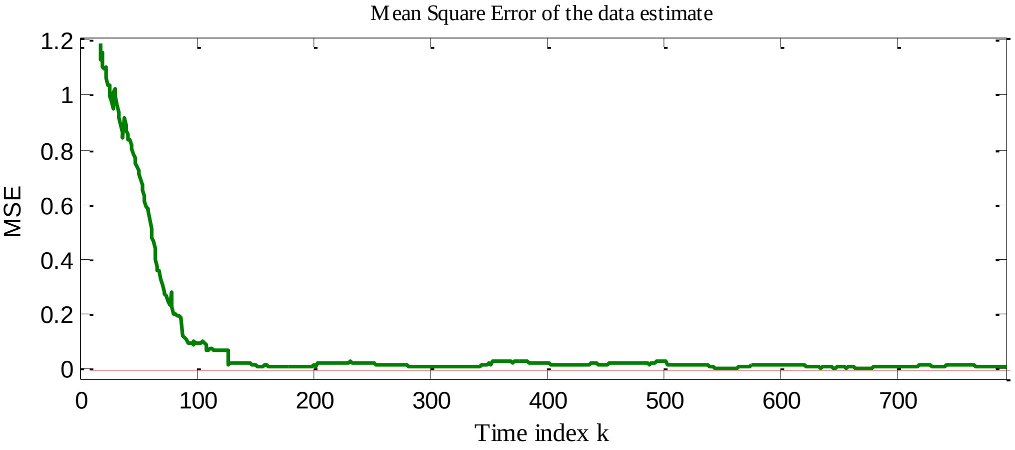

Figure 4-9 Mean Square Error (MSE) averaged over a moving window of 50 steps

There are only a total of 7 bit errors. The data bit error figure is zoomed in the first 100 steps because no further bit error occurs for another 2000 bits of data exchanged.

To show the effect of removing the delay adjustments we use the last example and give the same performance graphs when everything else has been kept constant except for the delays. This change simplifies equation (4-7) to $f_i[k] = u_i[k]$; $i = 1, 2, \dots, S$. Figure 4-10 shows significant deterioration in the performance as seen from $e_T[k]$ versus the input symbol number k from the very beginning of the transmission and the error $e_s[k] = a[k-d] - \hat{s}[k]$ versus the symbol number k for the case when the delay adjustments have been removed.

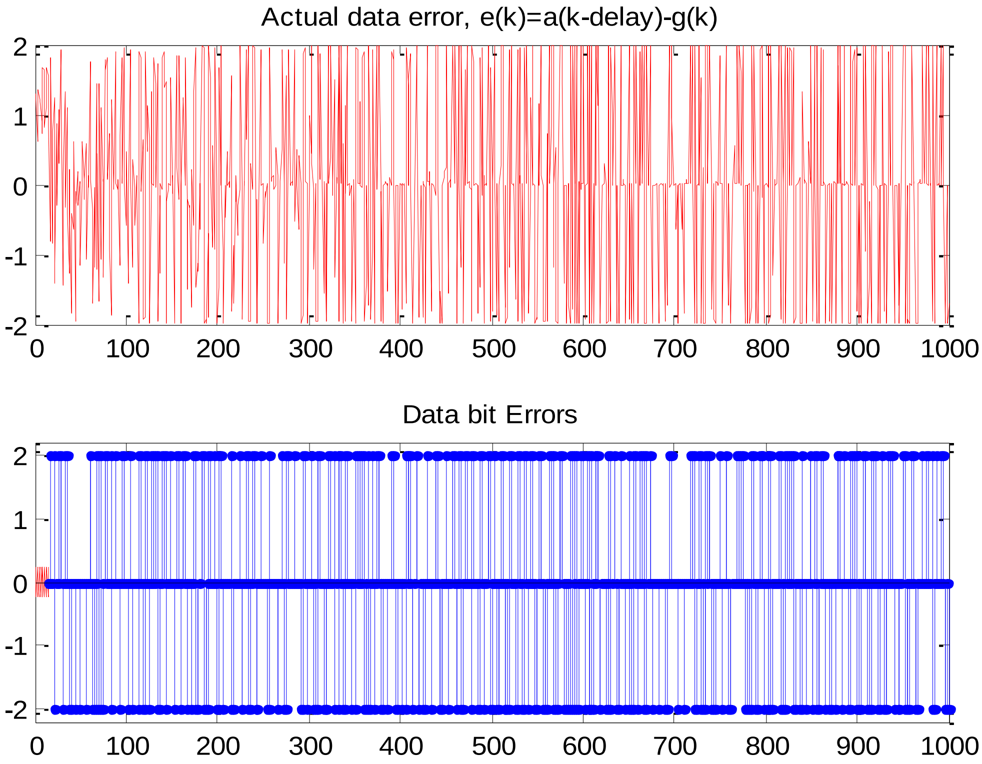

Figure 4-10 Instantaneous error (top) and the bit errors for the case without the delay adjustments (bottom).

Figure 4-11 plots the mean square error for this case.

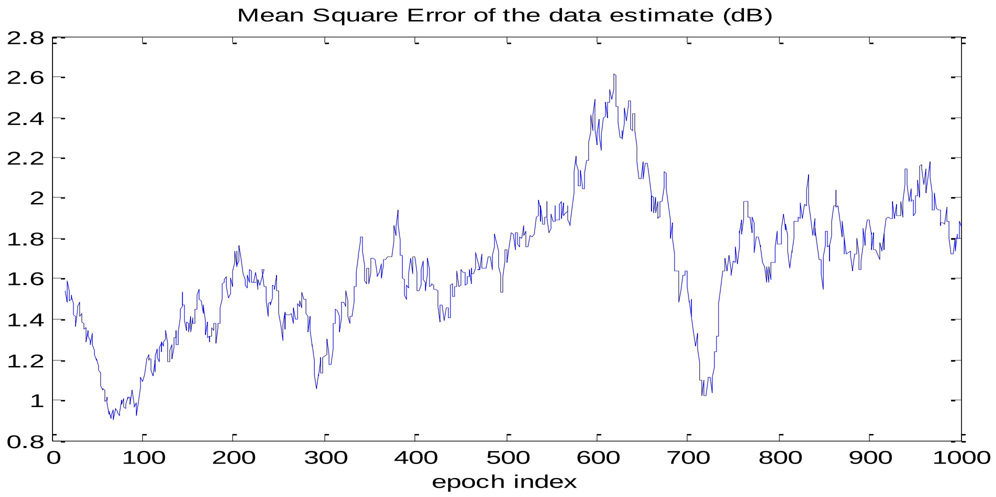

Figure 4-11 Mean Square Error (MSE) without the delay adjustments

Increasing the training period to 100 data bits or steps will still result in a converged equalizer as shown in Figure 4-12. It seems that the delays have shortened the training period for this example.

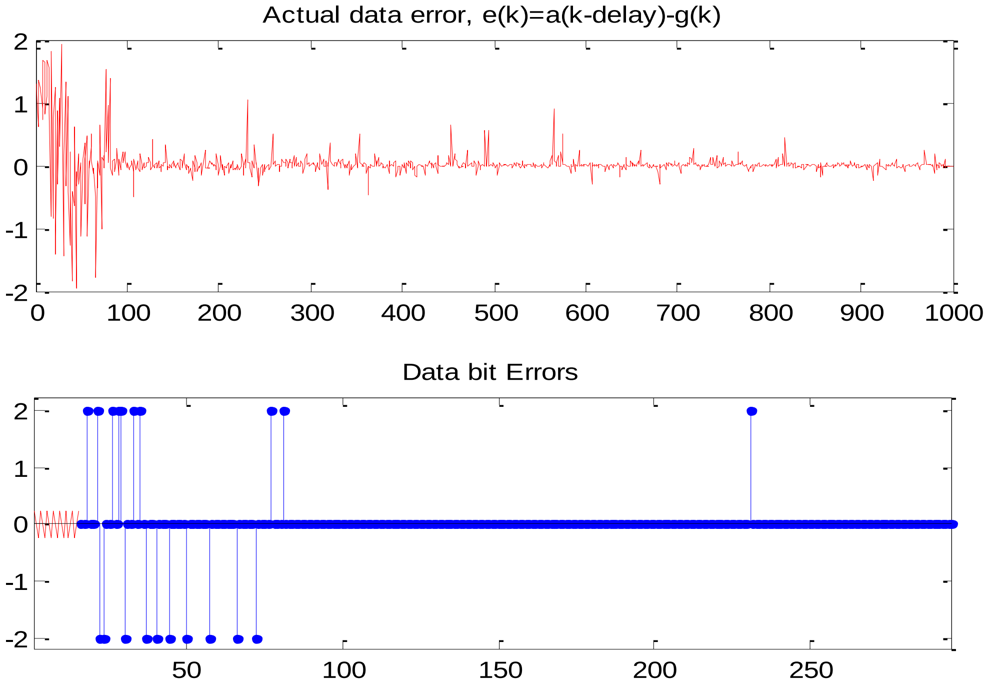

Figure 4-12 Instantaneous error (top) and the bit errors (bottom) for the case without the delay adjustments after increasing the training period from 40 to 100 steps.

The third channel has been used by Chang, Yang, and Ho [17] and has the impulse response $h = [0.3482, 0.8704, 0.3482]$ with norm $\|h\| = 1$.

The corresponding transfer function is given by

$$H(z) = 0.384 + 0.870z^{-1} + 0.384z^{-2}$$

The final channel is created by the sum $H_a(z) = H(z) + 0.2H^2(z)$ with $H(z)$ given by the above equation. Thus the final transfer function turns out to be:

$$H_a(z) = 0.3724 + 0.9916\mathrm{z}^{-1} + 0.5481\mathrm{z}^{-2} + 0.1212\mathrm{z}^{-3} + 0.0242z^{-4}.$$

The transfer function zeros are located at $-2, -0.5,\ 0.2551e^{\pm j108}$ and have relatively wide distribution in magnitude. In this case 80 steps or epochs have been used for training including delay; the input layer is selected to have $S = 9$ neurons, each having $L = 11$ synaptic connection weights, the offset $\ell = 1$, and the symbol bit energy to noise spectral density ratio is $\frac{E_b}{N_o} = 17$ dB. The step sizes for the input and output layer adaptations are $\eta_2 = \eta_1 = 0.10$, that are changed to $\eta_2 = \eta_1 = 0.03$ after initial convergence; the overall network delay between the network estimate and the channel input data d is set to 16.

Figure 4-13 shows the instantaneous actual error among the channel input data and the network output (to the decision device) $g[k]$ and the data error that occurred from the very beginning of the transmission. Obviously the first 16 data estimates $\hat{s}[k]$ of the network have not been used due to the overall delay of the channel and the network.

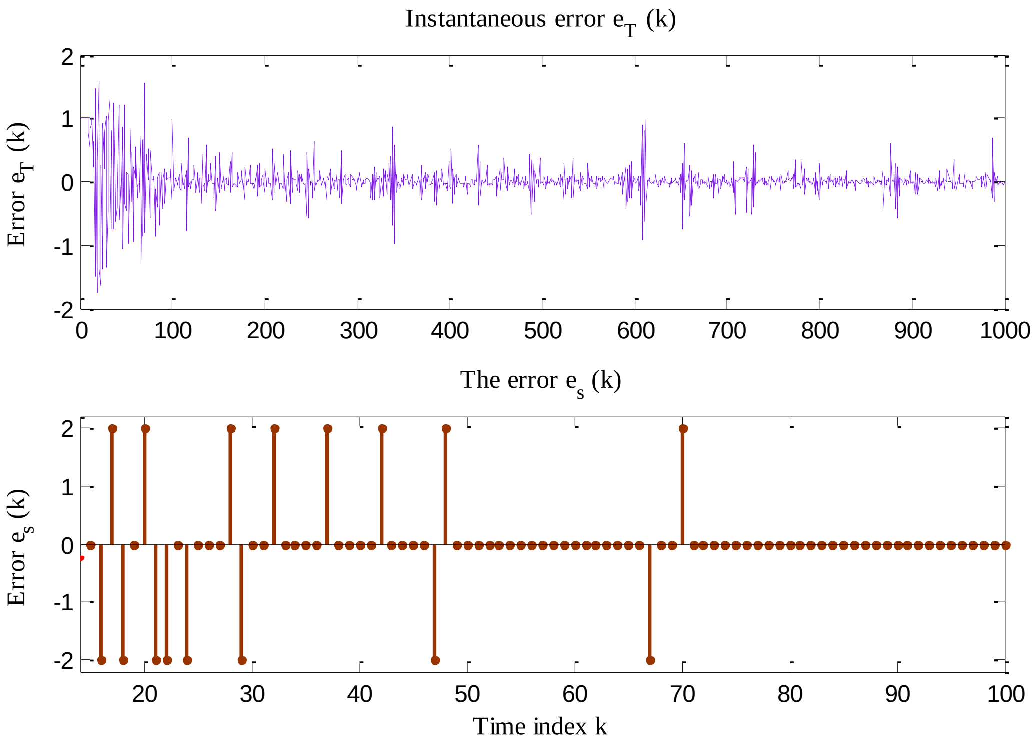

Figure 4-13 Instantaneous error (top) and the only bit errors that have occurred during the adaptation process (bottom)

There are only a total of 16 bit errors. The data bit error figure is zoomed-in for the first 100 steps because no further bit error occurs for another 2000 bits of data exchanged. As may be deduced from the simulation results presented here, the proposed equalizer architecture exhibits fast convergence in all the cases considered for simulations. In all cases good convergence is achieved within 100 iterations and, except for the last case, convergence is achieved in about 25 iterations of the algorithm.

Similarly, Figure 4-14 depicts the Mean Square Error in this case.

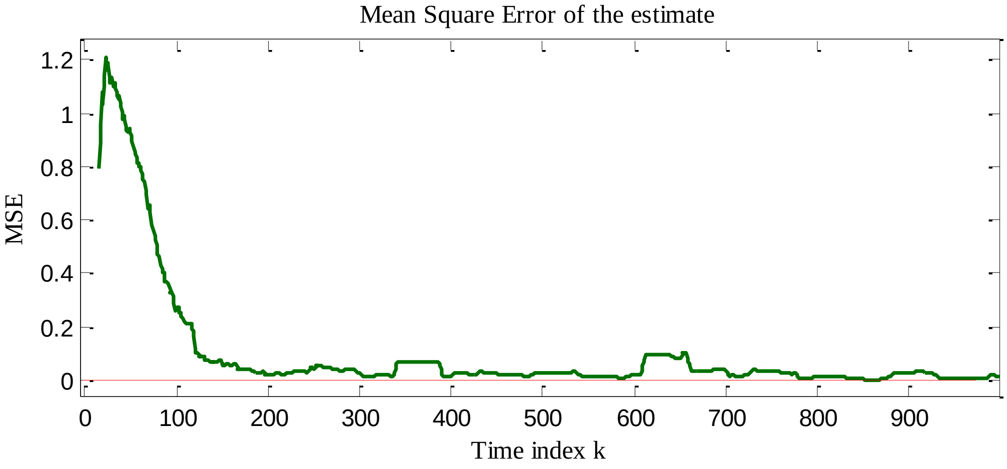

Figure 4-14 Mean Square Error (MSE) averaged over a moving window of 50 steps

We show the effect of removing the delay adjustments for the last example when all the other parameters have been kept constant in the graphs of Figure 4-15. The instantaneous actual error $e_T[k]$ and the error $e_s[k] = a[k-d] - \hat{s}[k]$ are shown for this case.

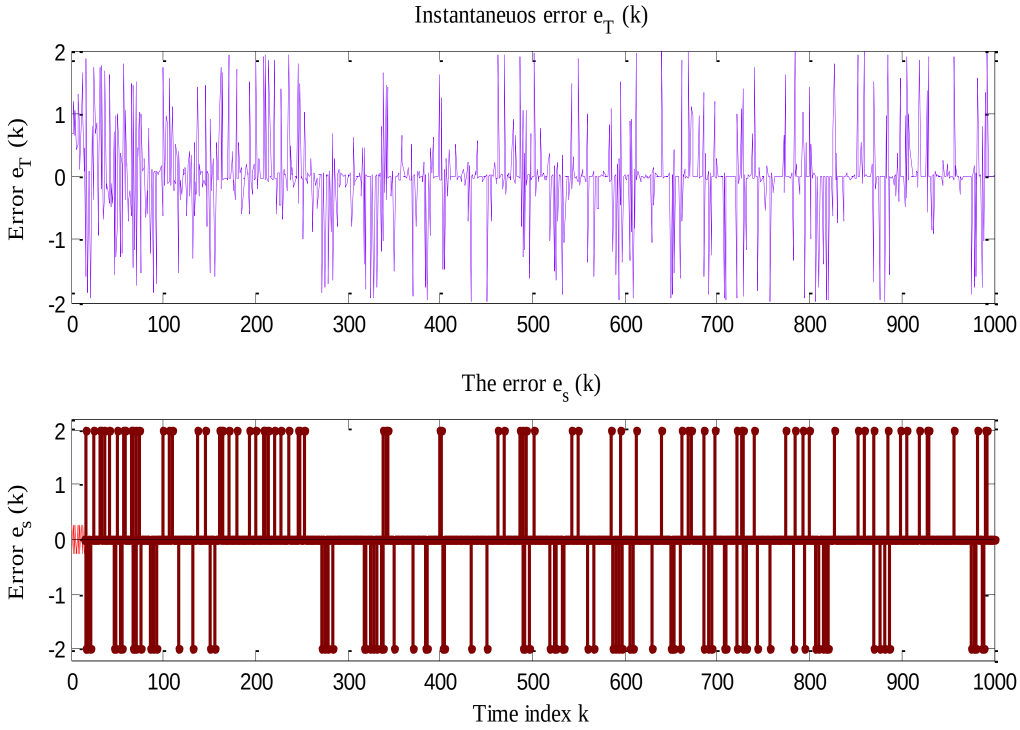

Figure 4-15 Instantaneous error (top) and the data errors (bottom) versus iteration number k.

The importance of the time adjustments for the network performance can be seen from the significant increase in the number of data errors. Increasing the training steps to larger length did not lead to convergence, that is, convergence could not be achieved without the delays for this channel.

In summary, we have shown that the proposed architecture and the introduction of the delay adjustments have shortened the training period for some channels, and for harder channel examples have made the convergence possible that otherwise could not be done with commonly used configurations even with relatively long training periods. In fact, long training periods defy our goal of making the equalization process efficient.

4.7 Convergence Analysis

The properties of convergence of multi-layer neural nets are mostly unknown. Here we give a weak convergence analysis using some convenient assumptions that might provide indications about network convergence. Our approach is based on the proposed network and is done by investigating one synaptic connection in each layer of neurons with the presumption that all the other weights in all layers have already reached their final and correct values.

First, we conjecture that there are infinitely many solution points in the *S*-dimensional space for the output layer neuron and *L*-dimensional space for the input layer neurons. This can be seen by a simple example. Consider the network of Figure 4-16. For simplicity we use the activation function $\varphi(x) = x$; we also remove the delay adjustments as it seems that they have no impact on the number of possible solutions:

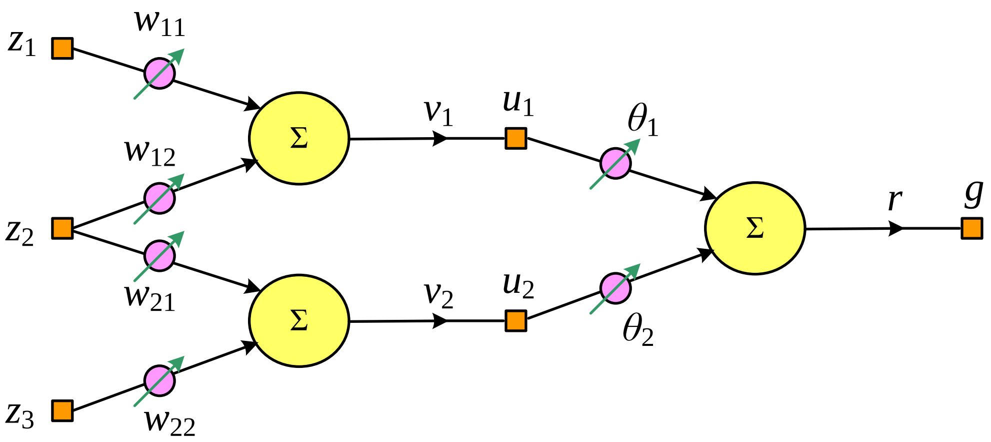

Figure 4-16 A simplified and low-dimensional example of two-layer network

The equations, simplified with convenient assumptions in terms of the weights of the input and the output layer neurons, can be written. The network output that is the required optimal value (but not unique) are denoted by $g^* = r^*$:

$$\begin{bmatrix} v_1 \\ v_2 \end{bmatrix} = \begin{bmatrix} w_{11} & w_{12} & 0 \\ 0 & w_{21} & w_{22} \end{bmatrix} \begin{bmatrix} z_1 \\ z_2 \\ z_3 \end{bmatrix} \qquad (4-29)$$

$$g^* = r^* = [\theta_1\ \theta_2] \begin{bmatrix} w_{11} & w_{12} & 0 \\ 0 & w_{21} & w_{22} \end{bmatrix} \begin{bmatrix} z_1 \\ z_2 \\ z_3 \end{bmatrix} \qquad (4-30)$$

The network weights acting on the arbitrary set of triple inputs are:

$$[\theta_1\ \theta_2] \begin{bmatrix} w_{11} & w_{12} & 0 \\ 0 & w_{21} & w_{22} \end{bmatrix} = [\theta_1 w_{11} \quad \theta_1 w_{12} + \theta_2 w_{21} \quad \theta_2 w_{22}]. \qquad (4-31)$$

Now suppose a certain known solution is given by $[a \quad b \ \ c]$, and we need to have

$$[\theta_1 w_{11} \quad \theta_1 w_{12} + \theta_2 w_{21} \quad \theta_2 w_{22}] = [a \ \ b \ \ c]. \qquad (4-32)$$

It can be seen that any of the equations $\theta_1 w_{11} = a$, $\theta_1 w_{12} + \theta_2 w_{21} = b$, and $\theta_2 w_{22} = c$ has many pairs of solution that must be on the same curve in the parameters space. Replacing the activation function with $\varphi(x) = \tanh x$ does not change this result as the hyperbolic tangent is a one-to-one function.

According to this conjecture it is reasonable to assume that the space of the synaptic weights has infinitely many solutions so that any random initial weight vector, with which the adaptation starts, is in the neighborhood of one of the solution vectors and hence a local convergence condition suffices for the network to take on one of the possible solutions. Moreover, the use of hyperbolic tangent relaxes the convergence requirements as we show in the following.

In the case of binary data input there will be only two cases, the case that the actual and delayed data input to the channel is $a[k-d] = +1$ (designated by Case + 1), and the case of $a[k-d] = -1$ (designated by Case – 1). We consider these cases separately. Starting with the output layer synaptic weights updates from Equation (4-12), we postulate that all of the parameters that are actually input layer connection weights have already converged to their corresponding solution values:

$$\theta_i[k+1] = \theta_i[k] + \eta_1 e[k](1 - g^2[k]) f_i[k]\ ; i = 1, 2, \dots, S \quad (4-12)$$

$$\text{Case } +1: \qquad e[k] = a[k-d] - g[k] \qquad (4-33)$$

$$\text{Case } -1: \qquad e[k] = a[k-d] - g[k] \qquad (4-34)$$

Applying the actual (training mode) error to adaptation equation according to the back propagation algorithm we obtain

$$\text{Case } +1: \qquad \theta_i[k+1] = \theta_i[k] + \eta_1 (1 - g[k])^2 (1 + g[k]) f_i[k] \qquad (4-35)$$

$$\text{Case} - 1: \qquad \theta_i[k+1] = \theta_i[k] - \eta_1 (1 - g[k])(1 + g[k])^2 f_i[k]. \qquad (4-36)$$

Let the difference between the output layer weights and the exact local solution be denoted as $\Delta_i[k] = \theta_i[k] - \theta_i^*$ at the k^{th} epoch. The last equations can be written in terms of $\Delta_i[k]$ as follows (by subtracting θ_i^* from each side of the equation) .

$$\text{Case } +1: \qquad \Delta_i[k+1] = \Delta_i[k] + \eta_1 (1 - g[k])^2 (1 + g[k]) f_i[k] \qquad (4-37)$$

$$\text{Case} - 1: \qquad \Delta_i[k+1] = \Delta_i[k] - \eta_1 (1 - g[k])(1 + g[k])^2 f_i[k] \qquad (4-38)$$

When the network parameters and the corresponding functions have converged to a local solution they settle at that point in the multidimensional space because either $(1 - g[k]) = 0$ or $(1 + g[k]) = 0$ in the adaptation equation for Case + 1 and – 1 respectively and no more adjustment will be made to the parameters. This of course applies to the first layer outputs after delays namely $f_i^*, i = 1, 2, \dots, S$ in Equation (4-37) and (4-38).

We need to compute network general output $g[k]$ with the assumption that all other weights have reached their local solution values except the one that is being analyzed, the i^{th} weight in the single output neuron $\theta_i[k] = \theta^* + \Delta_i[k]$.

$$g[k] = \tanh\left(\sum_{j=1}^{S} \theta_j[k] f_j[k]\right) = \tanh\left(\sum_{j=1}^{S} \theta_j^* f_j^* + \Delta_i[k] f_i^*\right)$$

$$= \frac{\tanh\left(\sum_{j=1}^{S} \theta_j^* f_j^*\right) + \tanh(\Delta_i[k] f_i^*)}{1 + \tanh\left(\sum_{j=1}^{S} \theta_j^* f_j^*\right) \tanh\left(\Delta_i[k] f_i^*\right)} \qquad (4-39)$$

We have assumed that the adaptation has reached its local solution except for one parameter or weight that is also assumed to be close to the solution point in the *S*-dimensional space. Based on these assumptions it is fair to consider that $\left|\tanh\left(\sum_{j=1}^{S} \theta_j^* f_j^*\right)\right| \approx 1$ and $|\Delta_i[k] f_i^*| \ll 1$. Consequently, the following approximations are justified.

$$\tanh(\Delta_i[k] f_i^*) \approx \Delta_i[k] f_i^* \qquad (4-40)$$

$$\text{Case } +1: \quad 1 + \tanh\left(\sum_{j=1}^{S} \theta_j^* f_j^*\right)(\Delta_i[k] f_i^*) \approx 1 + \Delta_i[k] f_i^* \approx 1 \qquad (4-41)$$

$$\text{Case } -1: \quad 1 + \tanh\left(\sum_{j=1}^{S} \theta_j^* f_j^*\right)(\Delta_i[k] f_i^*) \approx 1 - \Delta_i[k] f_i^* \approx 1 \qquad (4-42)$$

Notice that keeping the second terms in Equation (4-41) and (4-42) leads to even smaller terms in the adaptation equations due to the assumption $|\Delta_i[k] f_i^*| \ll 1$ (one can use approximations $\frac{1}{1+\epsilon} = 1 - \epsilon$ and $\frac{1}{1-\epsilon} = 1 + \epsilon$ to investigate this claim.) Inserting the approximations for the network output in both cases we have:

$$g[k] = \frac{\tanh\left(\sum_{j=1}^{S} \theta_j^* f_j^*\right) + \Delta_i[k] f_i^*}{1 + \tanh\left(\sum_{j=1}^{S} \theta_j^* f_j^*\right)\left(\Delta_i[k] f_i^*\right)} = \tanh\left(\sum_{j=1}^{S} \theta_j^* f_j^*\right) + \Delta_i[k] f_i^*. \qquad (4-42)$$

We use the approximate network output in addition to $\tanh\left(\sum_{j=1}^{S} \theta_j^* f_j^*\right) \approx 1$ for Case + 1 and $\tanh\left(\sum_{j=1}^{S} \theta_j^* f_j^*\right) \approx -1$ for Case – 1 in the adaptation equations as follows:

Case + 1: $1-g[k]=-\Delta_i[k]f_i^*$ and $1+g[k]=2+\Delta_i[k]f_i^*$

$$\Delta_i[k+1]=\Delta_i[k]+\eta_1(-\Delta_i[k]f_i^*)^2(2+\Delta_i[k]f_i^*)f_i^* \qquad (4-43)$$

$$\Delta_i[k+1]=\Delta_i[k]+2\eta_1\Delta_i^2[k]{f_i^*}^3+\eta_1\Delta_i^3[k]{f_i^*}^4 \qquad (4-44)$$

Case – 1: $1-g[k]=2-\Delta_i[k]f_i^*$ and $1+g[k]=\Delta_i[k]f_i^*$

$$\Delta_i[k+1]=\Delta_i[k]-\eta_1(2-\Delta_i[k]f_i^*)(\Delta_i[k]f_i^*)^2f_i^* \qquad (4-45)$$

$$\Delta_i[k+1]=\Delta_i[k]-2\eta_1\Delta_i^2[k]{f_i^*}^3+\eta_1\Delta_i^3[k]{f_i^*}^4 \qquad (4-46)$$

Finally, since the contribution of the misadjustment through *tanh* function to the network output $g[k]=\tanh\left(\sum_{j=1}^{S}\theta_j^*f_j^*+\Delta_i[k]f_i^*\right)$ is by the factor $\Delta_i[k]f_i^*$ we multiply both sides of the equations by f_i^* to get:

$$\text{Case}+1: \quad \Delta_i[k+1]f_i^*=\Delta_i[k]f_i^*+2\eta_1\Delta_i^2[k]{f_i^*}^4+\eta_1\Delta_i^3[k]{f_i^*}^5 \qquad (4-47)$$

$$\text{Case}-1: \quad \Delta_i[k+1]f_i^*=\Delta_i[k]f_i^*-2\eta_1\Delta_i^2[k]{f_i^*}^4+\eta_1\Delta_i^3[k]{f_i^*}^5. \qquad (4-48)$$

Before checking the adaptation trend for each case it might be useful to looks at the hyperbolic tangent function.

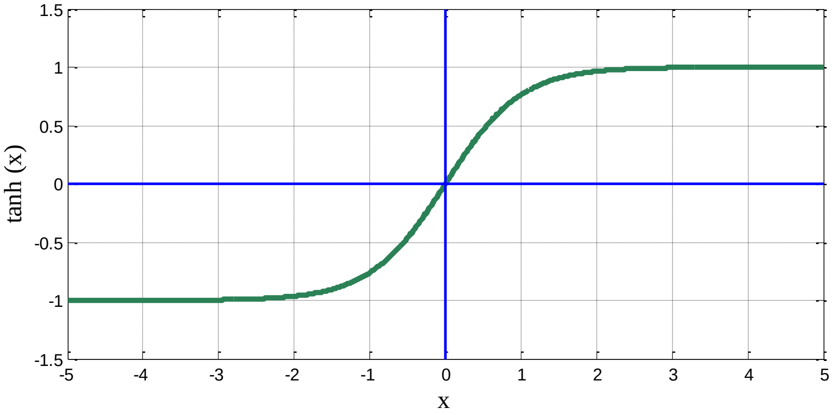

Figure 4-17 A graph of hyperbolic tangent function

Case + 1: First we modify Equation (4-47) to the following:

$$\Delta_i[k+1]f_i^* = \Delta_i[k]f_i^* + \eta_1\left(\Delta_i[k]f_i^{*2}\right)^2[2 + \Delta_i[k]f_i^*]\,. \qquad (4-49)$$

a) If $\Delta_i[k]f_i^* > 0$ then we have $\Delta_i[k+1]f_i^* > \Delta_i[k]f_i^* > 0$ because the second term in (4-49) is positive. This helps by forcing $g[k] = \tanh\left(\sum_{j=1}^{S}\theta_j^* f_j^* + \Delta_i[k]f_i^*\right)$ closer to $+1$.

b) If $\Delta_i[k]f_i^* < 0$ that means its contribution is in the opposite direction, pushing $g[k]$ backward from $+1$. In this case the second term in (4-49) is still positive $[2 + \Delta_i[k]f_i^*] > 0$ because we assumed that $|\Delta_i[k]f_i^*| \ll 1$. This updates the misadjustment in the correct direction $\Delta_i[k+1]f_i^* > \Delta_i[k]f_i^*$ that implies the output $g[k]$ closer to $+1$. Now if $\Delta_i[k+1]f_i^* > 0$ it will follow the case a above, otherwise if $\Delta_i[k+1]f_i^* < 0$ then the next change $\Delta_i[k+2]f_i^* > \Delta_i[k+1]f_i^*$ and the convergence continues in the correct direction.

Case – 1: Again we modify Equation (4-48) to the following

$$\Delta_i[k+1]f_i^* = \Delta_i[k]f_i^* - \eta_1\left(\Delta_i[k]f_i^{*2}\right)^2[2 - \Delta_i[k]f_i^*]\,. \qquad (4-50)$$

a) If $\Delta_i[k]f_i^* < 0$ then we have $\Delta_i[k+1]f_i^* < \Delta_i[k]f_i^* < 0$ because the second term in (4-50) is negative ($[2 - \Delta_i[k]f_i^*] > 0$). This helps by forcing $g[k] = \tanh\left(\sum_{j=1}^{S}\theta_j^* f_j^* + \Delta_i[k]f_i^*\right)$ to get closer to -1.

b) If $\Delta_i[k]f_i^* > 0$, that means that its contribution is in the opposite direction, pushing $g[k]$ backward from -1. The second term in (4-50) is still positive $[2 - \Delta_i[k]f_i^*] > 0$ because we assumed that $|\Delta_i[k]f_i^*| \ll 1$. This updates the misadjustment in the correct direction that is $\Delta_i[k+1]f_i^* < \Delta_i[k]f_i^*$ that implies the output $g[k]$ gets closer to -1. Now if $\Delta_i[k+1]f_i^* < 0$ it will follow the above, otherwise if $\Delta_i[k+1]f_i^* > 0$ then the next change $\Delta_i[k+2]f_i^* < \Delta_i[k+1]f_i^*$ and the convergence continues in the correct direction.

The adaptation equations for the input layer neurons become complicated as their corresponding gradients involve many free parameters. From Equation (4-28) for updating the j^{th} weight of synaptic connection of the i^{th} neuron in the input layer we have the gradients as:

$$\nabla_i[k] = -e[k](1 - g^2[k])\theta_i[k]\left(1 - f_i^2[k]\right)z[k - (S-1)\ell - j + 1]; \;\; i = 1, 2, \dots, L \qquad (4-51)$$

where $e[k] = 1 - g[k]$ for Case + 1, and $e[k] = -(1 + g[k])$.

Although there is a similar term in the gradient $\left(1 - f_i^2[k]\right)$ having about the same relation to the synaptic weights w_{ij}, a similar path of reasoning cannot follow because the similar assumption $|f_i[k]| = \left|\tanh\left(\sum_{j=1}^{S} w_{ij}[k]z[k - (S-1)\ell - j + 1]\right)\right| \approx 1$ for nearly converged network cannot be made. Moreover, the convergence of the output layer depends on the input layer convergence and not the other way around.

It is the intention of the author to pursue possible approaches to the complete convergence analysis of the proposed network or multilayer neural network in general in future research.

4.7 References

[7] Botoca, C., Budura, G., “Symbol Decision Equalizer using a Radial Basis Functions Neural network”, Proc. of WSEAS International Conference on Neural networks, Cavtat, Croatia, June 2006.

[8] Bradley, M.J., Mars, P., “A Critical Assessment of Recurrent Neural Networks as Adaptive Equalizers in Digital Communications”, Application of Neural Networks to Signal Processing (Digest No 1994/248), IEE Colloquium on.

[9] Bradley, M.J., Mars, P., “Application of Recurrent Neural Networks to Communication Channel Equalization”, International Conference on Acoustics, Speech, and Signal Processing (ICASSP), 1995.

[10] Carpenter, G.A., Grossberg, S., “A massively parallel architecture for a self-organizing neural pattern recognition machine,” Computer Vision, Graphics, and Image Processing, Vol. 37, 1983, pp. 54-115.

[11] Chang, Y.J., Yang, S.S., Ho, C.L., “Fast Self-Constructing Fuzzy Neural Network-Based Decision Feedback Equalizer in Time-Invariant and Time-Varying Channels”, IET Communications, 2010, Vol. 4, Issue 4.

[12] Chen, J.R., Mars, P., “The Feasibility of Using MLP Neural Networks for System Identification”, Neural Network for Systems: Principles and Applications, IEE Colloquium on, 1991.

[13] Fang, Y., Chow, T.W.S., “Blind Equalization of a Noisy Channel by Linear Neural Network”, IEEE Transactions on Neural Networks, July 1999.

[14] Feng, J., Tse, C.K., Lau, F.C.M., “A Neural Network Based Channel Equalization Strategy for Chaos-Based Communication Systems”, IEEE Trans. on Circuits and Systems, Vol. 50, No. 7, July 2003.

[15] Gibson, G.J., Siu, S., Cowan, C.F.N., "Multilayer Perceptron structures applied to adaptive equalizers for data communications", Proc. ICASSP'89, May 1989.

[16] Grossberg, S., "Adaptive Pattern Classification and Universal Recording , II: Feedback, expectation, olfaction, and illusions," Bilog. Cybernetics, Vol. 23, 1976, pp. 187-202.

[17] Haykin, S., "Neural Network and Learning machines", 3rd Edition, Pearson Education, 2009.

[18] Hecht-Nielson, R., "Kolmogrov's Mapping neural Network Existence Theorem", IEEE International Conference on Neural Network, Vol. 2, 1987.

[19] Hecht-Nielson, R., "The Theory of the Back propagation Neural Network", International Joint Conference on Neural Networks (IJCNN), 1989.

[20] Hopfield, J.J., "Neural networks and physical Systems with emergent collective computational abilities," Proc. Natl. Acad. Sci., Vol. 79, 1982, pp. 2554-2558.

[21] Jeffrey, A. "Handbook of Mathematical Formulas and Integrals," 3rd edition, Elsevier Academic Press, 2004.

[22] Kechriotis, G., Zervas, E., Manolakos, E.S., "Using Recurrent Neural Networks for Adaptive Communication Channel Equalization", IEEE Trans. on Neural Networks, Vol. 5, No. 2, 1994.

[23] Kosko, B., "Neural Network and Fuzzy Systems," Prentice-Hall, New Jersey, 1992.

[24] Kumar, R., Jalali, S.M., "Super Fast and Efficient Channel Equalizer Architecture Based on Neural Network," IEEE Conf. on Aerospace, March 2012.

[25] Lau, C., Editor, "Neural networks Theoretical Foundation and Analysis", IEEE Press, 1992.

[26] Lee, C., Go, J., Kim, H., "Multigradient for Neural Networks for Equalization", Systems, Cybernetics and Informatics, Vol. 1, No. 3, 2003.

[27] Li, M.B., Er, M.J., "Channel Equalization Using Dynamic Fuzzy Neural Networks", Proc. of The 17th World Congress The International Federation of Automatic Control, Seoul, Korea, July 2008.

[28] Lippman, R.P., "An Introduction to Computing with Neural Networks," IEEE ASSP Magazine, April 1987, pp. 4-22.

[29] McCullah, W.S., Pitts, W.,”A Logical calculus of the ideas immanent in nervous activity,” Bulletin of Mathematical Biophysics, Vol. 5, 1943, pp. 115-133.

[30] Minsky, M.L., Papert, S.A., “Perceptrons,”, MIT Press, Cambridge, MA. 1969.

[31] Minsky, M.L., Selfridge, O.G., “Learning in random nets,” Information Theory, Fourth London Symposium, London, Buttenvorths, 1961.

[32] Mo, S., Shafai, B., “Blind equalization using higher order cumulants and neural networks”, IEEE Trans. Signal Processing, Vol. 42, No. 11, Nov. 1994.

[33] Parker, D., “Learning Logic”, Technical Report TR-47, Center for Computational research in Economics and Management Science, MIT, Apr. 1985.

[34] Rosenblatt, F., “Principles of Neurodynamics: Perceptrons and the theory of brain mechanisms,” Spartan Books, Washington DC, 1962.

[35] Rosenblatt, F., “The Perceptron: A Probablilistic model for information storage and organization in the brain,” Psychological Review, Vol. 65, 1958, pp. 386-408.

[36] Rui, L., Saratchandran, P., Sundarajan, N., “Blind Equalization Using Higher Order Statistics and Neural Networks: A Comparison Between Multilayer Feed Forward Network and Radial Function Network”, Proc. of IEEE Signal Processing Workshop on Higher Order Statistics, 1999.

[37] Rumelhart, D.E., Hinton, G.E., Williams, R.J., “Learning internal representations by error propagation,” ICS report 8506, Institute for Cognitive Sciense, University of California at San Diego, La Jolla, CA, Sept. 1985.

[38] Rumelhart, D.E., Hinton, G.E., Williams, R.J., “Learning internal representations by error propagation,” Parallel Distributed Processing, Vol. 1, Ch. 8, Cambridge, MA, MIT Press, 1986.

[39] Sarajedini, A., Hecht-Nielson, R., “The Best of Both Worlds: Casasent Networks Integrate Multilayer Perceptron and Radial basis Functions”, International Joint Conference on Neural Networks (IJCNN), 1992.

[40] Satapathy, J.K., Subhushini, K.R., "A Highly Efficient Channel Equalizer for Digital Communication System in Neural Network Paradigm", 2009 Conference on Innovative Technologies in Intelligent Systems and Industrial Applications, July 2009.

[41] Veelenturf, L.P.J., "Analysis and Applications of Artificial Neural Networks", Prentice Hall International (UK), 1995.

[42] Widrow, B., Lehr, M.A., "30 years of Adaptive Neural Networks: Perceptron, Madaline, and Backpropagation," Proc. IEEE, Vol. 78, No. 9, Sept. 1990, pp. 1415-1442.

[43] Widrwo, B., "Generalization and information storage in network of Adaline neurons," Self-organizing Systems, Spartan Books, Washington DC, 1962, pp. 435-461.

[44] Widrow, B., Stearns, S.D., "Adaptive Signal Processing," Prentice-Hall, New Jersey, 1985.

[45] Werbos, P., "Beyond Regression: New Tools for Prediction and Analysis in the Behavioral Sciences," Ph.D. Thesis, Harvard University, Cambridge, MA, Aug. 1974.

[46] Xie, N., Leung, H., "Blind Equalization using a Perdictive Radial Basis Function Neural Networks," IEEE Trans. On Neural Networks, Vol. 16, No. 3, May 2005.

[47] Zhang, L., Liu, T., Sun, Y., Chen, L., "Research on Neural Network Blind Equalization Algorithm with Structure Optimized by Genetic Algorithm", IEEE Sixth International Conference on Natural Computation (ICNC), 2010.

Chapter 5: Adaptive Simulated Annealing

5.1 Introduction

Every optimization problem should be based on minimization (or maximization) of a cost or objective function, which usually is a function of a weight vector or state variable of many dimensions. The weight vector needs to be adjusted to some optimum point in its space. The cost function in the problem of channel equalization has several uncertainties associated with it (see section 2.5 and Equation (2-19) and (2-20)). Other than the channel that is modeled by a linear transversal impulse response with slow varying tap gains, there is channel noise and the desired output that is unknown in the blind mode case. Furthermore, the cost function is normally complicated. Let us assume the binary data input to the channel normalized to $\{\pm 1\}$ and the channel that is considered fixed for the period of adaptation, then the cost function is composed of terms of the form given in Equation (5-1). The random noise samples n_p in Equation (5-1) represent channel noise and the dependence on the time steps are dropped for clarity in the equation.

$$\mathcal{J} = \mathbb{E}\left\{e^2 = \cdots \pm h_k^2 w_\ell^2 \pm h_i h_j w_m w_n \pm \cdots + n_p w_q + \cdots\right\} \qquad (5-1)$$

One has to acknowledge that the equalizer weights in Equation (5-1) themselves change at each step according to another mathematical equation. If we take the LMS iterative update equation for the equalizer weight vector, they will be dependent on the error in each step. In the blind mode an estimate of the input data is incorporated that is determined by a nonlinearity of the form

$$\hat{s} = K\mathrm{sgn}\left(\cdots \pm h_i w_j \pm \cdots\right). \qquad (5-2)$$

Equation (5-2) represents what is also known as slicer, or quantizer, which adds to the complexity of the cost function. In either case the cost function behavior or characteristics is difficult to be pictured in advance. It is quite possible that the iterative algorithm becomes trapped in a local minimum of the cost function (see Mazo [10]), some of these local points are not acceptable in terms of their performance measured by residual ISI. A mechanism to catapult the weight vector out of the local traps is needed to enhance the performance of the algorithms, lacking a workable plan to attain the global minimum or optimum point of the cost function. In evaluating each algorithm performance it must be conceded that many possible local stationary points with acceptable and close to global optimum residual ISI exist. In fact, that is the reason many simple blind mode equalizer techniques are known to achieve an acceptable convergence. Even when an almost-sure convergence to the global minimum exists, it is definitely associated with a sophisticated algorithm and costly procedure.

Addition of a zero-mean noise to the adaptive equalization process was introduced by Kumar in 1981 [8-9]. This process was referred to as simulated annealing in the subsequent literature. Kumar has explained additional noise benefits in the statement: “In very intuitive terms the noise sequence $\{v[k]\}$ and/or $\{n[k]\}$ compensate for a non-continuous distribution of $\{s[k]\}$ and thus ensure a priori convergence of the adaptive algorithm. It will become apparent later that in the absence and with discrete distribution of $\{s[k]\}$ one could always find an initial estimate of the equalizer parameters which will not cause convergence.” The configuration of [8-9] according to the notation and format of this thesis is shown in Figure 5-1. References [8-9] also provide mathematical proof of extension of convergence domain with the addition of annealing noise.

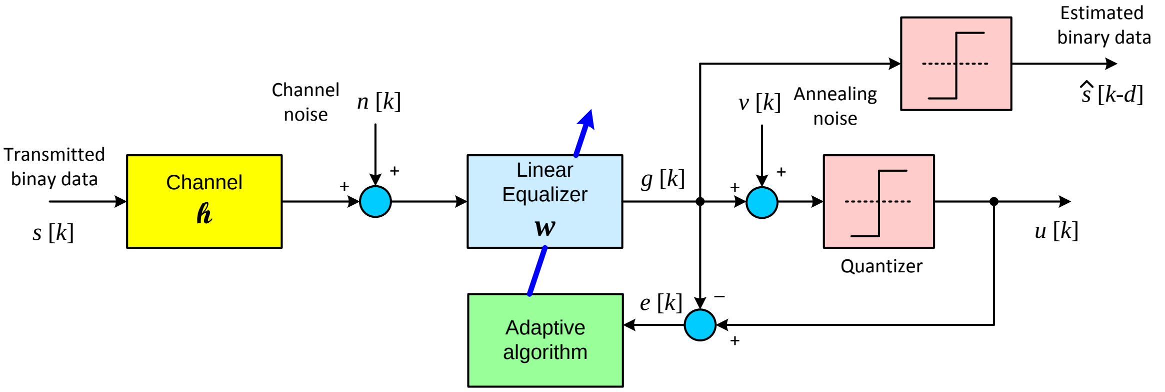

Figure 5-1 The decision-directed system configuration to include random noise application

It can also be said that the additional noise facilitates the release of an entrapped process from the local minima with unacceptable performance. White, et. al, in their 1995 paper [14] state: “We observe that the noisier the observations are, the faster the algorithm converges. It results from a better conditioning of the information matrix.” This observation and many similar ones justify the addition of noise.

In section 3.6 of [15], Widrow and Walach, show that the LMS algorithm converges to the optimum point measured by the mean squared error substantiated in a sum of exponentials, which have time constants inversely proportional the eigenvalues of the autocorrelation matrix of the received input process. It is well-known that the higher eigenvalue spread of the auto-covariance or autocorrelation matrix of the channel generates a harder problem with longer adaptation. In Appendix A, we show some basic idea that encourages the addition of random noise samples to change the process of adaptive equalization behavior with variable results, though positive and promising in many cases.

The idea of random noise injection (with zero mean) gained momentum in the research community in order to solve problems in different areas of interest and has become known as *Simulated Annealing* (the term first time used by Kirkpatrick, et. al in [6] and [7]). Some of the tough problems such as the Travelling Salesman Problem (TSP), and the floor planning in particular, optimization of the Integrated Circuit layout, are among the class of combinatorial optimization problems often tackled by simulated annealing. The theory of Adaptive Simulated Annealing (ASA) is covered in [4, 5, 6, 7, 8, 9, 12, and 13] with some interesting applications demonstrated in [1, 2, 3, and 11].

Van Laarhoven and Aarts [13] explain a required “generation mechanism” in the randomized optimization (a new state is generated using a random transition in a specified way) that generates a transition from the current state to another state selected from the current neighborhood. If the new state has lower cost it replaces the current one, otherwise another randomized transition is generated and examined. They also define the final stopping point by the following method: “the algorithm terminates when a configuration is obtained whose cost is no worse than any of its neighbors." Hence, ASA requires 3 main components, namely a generation mechanism, and method by which to evaluate the current cost to make the decision whether to keep or reject the new transition, and of course a method to stop the procedure. The second component is the prominent difference between Kumar's proposed system and common ASA implementations.

5.2 Adaptive Simulated Annealing in Channel Equalization

From the discussion in section 5.1, it is reasonable to seek answers to three important questions. What system setup to deploy that includes the random noise (we will call it annealing noise) addition point. How to choose noise power in terms of standard deviation, and how to vary (decrease) the noise power as the final point is approached. Accurately answering these questions requires intensive research and mathematical analysis extending the work of Kumar in [8-9]. Here we propose two basic system configurations, one illustrated in Figure 5-1, and an additional one characterized by small change in the way the system error is computed in Figure 5-2.

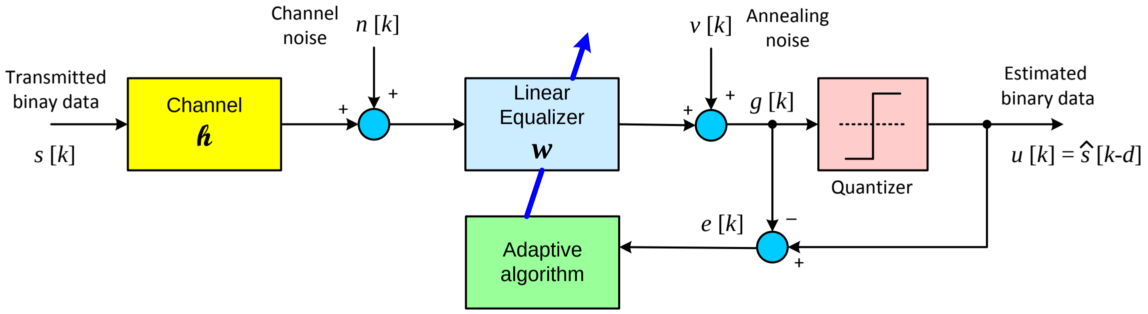

Figure 5-2 The alternative system configuration to include additional random noise

A preliminary study of the basics of Adaptive Simulated Annealing in wireless channel equalization is championed in this chapter. In particular, we apply only low power Gaussian noise samples with zero-mean that is kept constant during the adaptation. Experimenting with the similar channels as in chapter 3 and 4, we have reached an interesting and promising conclusion summarized in 5.4.

5.3 Simulation Results on Different Channels

Channel 1

The first channel is symmetric with five taps (non-minimum phase) specified by the impulse response of (introduced in Chapter 3)

$$h = -0.2287\delta[k] + 0.3964\delta[k-1] + 0.7623\delta[k-2] + 0.3964\delta[k-3] - 0.2287\delta[k-4].$$

The optimum LS optimum equalizer of the same size as CIR for known CIR produces only -3.22 dB. The application of ASA for EWRLS case with $\mu = 1.0$ shows considerable improvement with final $ISI_R = -4.2$ dB as seen in Figure 5-3. As may be inferred form Figure 5-3, in the absence of ASA, the convergence is very poor with the ISI to signal power of about 2 dB.

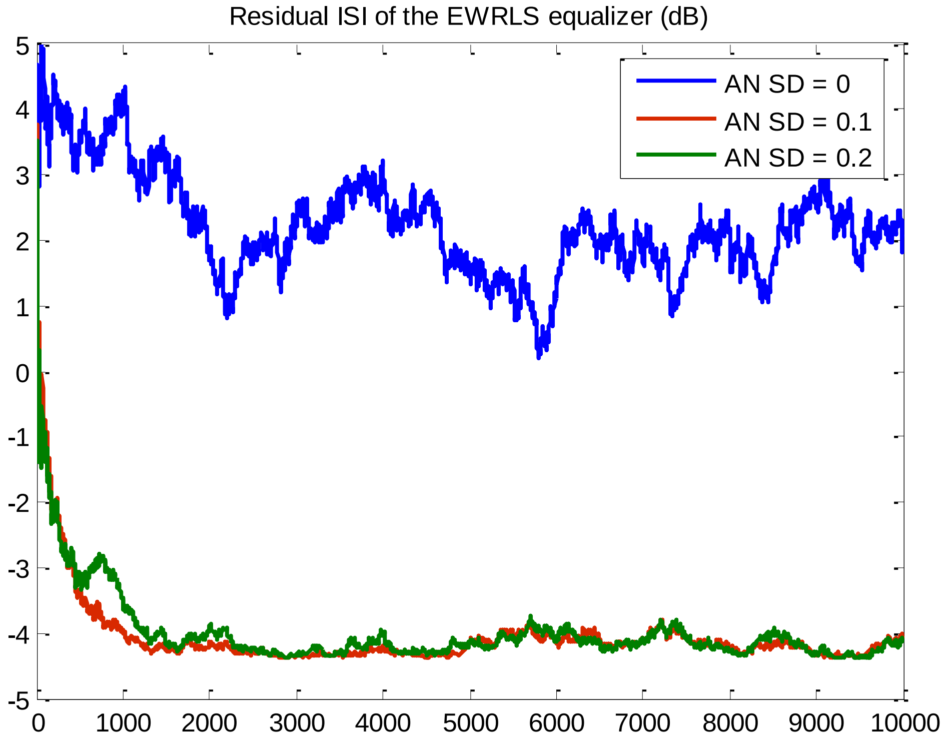

Figure 5-3 Comparison of residual ISI for the case of EWRLS

Channel 2

The second channel with eleven taps is specified by the impulse response of

$$h = 0.04\delta[k] - 0.05\delta[k-1] + 0.07\delta[k-2] - 0.21\delta[k-3] - 0.5\delta[k-4] + 0.72\delta[k-5] + 0.36\delta[k-6] + 0.21\delta[k-8] + 0.03\delta[k-9] + 0.07\delta[k-10].$$

The optimum LS optimum equalizer for known CIR produces -24.7 dB. The application of ASA for EWRLS algorithm with $\mu = 1.0$ shows a variable final residual ISI as seen in Figure 5-4. This result is an indicator that the equalizer converges to the different final points in the weight vector space. The residual ISI is reduced about 6 dB with ASA compared to that obtained without the ASA after 5000 iterations. Furthermore, higher variance of the annealing noise shows better convergence.

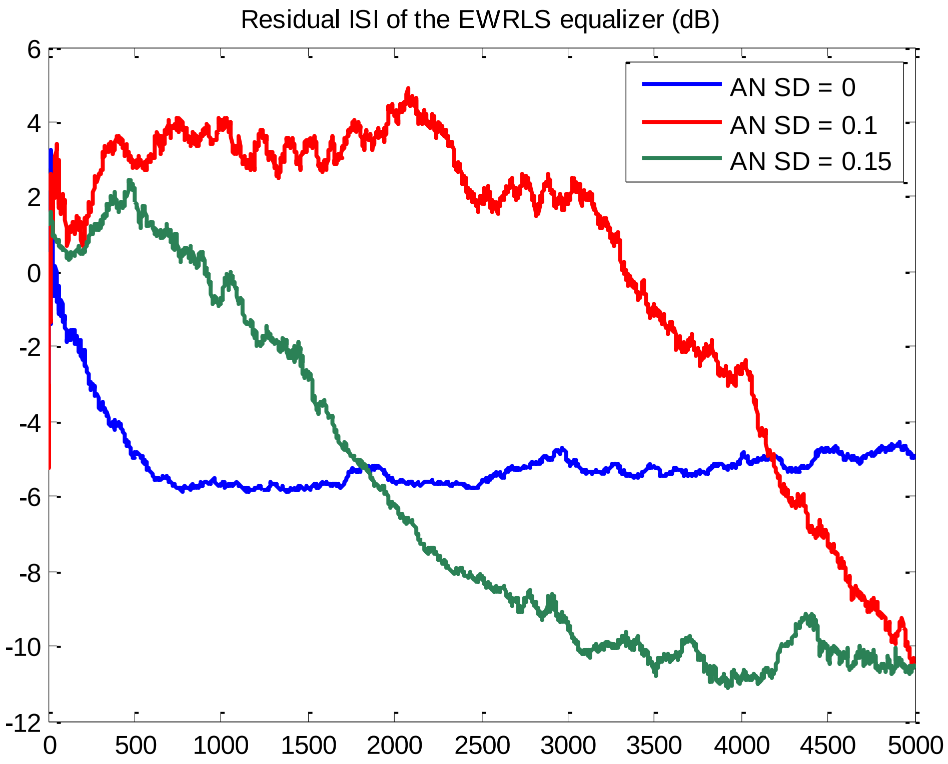

Figure 5-4 Comparison of residual ISI for the case of EWRLS

Figure 5-5 depicts the convolution of the equalizer final weight vectors with the channel CIR for different annealing noise powers. It is seen that the system converges to different final points with varied residual ISI.

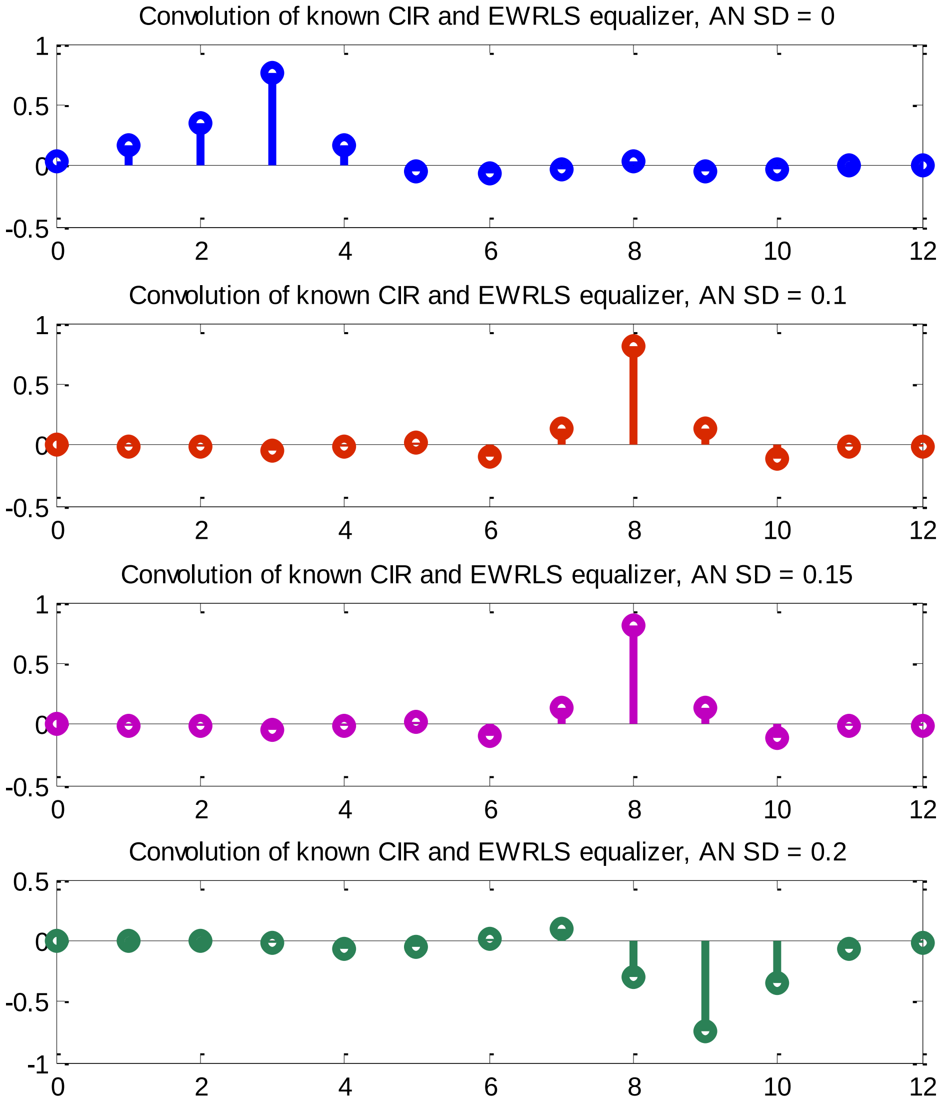

Figure 5-5 Comparison of final equalizer convolution with the CIR

Channel 3

The third channel with eleven taps is specified by the impulse response of

$$h = 0.04\delta[k] - 0.05\delta[k-1] + 0.07\delta[k-2] - 0.21\delta[k-3] - 0.5\delta[k-4] + 0.72\delta[k-5]$$
$$+ 0.36\delta[k-6] + 0.21\delta[k-8] + 0.03\delta[k-9] + 0.07\delta[k-10].$$

The optimum LS optimum equalizer for known CIR gets -15.7 dB. The application of ASA for EWRLS algorithm with $\mu = 1.0$ shows a variable final residual ISI as seen in Figure 5-6. This result is again an indicator that the equalizer converges to different final points in the weight vector space.

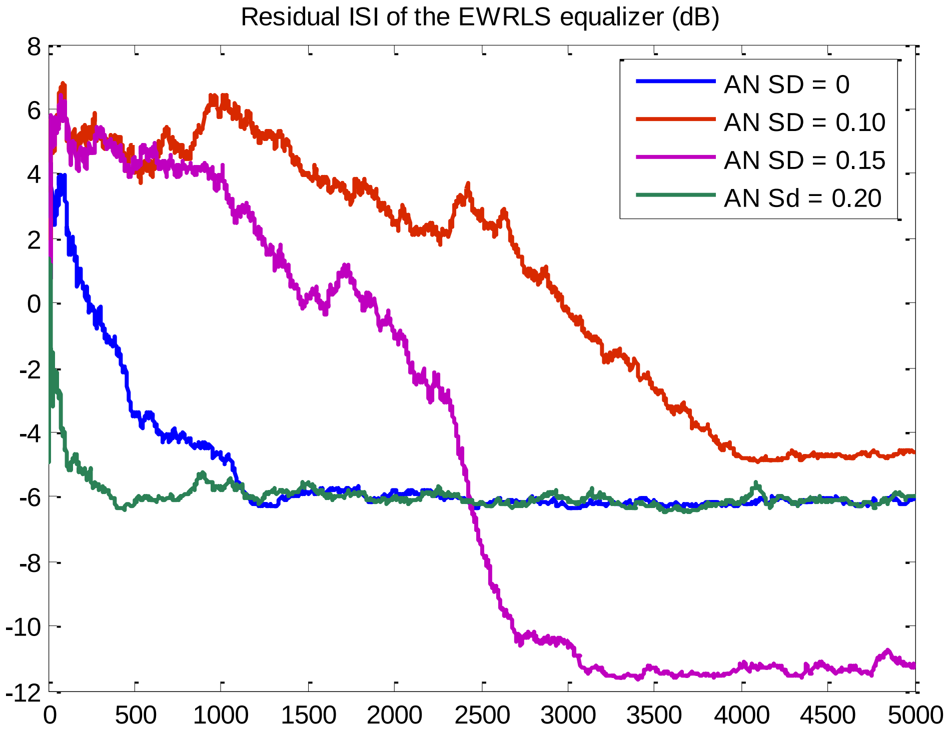

Figure 5-6 Comparison of residual ISI for the case of EWRLS

Figure 5-7 shows the convolution of the equalizer final weight vectors with the channel CIR for different annealing noise powers. It is seen that the system converges to different final points with varied residual ISI.

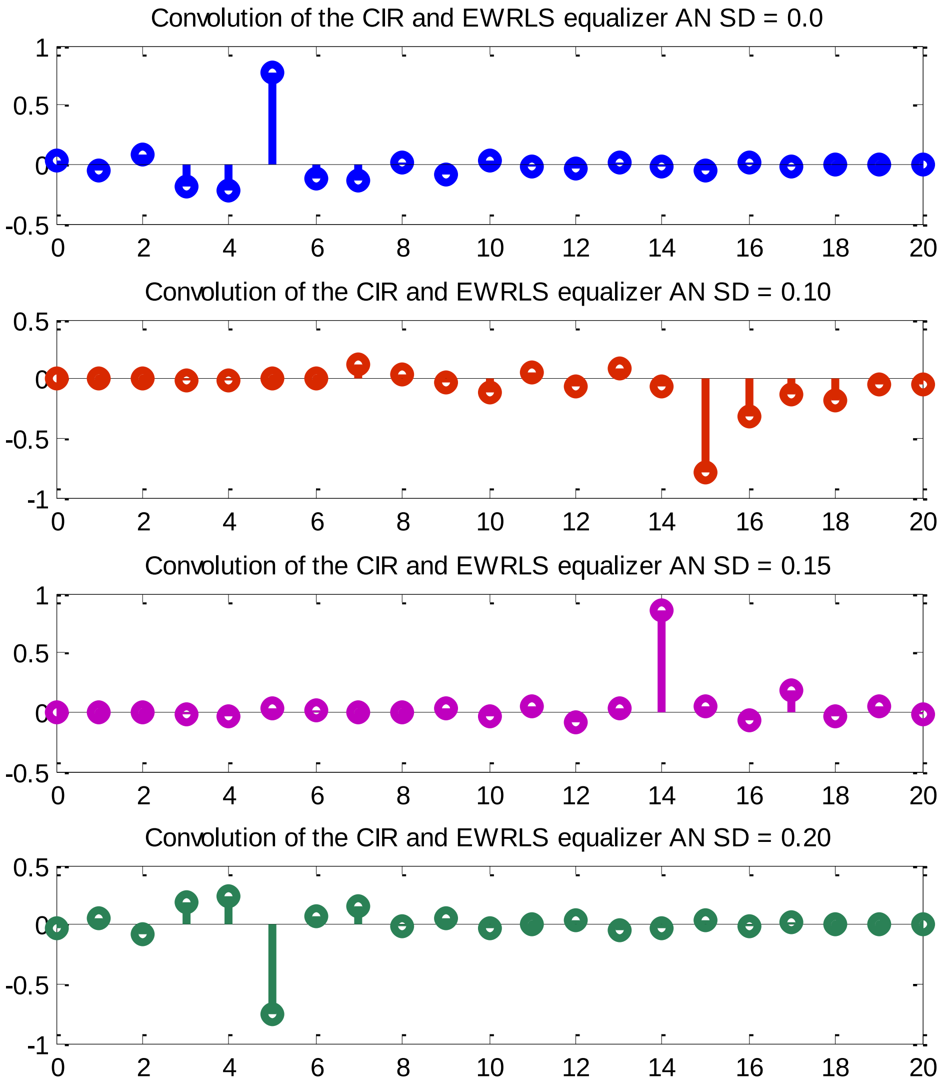

Figure 5-7 Comparison of final equalizer convolution with the CIR

Channel 4

The fourth channel with nineteen taps is specified by the impulse response of

$$\begin{aligned} h = 0.005\delta[k] - 0.007\delta[k-1] - 0.012\delta[k-2] + 0.005\delta[k-3] - 0.015\delta[k-4] \\ - 0.008\delta[k-5] + 0.017\delta[k-6] + 0.023\delta[k-7] + 0.13\delta[k-8] \\ + 0.042\delta[k-9] + 0.21\delta[k-10] + 0.036\delta[k-11] + 0.01\delta[k-13] \\ + 0.004\delta[k-13] - 0.002\delta[k-14] + 0.009\delta[k-15] + 0.004\delta[k-16] \\ + 0.001\delta[k-17] - 0.0006\delta[k-18] \end{aligned}$$

The optimum LS optimum equalizer for known CIR achieves -34.4 dB. The application of ASA for LMS algorithm with $\mu = 0.004$ shows the same final $ISI_R = -12$ dB as seen in Figure 5-8. Therefore the final points of convergence are the same for the applied noise powers.

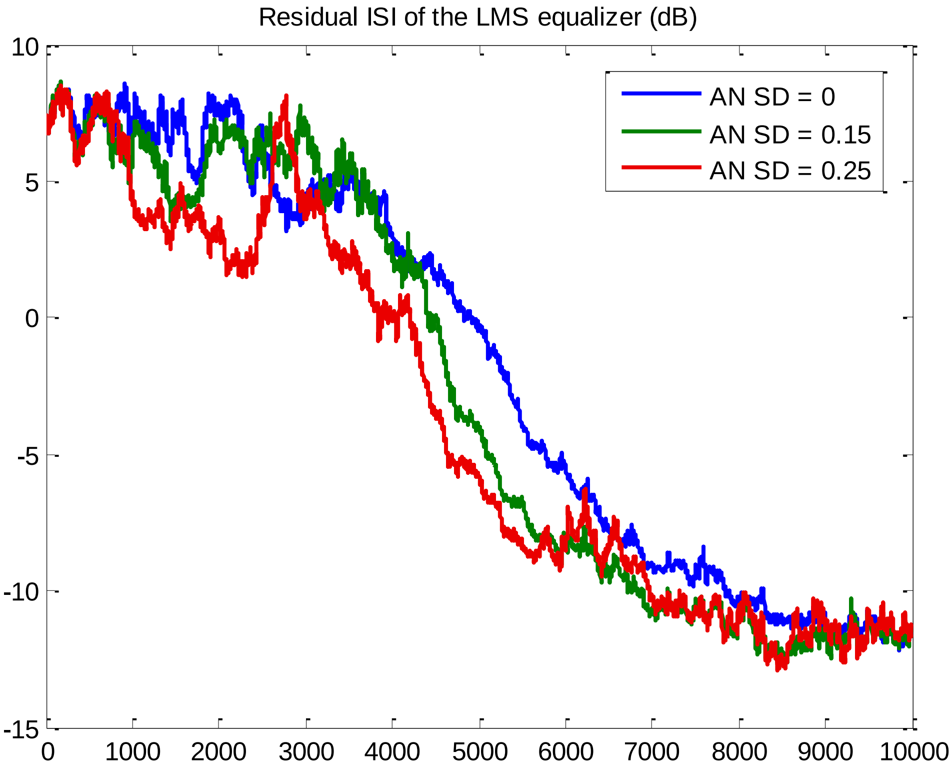

Figure 5-8 Comparison of residual ISI for the case of EWRLS

Figure 5-9 gives the convolution of the equalizer final weight vectors with the channel CIR. It is seen that the system converges to the final point with the same residual ISI, even though there is an associated sign inversion.

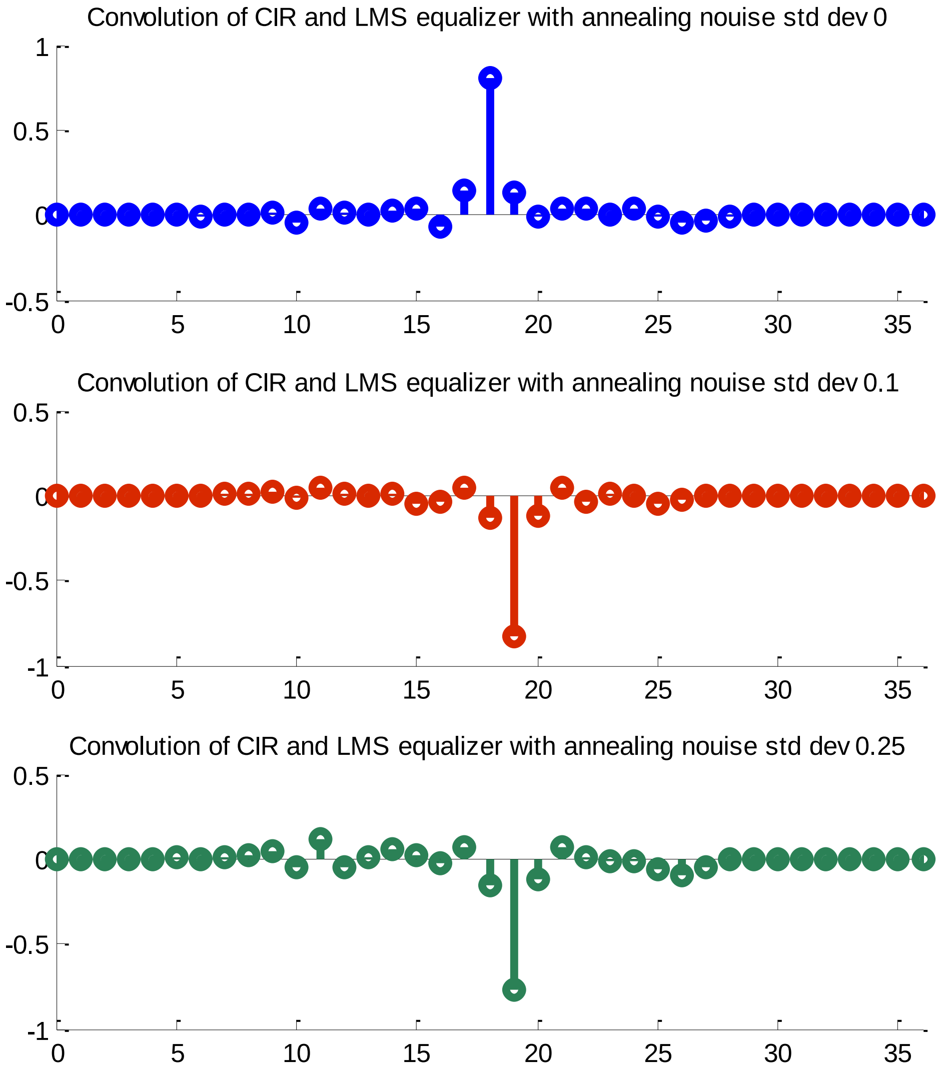

Figure 5-9 Comparison of final equalizer convolution with the CIR

For the same channel the ASA technique is applied to the EWRLS algorithm with $\mu = 1.0$. The results show a variable residual ISI as seen in Figure 5-10. Therefore there are different final converged points based on the different annealing noise power.

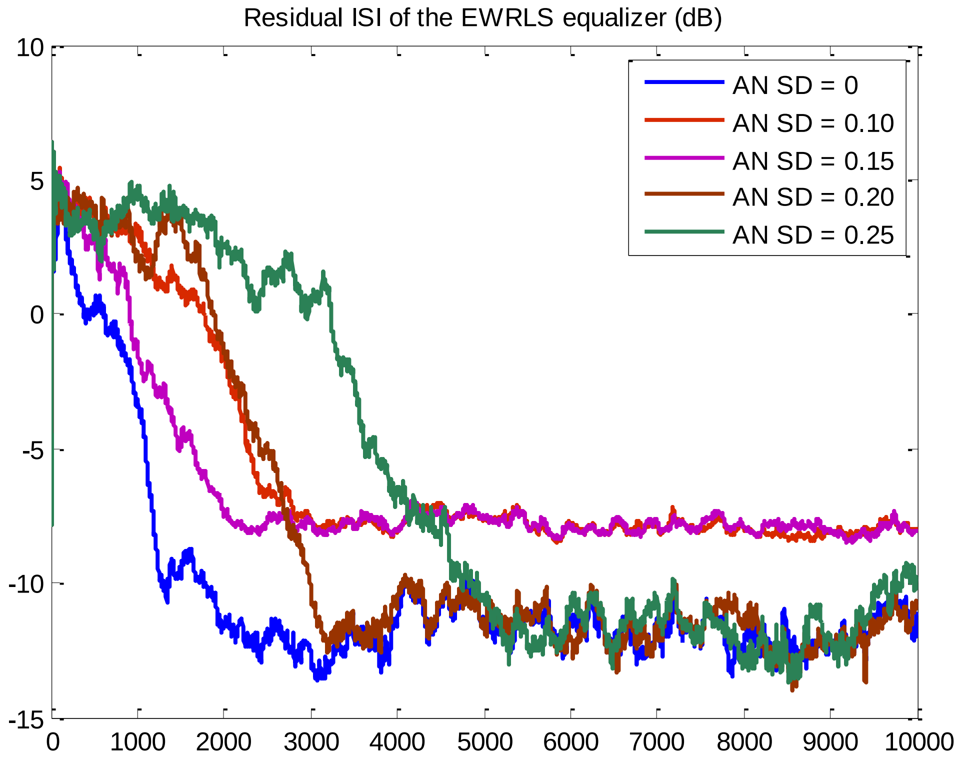

Figure 5-10 Comparison of residual ISI for the case of EWRLS

Figure 5-11 confirms the varied final converged points offering the convolution of the equalizer final weight vectors with the channel CIR. It seems that some local minima have been reached and ASA method has the catapulting effect, at least in some cases that were examined.

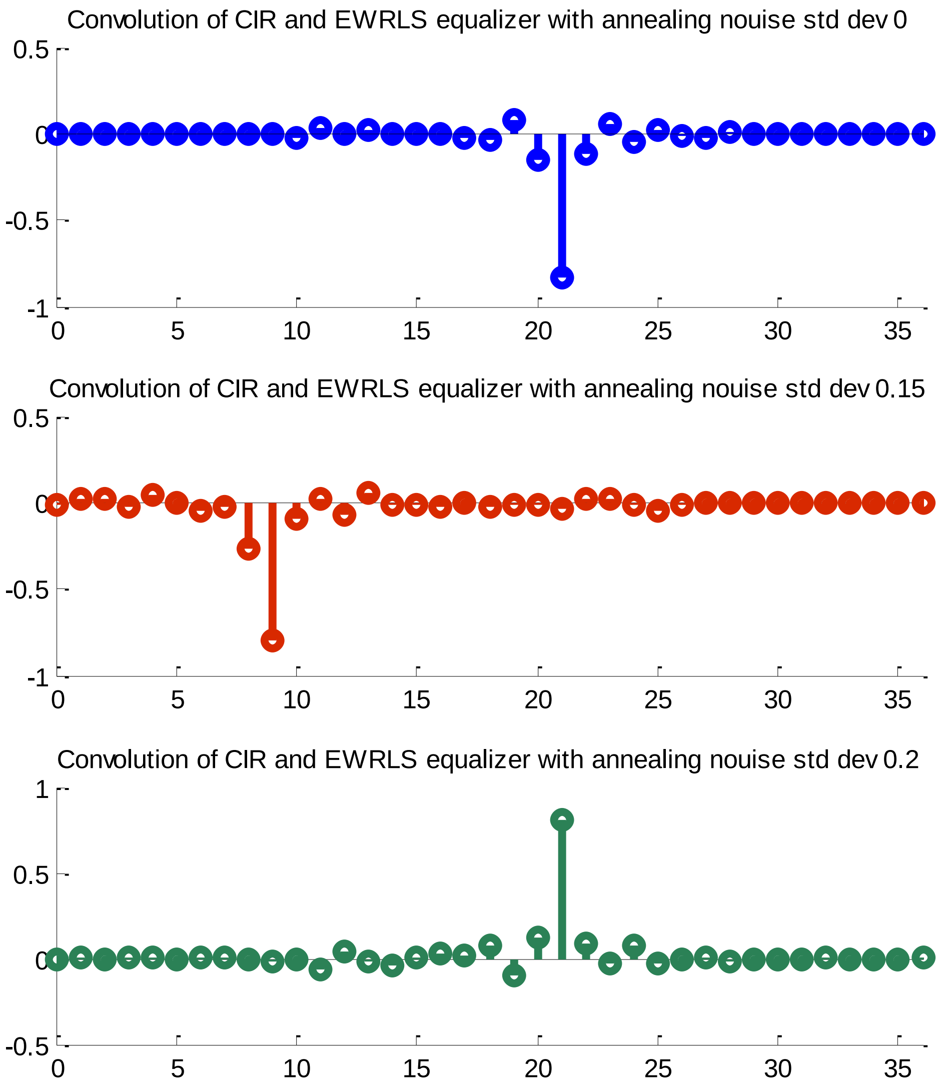

Convolution of CIR and EWRLS equalizer with annealing nouise std dev 0

Convolution of CIR and EWRLS equalizer with annealing nouise std dev 0.15

Convolution of CIR and EWRLS equalizer with annealing nouise std dev 0.2

Figure 5-11 Comparison of final equalizer convolution with the CIR

Channel 5

There is yet another channel with five taps and specified by the impulse response of

$$h = 0.04823\delta[k] + 0.0194\delta[k-1] - 0.5889\delta[k-2] + 0.6285\delta[k-3] - 0.1586\delta[k-4].$$

The optimum LS optimum equalizer for known CIR achieves only -1.3 dB. The application of ASA for LMS algorithm with $\mu = 0.004$ shows variable convergence speed with the final $ISI_R = -5$ dB as seen in Figure 5-12. This result is an indicator that the equalizer converges to the same final points in the weight vector space with variable convergence speed.

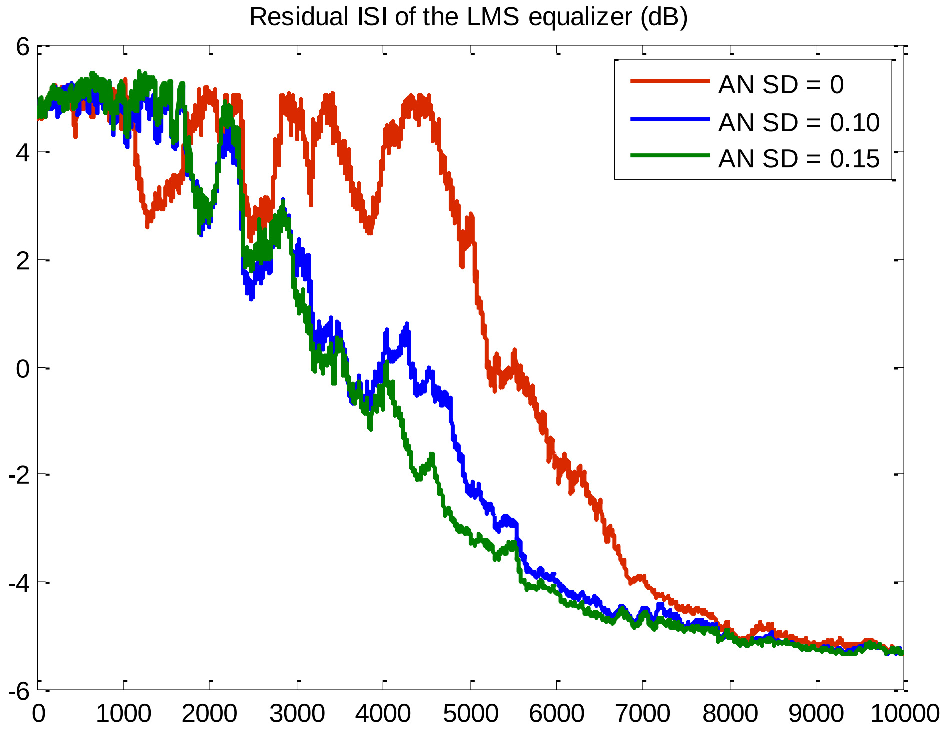

Figure 5-12 Comparison of residual ISI for the case of EWRLS

For the EWRLS algorithm with $\mu = 1.0$ the ASA technique also shows variable convergence speed with a final $ISI_R = -6.2$ dB as seen in Figure 5-12.

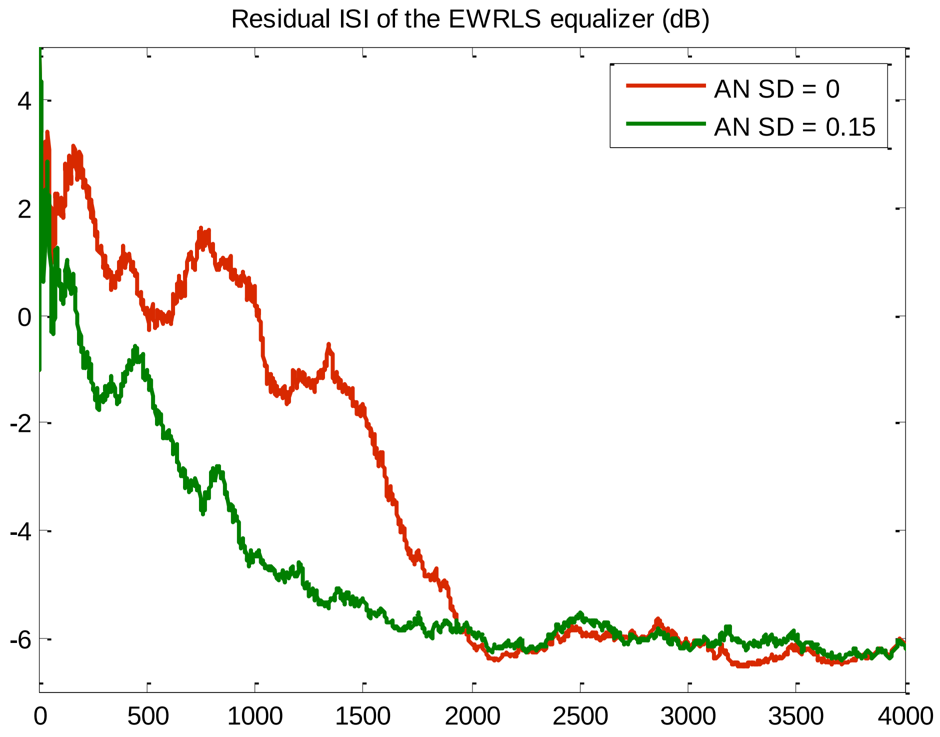

Figure 5-13 Comparison of residual ISI for the case of EWRLS

5.4 Chapter Conclusion

Important results have been achieved that are expected to some extent. Simulated annealing produced many positive changes to the speed of convergence and/or final measure of equalization, residual ISI. The latter is an indication of a trapped adaptation in which the weight parameters are stuck in a local minimum with acceptable or unacceptable performance measures.

Applying the ASA techniques generate results demonstrating the improvement in the convergence speed and the final ISI. However, the final residual ISI is changed only if convergence is made to another location of the available local minima. In other words, adding the annealing noise in any of the different channel models will not change the performance in terms of final ISI as long as the equalizer converges to the same point.

Another interesting observation was made about the number of local stationary points in each algorithm. It has been seen that QS-2 algorithm shows the least number of change in the final stationary points. The LMS algorithm comes second, and the EWRLS is first with the highest number of change in final adapted point.

Changing the system model of Figure 5-1 to 5-2 is not associated with significant change in the equalizers performance and behavior.

5.5 References

[48] Benvenuto, N., Marchesi, M., “Digital Filter Design by Simulated Annealing”, IEEE Transactions on Circuits and Systems, Vol. 36, No. 3, March 1989.

[49] Bohm, M., et al., “On the Use of Simulated Annealing to Automatically Assign Decorrelated Components in Second-Order Blind Source Separation”, IEEE Transactions on Biomedical Engineering, Vol. 53, No. 5, May 2006.

[50] Courat, J.P., Raynaud, G., Wad, I., Siarry, P., “Electronic Component Model Minimization Based on Log Simulated Annealing”, IEEE Transactions on Circuits and Systems, Vol. 41, No. 12, December 1994.

[51] Gelfand, S.B., Mitter, S.K., “Simulated Annealing Type Algorithms for Multivariate Optimization,” Algorithmica, pp 419-436, No. 6, 1991.

[52] Gelfand, S.B., Mitter, S.K., “Analysis of Simulated Annealing for Optimization,” Proc. 24th Conference on Decision and Control, December 1985, pp779-786.

[53] Kirkpatrick, S, Gelatt Jr., C.D., Vecchi, M.P., “Optimization by Simulated Annealing,” IBM Research Report RC 9355, 1982.

[54] Kirkpatrick, S, Gelatt Jr., C.D., Vecchi, M.P., “Optimization by Simulated Annealing,” Science, Volume 220, No. 4598, May 1983.

[55] Kumar, R., “Convergence of Decision-Directed Adaptive Equalizer,” Technical Report, Lefschetz Center for Dynamical Systems, Brown University, Providence RI, September 1981.

[56] Kumar, R., “Convergence of a Decision-Directed Adaptive Equalizer,” The 22nd IEEE Conference on Decision and Control, Dec. 1983.

[57] Mazo, J.C., “Analysis of Decision-Directed Equalizer Convergence,” Bell System Technical Journal, Vol. 59, No. 10, pp 1857-1876, December 1980.

[58] Qin, Z., Cai, K., Zou, X., “A Reduced-Complexity Iterative Receiver Based on Simulated Annealing for Coded partial-Response Channels”, IEEE Transactions on Magnetics, Vol. 43, No. 6, June 2007.

[59] Rutenbar, R.A., “Simulated Annealing Algorithm: An Overview”, IEEE Circuits and Devices magazine, Vol. 5, Issue 1, January 1989.

[60] Van Laarhoven, P.J.M., Arrts, E.H.L., “Simulated Annealing: Theory and Applications’”, D. Reidel Publishing Company, Holland, 1987.

[61] White, L.B., Perreau, S., Duhamel, P., “Reduced Computation Blind Equalization for FIR channel input Markov Models,” IEEE International Conference on Communications, “Gateway to Globalization,” Seattle, 1995.

[62] Widrow, B, Walach, E., “Adaptive Inverse Control: A Signal Processing Approach,” Wiley-IEEE Press, Nov. 2007.

Appendix A

Auto-covariance matrix of a random process $\boldsymbol{C_x} = \mathbb{E}\{(\boldsymbol{x} - \overline{\boldsymbol{x}})(\boldsymbol{x} - \overline{\boldsymbol{x}})^T\}$ wof the random vector $\boldsymbol{x}$ with zero mean reduces to the autocorrelation matrix $\boldsymbol{R_x} = \mathbb{E}\{(\boldsymbol{x})(\boldsymbol{x})^T\}$ with the following properties. We are to show that the addition of white noise to the process output can possibly improves the eigenvalue spread in a worst case analysis method. With the fair assumption of stationary process the autocorrelation matrix is symmetric and also Toeplitz. Furthermore, the main diagonal elements are all positive that can be normalized to unity. Symmetry in addition to semi-definite properties of the autocorrelation matrix leads to real and positive eigenvalues (see Papoulis [2]).

Let us denote the elements in a complex and square matrix order N by $\{a_{ij} \in \mathbb{C}\},\ i,j = 1$ to N, and let $Z_i$denote the circles with center a_{ii} and radius $r_i = \sum_{\substack{j=1 \\ j\neq i}}^{N} |a_{ij}|$ that is

$$Z_i = \{z \in \mathbb{C} \mid |z - a_{ij}| \leq r_i\}. \qquad (A-1)$$

The Greschgorin theorem states that any eigenvalue of the matrix λ belongs to one of the circles Z_i (see Atkinson [1]). Since the eigenvalues of autocorrelation matrix of a stationary process are real and positive, the Greschgorin discs geography should look like the ones in Figure A-1. Notice that the disc centers are all equal to diagonal value a_{ii}. In worst case, the eigenvalue spread is $\frac{\lambda_{max}}{\lambda_{min}}$ with λ_{max} and λ_{min} as shown in Figure A-1.

Addition of white noise $\sigma_n^2\boldsymbol{I}$ to the output of the process will only affect the diagonal elements to new value $a_{ii} + \sigma_n^2$. The new autocorrelation matrix has the discs geography shown in Figure A-2. In Figure A-2 one can see the discs are all moved in the positive direction of real axis by σ_n^2. Consequently the new eigenvalue spread in the worst case is $\frac{\lambda_{max}+\sigma_n^2}{\lambda_{min}+\sigma_n^2}$.

Finally, the behavior of the autocorrelation matrix is likely to improve because its worst case eigenvalue spread is smaller. That is

$$\frac{\lambda_{max} + \sigma_n^2}{\lambda_{min} + \sigma_n^2} < \frac{\lambda_{max}}{\lambda_{min}} \qquad (A-2)$$

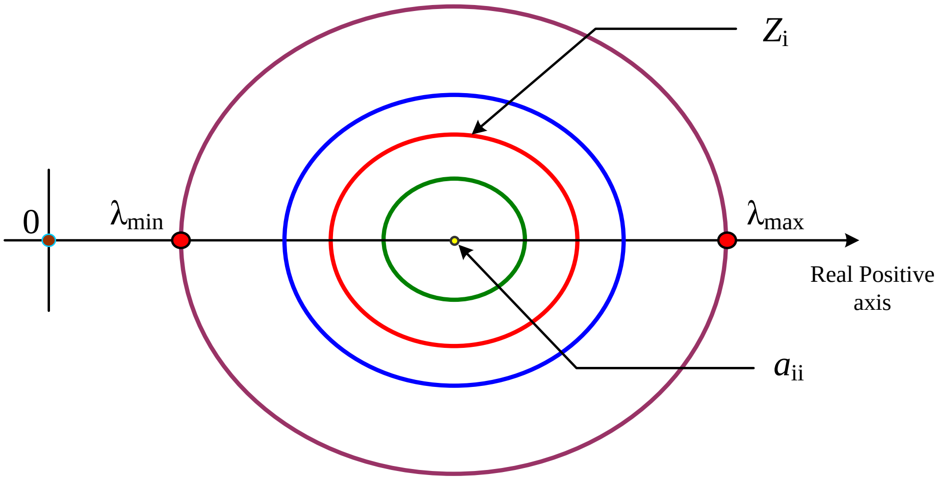

Figure A-1 Greschgorin discs for the autocorrelation matrix of a stationary process

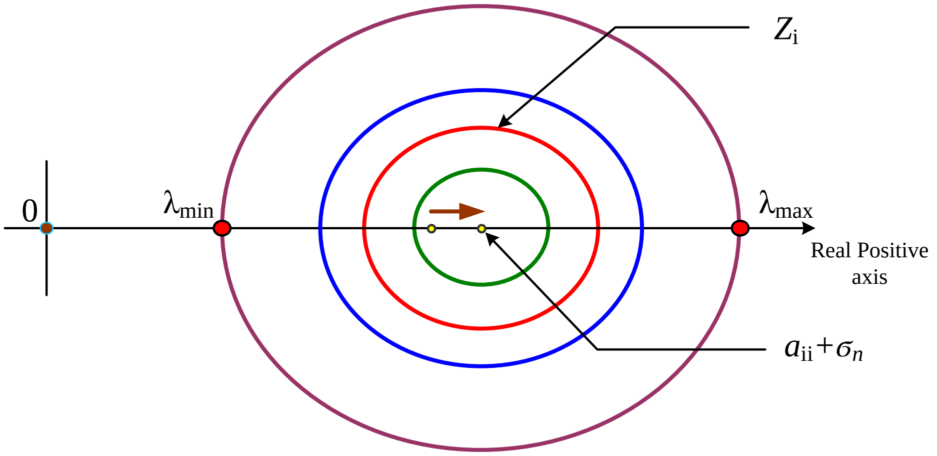

Figure A-2 Greschgorin discs for the autocorrelation matrix plus the white noise

A.1 References

[1] Atkinson, K.E., “An Introduction to Numerical Analysis,” 2nd Edition, John Wiley & Sons, 1989.

[2] Papoulis, A., Pillai, S.U., “Probabilty, Random Variables and Stochastic Processes,” 4th Edition, McGraw-Hill Higher Education, 2002.

Chapter 6: Concluding Remarks and the Future Research

The main problem that is being addressed in this thesis is related the most important issues associated with the wireless communication channels, namely Inter-Symbol Interference (ISI) caused by multipath nature and the communicators mobility. A complete introduction to the modeling and characteristics of this kind of channels are given in Chapter 1. It was also explained in Chapter 2 that ISI is causing data errors and hence the main obstacle in the way of reliable and fast wireless digital communications. The common methods to eliminate or sufficiently mitigate the effect of distortion caused by ISI are collectively known as channel equalization.

The approach in this thesis is based not only on one methodology but several algorithms and configurations that are offered and examined to tackle the ISI problem. There are two main categories of channel equalization, supervised and blind modes. We have studied the application of a new specially modified neural network requiring very short training period for the proper channel equalization in Chapter 4. The demonstrated success in given examples motivated some convergence analysis.

For blind modes two distinctive methodologies are presented and studied. Chapter 3 covers the concept of multiple "cooperative" algorithms for the cases of two and three cooperative algorithms. Several computationally effective algorithms are necessary to implement a diversified-algorithm system. The "select absolutely larger equalized signal" versus "majority vote" methods have been used in 2- and 3-algoirithm systems respectively, many of the demonstrated results are encouraging for further research.

Chapter 5 involves the application of general idea of simulated annealing to the target problem of this thesis in an adaptive. A limited strategy of constant annealing noise is experimented for testing the same various simple algorithms as in Multiple Algorithms systems. Convergence to local stationary points of the cost function in parameter space is clearly demonstrated and justifies the use of additional noise. The capability of the adding the random noise to release the algorithm from the local traps is established in several cases.

Each of the methods proposed and investigated invites future research and scholarly work.

1. The new supervised equalizer system based on the new neural network configuration can be augmented by the addition of at least one hidden layer. Additional layer seeks more computations for both the forward and the backward propagations however it is possible to obtain significant capability in particular for the cases of nonlinear channel models. More general convergence analysis for all layers can be attempted in the perspective regardless of how challenging this can be.
2. Adaptive simulated Annealing method has been studied in the limiting cases such as constant random noise power and the lack of a plan to adjust the noise power during the adaptation. Some practical measures that can represent the unknown channel parameters must be proposed for the noise power management. Besides, it is intuitively assumed that there should be modified or augmented algorithms to achieve robust and mighty ASA process with minimal constraints.
3. The algorithms with diversified adaptive techniques have been studied with limited number and limited variety of cooperating techniques. Although the methodology for the cooperation of algorithms can be seen to be final, there are capacities of improvements that require scholarly attentions.